Non-conventional Many-body Phases in Ultracold Dipolar Systems

Aleksey Fedorov

NNT : 2017SACLS580

Thèse de doctorat
de
L'Université Paris-Saclay
preparee a
L'Université Paris-Sud
Au sein Du Laboratoire de Physique Théorique et Modèles Statistiques

Ecole doctorale n° 564
Physique de l'Ile-de-France (PIF)

Spécialité de doctorat : Physique

par

M. Aleksey Konstantinovich Fedorov

Non-conventional Many-body Phases in Ultracold Dipolar Systems

Thèse présentée et soutenue à Orsay, le 28 juin 2017 :

Devant le jury composé de :

M. Christophe TEXIER, Professeur, Université Paris-Sud	Président
M. Mikhail BARANOV, Chercheur, Académie Autrichienne des Sciences	Rapporteur
M. Paolo PEDRI, Maître de Conférences, Université Paris Nord	Rapporteur
M. Andrey VARLAMOV, Professeur, Université de Rome "Tor Vergata"	Examinateur
M. Georgy SHLYAPNIKOV, Professeur, Université Paris-Sud	Directeur de thèse

Contents

Acknowledgment

I would like to begin by thanking my advisor Gora Shlyapnikov for making my time in Laboratoire de Physique Théorique et Modèles Statistiques (LPTMS) such an incredible experience.

It was a great pleasure to work with Vladimir Yudson. I am very grateful to Vladimir for teaching me the intricacies of theoretical physics and for kind attention to my other research activities.

The significant part of this Thesis has been completed under the influence of the joint work with Yury Lozovik and his group, especially Igor Kurbakov. The work with the group of Yury Lozovik is a great experience.

It was a great pleasure to discuss and/or collaborate with numerous of outstanding people at Russian Quantum Center (RQC) and LPTMS including Evgeniy Kiktenko, Yulia Shchadilova, Oleg Lychkovsky, Ilya Fedorov, Alexander Ulanov, Alexandra Sheremet, Nina Voronova, Anton Trushechkin, Dmitry Kronberg, Sergey Matveenko, Denis Kurlov, Giulio Bertoli (it was a pleasure to share office with you!), Kirill Plekhanov, Andrew Sykes, and Dmitry Petrov. I am grateful to my tutors Guillaume Roux and Mikhail Zvonarev at LPTMS for kind attention to my work. I thank Claude Pasquier and École Doctorale de Physique en Île-de-France as well as Emmanuel Trizac and Claudine Le Vaou for perfect support. I also thank the RQC team and Ruslan Yunusov for supporting me.

I feel lucky that about 6 years ago Alex Lvovsky replied to my letter to *mail@iqct.org* regarding an internship at just formed RQC. The invitation to the University of Calgary and our collaboration during 2011-2013 opened a way to my future. I sincerely hope that my efforts in organization of the laboratory were helpful for the Lvovsky group. It is a great honor for me to be the first diploma student of Yury Kurochkin, whose belief and vision of the future are truly inspiring.

I am happy to thank here first scientific advisors in my life, Alexander Ovseevich, Vladimir Man'ko, and Stanislav Yurchenko. I would like also thank Eugene Demler and Mikhail Lukin for their support and numerous of inspiring discussions during my visit to Harvard University in 2013-2014.

My friends are a very important part of my life. The most wonderful thing characterising my close friends is that they are more confident in my success than I am. Last but not least, I would like to thank my family, my parents, my grandparents, and my brother. This Thesis is dedicated to them.

The research leading to these results has received funding from the European Research Council under European Community's Seventh Framework Programme (FR7/2007-2013 Grant Agreement no. 341197).

Aleksey K. Fedorov

Paris, date

Thesis are based on the following publications:

1. A.K. Fedorov, I.L. Kurbakov, Y.E. Shchadilova, and Yu.E. Lozovik, Phys. Rev. A **90**, 043616 (2014).

2. A.K. Fedorov, I.L. Kurbakov, and Yu.E. Lozovik, Phys. Rev. B **90**, 165430 (2014).

3. A.K. Fedorov, S.I. Matveenko, V.I. Yudson, and G.V. Shlyapnikov, Sci. Rep. **6**, 27448 (2016).

4. A.K. Fedorov, V.I. Yudson, and G.V. Shlyapnikov, Phys. Rev. A **95**, 043615 (2017).

Synthèse en français

Le problème de la détection et de la description des nouveaux états quantiques macroscopiques, caractérisés par des propriétés exotiques et non-conventionnelles, est d'importance fondamentale dans la physique moderne. Ces états offrent des perspectives fascinantes dans le domaine du traitement de l'information, des simulations quantiques et de la recherche des nouveaux types de matériaux. Dans ce travail de thèse, nous développons une théorie qui permet de décrire des phases non-conventionnelles dans des systèmes de gaz ultra-froids dipolaires. Ces systèmes sont activement étudiés expérimentalement en utilisant des atomes à grand spin, des molécules polaires et des excitations dipolaires dans des semiconducteurs. Nous mettons l'accent sur le rôle des interactions dipôle-dipôle à longue portée.

L'exemple primordial est la phase topologique a plusieurs corps décrite par un nombre significative des états fondamentaux et son caractère non-local. Ses systèmes peuvent être appliqués dans le domaine du traitement d'information quantique qui peut être protégé topologiquement [2,3]. Le prix Nobel de l'année 2016 en Physique (J. Kosterlitz, D. Haldane, and D. Thouless) a été attribuée pour la recherche séminal sur les transitions des phases topologiques et des phases de matériaux topologiques. Cependant, la réalisation expérimentale de ces phases exotiques possède un nombre des difficultés sérieuses, et exige des approches nouvelles.

L'exemple primordial est la phase topologique à plusieurs corps décrite par un nombre significatif des états fondamentaux et son caractère non-local. Ses systèmes peuvent être appliqués dans le domaine du traitement d'information quantique qui peut être protégé topologiquement [2,3]. Le prix Nobel de l'année 2016 en Physique (J. Kosterlitz, D. Haldane, and D. Thouless) a été attribuée pour la recherche séminale sur les transitions des phases topologiques et des phases de matériaux topologiques. Cependant, la réalisation expérimentale de ces phases exotiques possède un nombre des difficultés sérieuses, et exige des approches nouvelles.

L'une des découvertes les plus avancées de ces dernières décennies est l'observation du condensat de Bose-Einstein (BEC) de gaz atomiques dilués ultra-froids reporte par les groupes de E. Cornell et C. Wieman à JILA [4], W. Ketterle à MIT [5], et R. Hulet à RICE [6]. Cet accomplissement exceptionnel est devenu un point de départ pour des études consécutives dans le domaine de la matière ultra-froide. Une capacité de contrôle remarquable de tous les paramètres pertinents, tels que la densité, la force d'interaction et la dimensionnalité du problème, permet d'utiliser des gaz ultra-froids comme une base pour étudier les systèmes de matière condensée, qui peuvent révéler des phases nouvelles de la matière ultra-froide, et mettre en œuvre l'implémentation des nouvelles technologies quantiques [7-10].

Les interactions entre les particules jouent un rôle crucial et leur manipulation représente donc un outil évident pour générer de nouveaux états exotiques à plusieurs corps. Ceci a stimulé une étude théorique avancée des systèmes en interaction non-locales, comme par exemple, des systèmes des particules dipolaires ultra-froides (molécules polaires et atomes à spin grand). Ces particules interagissent entre eux via des forces dipolaires anisotropes à longue portée, ce qui change radicalement la nature des états dégénérés quantiques. Les découvertes importantes contiennent des résonances pointues lors de la

diffusion dipôle-dipôle [11], la dépendance du diagramme de stabilité des dipôles piégés pour la forme géométrique du piégeage [12], spectre d'excitation roton-maxon (voir Fig. 1.1) pour les bosons dipolaires dans la géométrie "pancake" [13], et la possibilité d'avoir l'appariement superfluide des ondes-p dans un gaz de Fermi dipolaire polarisé [14]. Une autre branche de cette recherche est liée à l'utilisation des dipôles ultra-froids comme une plate-forme dans le contexte de traitement de l'information quantique [15-18].

La physique des dipôles quantiques ultra-froides a connu une nouvelle vie après des expériences remarquables sur la création de nuages ultra-froids des molécules polaires diatomiques dans leur état fondamental [19-36], sur l'obtention des gaz dégénérés d'atomes avec des grands moments magnétiques [37-40], et sur la création des excitons à un grand temps de vie dans des systèmes de matière condensée [41-48]. Actuellement, il y a un nombre croissant de propositions pour étudier des nouveaux états quantiques à plusieurs corps dans ces systèmes (pour la revue, voir les Refs. [49-52]), qui comprennent la cristallisation [53-59], les motifs d'onde de densité [60-65], des vortices [66-69], de la physique des spins avec des dipôles [70,71], et beaucoup d'autres phénomènes intéressants. Un accomplissement important est la réalisation expérimentale de l'extension du modèle de Hubbard pour les gaz dipolaires dans les réseaux optiques [72]. Des résultats importants incluent aussi la découverte de nouveaux types de liquide de Fermi [73-75], de la dynamique à plusieurs corps [76], de la localisation à plusieurs corps [77], des ferrofluides quantiques [78], de la multifractalité des excitations dipolaires dans des systèmes aléatoires [79], ainsi que la physique des gouttelettes quantiques [80-82].

Cependant, il existe une grande variété de questions ouvertes, liées en particulier à la simulation des systèmes complexes de matière condensée et la supraconductivité à ondes-p et ondes-d ainsi que la création des états topologiques stables à plusieurs corps. Dans ce travail de thèse, nous nous focalisons exactement sur ces problèmes.

Manifestation du spectre d'excitation roton-maxon. Pour le gaz de Bose dipolaire condensé, l'une des questions clés était reliée à la présence de la caractéristique roton-maxon (ligne solide) du spectre d'excitation et à la possibilité d'obtenir des états supersolides. Cependant, l'idée d'obtenir un état supersolide lorsque le roton atteint zéro (ligne mixte) et le BEC uniforme devient instable n'a pas atteint le succès à cause de l'effondrement du système. Rotonisation est une caractéristique distincte du gaz de Bose dipolaire condensé, comparé aux gaz ultra-froids atomiques ordinaires avec des interactions à courte distance qui montrent un spectre quadratique (ligne pointillée).

Parmi les états exotiques à plusieurs corps des gaz dipolaires ultra-froids, l'état supersolide des bosons attirent beaucoup d'attention. Dans cet état supersolide, la fonction d'onde du condensat possède une structure de réseau au-dessus d'un fond uniforme [83-91]. La recherche expérimentale de cet état dans des systèmes de l'hélium liquide a duré des décennies [86,91] depuis la première prédiction théorique [88]. Cependant, la confirmation de l'observation expérimentale de cet état supersolide [92] dans l'hélium confiné dans le milieu poreux a été retiré [93].

Une idée remarquable sur la création de supersolidité dans l'espace libre est liée à la présence du spectre d'excitation roton-maxon et suppose que l'hélium se déplace dans un capillaire avec la vitesse critique, de telle sorte que dans le cadre mobile, le minimum de roton touche zéro [94]. Il a ensuite été prédit qu'il y a une transition de phase du système dans cet état avec des modulations périodiques de la densité (de la fonction d'onde de condensat). Cette belle idée, qui n'a cependant jamais été mise en œuvre dans des expériences d'hélium, est activement discutée dans le contexte général de la superfluidité des gaz de Bose circulant à des vitesses supérieures à la vitesse critique de

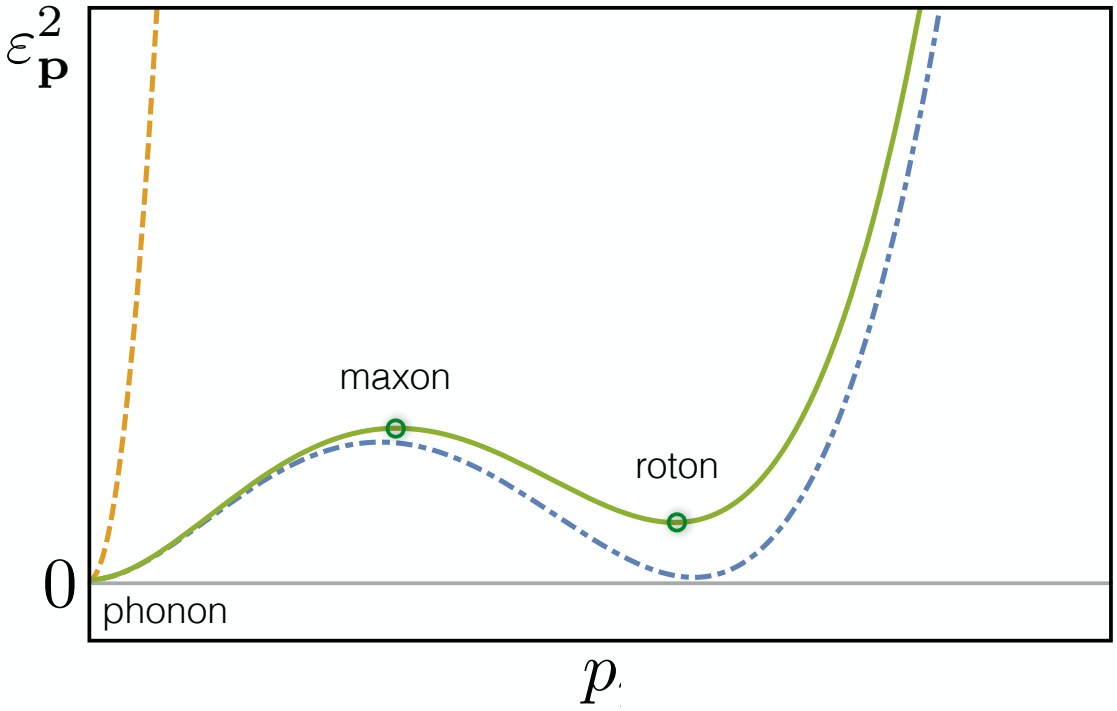

Figure 1: Manifestation du spectre d'excitation roton-maxon. Pour le gaz de Bose dipolaire condensé, l'une des questions clés était reliée à la présence de la caractéristique roton-maxon (ligne solide) du spectre d'excitation et à la possibilité d'obtenir des états supersolides. Cependant, l'idée d'obtenir un état supersolide lorsque le roton atteint zéro (ligne mixte) et le BEC uniforme devient instable n'a pas atteint le succès à cause de l'effondrement du système. Rotonisation est une caractéristique distincte du gaz de Bose dipolaire condensé, comparé aux gaz ultra-froids atomiques ordinaires avec des interactions à courte distance qui montrent un spectre quadratique (ligne pointillée)..

Landau [95].

Les gaz dipolaires dilués de bosons en deux dimensions (2D) peuvent montrer une structure de maxon du spectre des excitations si on ajuste le terme du potentiel d'interaction à courte distance. Ils peuvent être rendus instables par rapport aux modulations périodiques du paramètre d'ordre (instabilité du roton) [13]. Malheureusement, plutôt que de former un état supersolide à l'approche d'une telle instabilité, le gaz s'effondre [69, 96, 97].

À un stade ultérieur, plusieurs propositions ont été faites en vue de la création de l'état supersolide dans des gaz quantiques des bosons dipolaires [98-101] (pour une revue, voir la référence [85]). Les propriétés statiques et dynamiques des gaz dégénérés dipolaires piégés dilués ont été activement discutés en basant sur l'approche de Bogoliubov [102-104]. Cependant, les états supersolides obtenus dans cette approche nécessitent généralement un régime dense avec plusieurs particules dans la portée d'interaction, ce qui peut être difficile à atteindre expérimentalement. Le même résultat demeure pour les supersolides discutés dans le contexte des gaz de Bose dipolaires près de la transition de phase gaz-solide [53, 54, 57].

C'est donc une question importante de savoir si la supersolidité peut exister dans le régime dilué. Il a été démontré récemment que les gaz dipolaires dilués en 2D des bosons peuvent devenir supersolides lors de l'ajout d'une interaction de contact répulsive à trois corps en plus des interactions à deux corps habituelles ainsi que des interactions

dipolaires de contact à longue distance [105]. Au stade actuel, différentes possibilités d'obtenir l'instabilité du roton et la supersolidité dans les gaz dipolaires dilués des bosons sont d'un très grand intérêt.

Une autre prédiction notable concerne des phases superfluides non-conventionnelles. Des supraconducteurs et superfluides non-conventionnels attirent beaucoup d'intérêt grâce à leurs propriétés de transport non triviales et / ou comportement topologique [106-116].

Ce comportement a été activement discuté en 2D pour le superfluid $p_x + ip_y$ des fermions identiques, où les paires de Cooper ont un moment angulaire orbital égal à l'unité [117-123]. Les vortex quantifiés dans ces superfluides portent des modes de Majorana à l'énergie nulle à l'intérieur de leurs noyaux [108,124,125]. Ces modes rendent les vortices obéissant à la statistique d'échange non-abélienne, ce qui est indispensable pour réaliser l'informatique quantique topologiquement protégée [2, 3, 126, 127].

Malgré le progrès significatif d'un point de vue théorique [118,119,125,128-133], les superfluides $p_x + ip_y$ n'ont jamais été observés. L'obstacle crucial à la réalisation de ces phases pour les fermions atomiques en interactions provient d'une grandeur très petite de la force d'interaction d'onde-p. Par conséquent, pour obtenir une température de transition importante, il faut approcher de la résonance de Feshbach d'onde-p. Des résonances d'onde-p ont été étudiées dans des expériences de potassium fermionique [134-136] et des atomes de lithium [137-143]. Proche de la résonance, le taux de perte dû aux collisions inélastiques devient extrêmement important [144-146]. Ainsi, le superfluide des fermions atomiques interagissant à courte distance est décrit soit par une température critique très basse soit par l'instabilité due à des pertes générées par des collisions inélastiques.

Des expériences successives sur la réalisation des molécules polaires dans l'état fondamental ont ouvert la possibilité d'obtenir de superfluides non conventionnels. En particulier, des molécules polaires habillées par le champ micro-onde confinées en 2D peuvent acquérir une queue dipôle-dipôle attrayante dans le potentiel d'interaction, ce qui conduit à l'émergence du superfluide d'onde-p avec une température de transition atteignable expérimentalement [122, 123]. Cependant, l'utilisation des superfluides d'onde-p gazeux pour le traitement quantique tolérant rencontre des difficultés dues aux qubits d'adressage. Il est donc important de trouver des nouvelles configurations pour des superfluides topologiques, qui fournissent des températures de transition plus hautes et la possibilité d'avoir une grande capacité de contrôle des opérations avec des qubits.

En plus des applications possibles dans le domaine de traitement de l'information quantique, les gaz dipolaires ultra-froids sont prometteurs en tant que simulateur quantique des systèmes complexes de matière condensée. Des exemples de phénomènes intéressants, qui peuvent être étudiés avec des simulations quantiques sont la superfluidité non-conventionnelle (en particulier, la superconductivité d'onde-d) [147-149] et le magnétisme quantique [148, 150, 151].

Les phases non conventionnelles à plusieurs corps des systèmes dipolaires sont intéressantes dans les géométries bicouches [152-158] et multi-couches [60, 63, 159-162]. Des configurations bicouches dans lesquelles tous les dipôles sont orientés dans la même direction ont été activement discutés [63,152-158]. Il a été trouvé, qu'il y a une superfluidité d'onde-s entre les deux couches. Les paires de Cooper sont formées par des dipôles de différentes couches et ils sont générés par des interactions dipolaires d'onde-s entre eux [152].

Dans le contexte de la superfluidité non-conventionnelle, il est crucial de s'appuyer sur des réseaux de longueur inférieure aux longueurs d'onde, proposés récemment [163-174], où la constante de réseau (l'espacement entre couches dans le système bicouche)

peut atteindre moins de 60 nm. Ceci augmente fortement toutes les échelles d'énergie du problème, de telle sorte que même pour un facteur de remplissage petit, l'énergie de Fermi peut devenir de l'ordre de centaines de nano-Kelvins. Ces réseaux peuvent être conçus en utilisant un habillage adiabatique des réseaux dépendant de l'état [163], des transitions optiques multi-photons [164], des réseaux optiques dépendant du spin avec des modulations dépendant du temps [165], ainsi que des systèmes nano-plasmoniques [166], des réseaux de vortices dans des films supraconducteurs [167], dans le graphène [168], des puces atomiques des films magnétiques [169], et des cristaux photoniques [170-172] (voir aussi les références [173, 174]).

Ces propositions intéressantes ont déjà stimulé des études liées à la physique à plusieurs corps dans de tels réseaux, en particulier à l'analyse du modèle de Hubbard et de l'ingénierie des Hamiltoniens spin-spin [170].

Chapter 1

New frontiers of many-body physics with ultracold dipolar gases

1.1 Overview

Today, significant efforts of the physics community are concentrated on the problem of revealing and describing novel macroscopic quantum states characterized by exotic and non-conventional properties. The idea behind this is the fundamental importance of such states for modern physics and their potential applications in quantum information processing, quantum simulation, nanophysics, and material research [1].

A paramount example is a topologically protected many-body phase with an extremely large number of ground states and non-local character. Such systems have a great potential for applications in topologically protected quantum information processing [2, 3]. The seminal research on topological phase transitions and topological phases of matter was awarded by the Nobel Prize in Physics in 2016 (J. Kosterlitz, D. Haldane, and D. Thouless). However, realization of these interesting phases encounters a number of serious difficulties, and it demands novel approaches.

One of the most advances discoveries of recent decades is the observation of Bose-Einstein condensation (BEC) of ultracold dilute atomic gases by the groups of E. Cornell and C. Wieman at JILA [4], W. Ketterle at MIT [5], and R. Hulet at RICE [6]. This outstanding achievement has become a starting point for the progress in the studies of ultracold matter. A remarkable degree of control over all relevant parameters, such as density, interaction strength, and dimensionality, allows one to use ultracold quantum gases as a playground for investigating condensed matter systems, revealing novel interesting phases of ultracold matter, and implementing quantum technologies [7–10].

Interactions between particles play a crucial role and their manipulation is a clear way to generate novel many-body states. This stimulated an extended theoretical activity in the investigation of systems with a non-contact interaction between particles, in particular, ultracold dipolar particles (polar molecules and large-spin atoms). These particles interact with each other via anisotropic and long-range dipolar forces, which drastically changes the nature of quantum degenerate states. Important findings include shape resonances in the dipole-dipole scattering [11], the dependence of the stability diagram of trapped dipoles on the trapping geometry [12], roton-maxon excitation spectrum (for details, see Fig. 1.1) for pancaked dipolar bosons [13], and possibilities of p-wave superfluid pairing in a polarized dipolar Fermi gas [14]. Another branch of this research is related to the use of ultracold dipoles as a platform for quantum information processing [15–18].

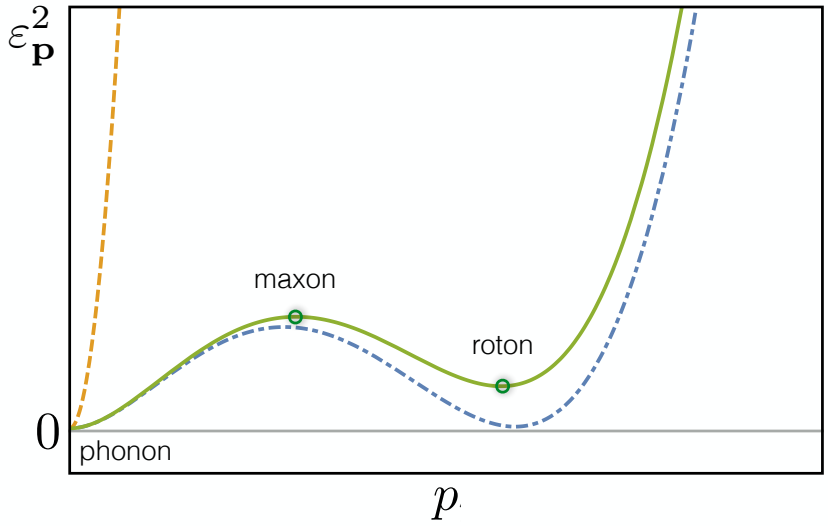

Figure 1.1: Manifestation of the roton-maxon excitation spectrum. For dipolar Bose-condensed gases, one of the key issues was related to the presence of the roton-maxon character (solid line) of the excitation spectrum and to the possibility of obtaining supersolid states. However, the idea of obtaining a supersolid state when the roton reaches zero (dot-dashed line) and the uniform BEC becomes unstable did not succeed because of the collapse of the system. Rotonization is a distinguished feature of dipolar Bose-condensed gases in compare with ordinary atomic ultracold gases with short-range interactions demonstrating a quadratic spectrum (dashed line).

The physics of ultracold quantum dipoles got a new life after remarkable experiments on creating ultracold clouds of ground-state diatomic polar molecules [19–36], on obtaining degenerate gases of atoms with large magnetic moments [37–40], and on creating long-lived excitons in condensed matter systems [41–48]. Presently, there is a growing number of proposals to study novel quantum many-body states in these systems (for a review, see Refs. [49–52]), which include crystallization [53–59], density-wave patterns [60–65], vortex structures [66–69], spinor physics with dipoles [70,71], and many others interesting phenomena. An important achievement is the experimental realization of the extension of the Hubbard model for dipolar gases in optical lattices [72]. Important findings also include novel types of Fermi liquid [73–75], many-body dynamics [76], many-body localization [77], quantum ferrofluids [78], multifractality of dipolar excitations in a random system [79], and the physics of quantum droplets [80–82].

However, there is a large variety of open questions, related in particular to the simulation of complex condensed matter systems with p-wave and d-wave superconductivity and to the creating of stable topological many-body states. In the present Theses we focus in these directions.

1.1.1 Rotonization and supersolidity of dipolar bosons

Among exotic many-body states of ultracold dipolar gases, the supersolid state of bosons attracts large attention. In this state the condensate wavefunction shows a lattice structure on top of a uniform background [83–91]. The search for this state in experiments with liquid helium has spanned decades [86,91] since the early theoretical prediction [88]. However, the claim of the observation of the supersolid state [92] in helium confined in a porous medium has been withdrawn [93].

A remarkable idea on creating supersolidity in free space is related to the presence of the roton-maxon excitation spectrum and assumes that helium is moving in a capillary with the critical velocity, so that in the moving frame the roton minimum touches zero [94]. It was then predicted that there is a phase transition of the system to the state with periodic modulations of the density (condensate wavefunction). This beautiful idea, which however was never implemented in helium experiments, is actively discussed in the general context of superfluidity in Bose gases flowing with velocities higher than the Landau critical velocity [95].

Dilute dipolar gases of bosons in two dimensions (2D) may demonstrate the roton-maxon structure of the spectrum by fine tuning the short-range part of the interaction potential and can be made unstable with respect to periodic modulations of the order parameter (roton instability) [13]. Unfortunately, instead of forming a supersolid state when approaching such an instability, the gas collapses [69, 96, 97].

In a later stage, several proposals have been made towards the creation of the supersolid state in quantum gases of dipolar bosons [98–101] (for a review, see Ref. [85]). The static and dynamical properties of dilute trapped dipolar degenerate gases have been actively discussed on the basis of the Bogoliubov approach [102–104]. However, the predicted supersolids typically require a dense regime with at least several particles within the interaction range, which can be difficult to achieve. The same holds for supersolids discussed for dipolar Bose gases near the gas-solid phase transition [53, 54, 57].

It is thus an important question of whether supersolidity can exist in the dilute regime. It has been recently demonstrated that 2D dilute dipolar gases of bosons can become supersolids when adding a contact three-body repulsion on top of the usual two-body contact and long-range dipolar interactions [105]. In the present stage different possibilities for obtaining the roton instability and supersolidity in dilute dipolar gases of bosons are of great interest.

1.1.2 Non-conventional superfluids of atoms and polar molecules

Another notable prediction is related to non-conventional superfluid phases. Non-conventional superconductors and superfluids attract a great deal of interest due to their non-trivial transport properties and/or topological behavior [106–116].

This behavior has been actively discussed in 2D for the $p_x + ip_y$ superfluid of identical fermions, where Cooper pairs have orbital angular momentum equal to unity [117–123]. Quantized vortices in this superfluid carry zero-energy Majorana modes on their cores [108, 124, 125]. These modes cause the vortices to obey non-Abelian exchange statistics, which is a basis for topologically protected quantum computing [2, 3, 126, 127].

Despite a significant progress in theory [118, 119, 125, 128–133], the $p_x + ip_y$ superfluid has not been observed. The crucial obstacle to achieve this phase for spinless short-range interacting atomic fermions comes from a small value of the p-wave interaction. Therefore, in order to obtain a sizable transition temperature one has to approach a p-wave Feshbach resonance. The p-wave resonances have been studied in experiments with fermionic potassium [134–136] and lithium [137–143] atoms. Close to the resonance the rate of inelastic collisional losses becomes extremely large [144–146]. Thus, the superfluid of short-range interacting atomic fermions is characterized either by vanishingly low critical temperature or by instability due to collisional losses.

Successful experiments on the creation of ground-state polar molecules opened fascinating prospects for obtaining non-conventional superfluids. In particular, microwave-

dressed polar molecules confined to 2D may acquire an attractive dipole-dipole tail in the interaction potential, which leads to the emergence of collisionally stable p-wave superfluid with a reachable transition temperature [122, 123]. However, the use of gaseous p-wave superfluids for fault-tolerant quantum information processing encounters difficulties with respect to addressing qubits. It is thus important to reveal novel setups for topological superfluids, which provide sizable transition temperatures and possibilities for high degree of control in the operation with qubits.

Besides possible applications in quantum information processing, ultracold dipolar gases are promising as quantum simulator of complex condensed matter systems. Examples of interesting phenomena, which can be studied via quantum simulations, include non-conventional superfluidity (in particular, d-wave) [147–149] and quantum magnetism [148, 150, 151].

Non-conventional many-body phases of dipolar systems are interesting in bilayer [152–158] and multilayer geometries [60, 63, 159–162]. Bilayer configurations with all dipoles oriented in the same direction have been actively discussed [63, 152–158]. As found, there is an interlayer s-wave superfluid, where Cooper pairs are formed by dipoles of different layers due to the s-wave dipolar interaction between them [152].

In the context of non-conventional superfluidity it is crucial to rely on the recently proposed subwavelength lattices [163–174], where the lattice constant (interlayer spacing in the bilayer system) can be as small as about 60 nm. This strongly increases all energy scales, and even for a small filling factor the Fermi energy may become of the order of hundreds of nanokelvins. Subwavelength lattices can be designed using adiabatic dressing of state-dependent lattices [163], multi-photon optical transitions [164], spin-dependent optical lattices with time-dependent modulations [165], as well as nanoplasmonic systems [166], vortex arrays in superconducting films [167], graphene [168], magnetic-film atom chips [169], and photonic crystals [170–172] (see also Refs. [173, 174]).

These interesting proposals already stimulated studies related to many-body physics in such lattices, in particular to the analysis of the Hubbard model and engineering of spin-spin Hamiltonians [170].

1.2 This Thesis

In this Thesis we develop a theory for describing non-conventional phases of ultracold dipolar gases. The main emphasis is on revealing the role of the long-range character of the dipole-dipole interaction. The results of the Thesis are linked to ongoing and future experimental studies.

In Chapter 2 we consider the effect of rotonization for a 2D weakly interacting gas of tilted dipolar bosons in a single homogeneous layer. The obtained roton-maxon excitation spectrum turns out to be anisotropic. In contrast to the case of dipoles perpendicular to the layer, in a wide range of tilting angles the condensate depletion remains small even when the roton minimum is infinitely close to zero. Predicted effects can be observed in a wide class of dipolar systems. We estimate optimal parameters for observing them with ultracold atoms and polar molecules. These results are published in Ref. [175].

In Chapter 3 we discuss the effect of rotonization for a weakly correlated Bose gas of dipoles in a layer. We calculate the stability diagram of the system. According to our estimates, the threshold of the roton instability for a bose-condensed gas with the roton-maxon spectrum is achievable experimentally, e.g., for excitons in GaAs semiconductor

layers. The results of this chapter are published in Ref. [176].

In Chapter 4 we consider p-wave superfluids of fermionic polar molecules in 2D lattices. The optical lattice potential manifests itself in an interplay between an increase in the density of states on the Fermi surface and the modification of the fermion-fermion interaction (scattering) amplitude. The density of states is enhanced due to an increase of the effective mass of atoms. In deep lattices the scattering amplitude is strongly reduced compared to free space due to a small overlap of wavefunctions of fermions sitting in the neighboring lattice sites, which suppresses the p-wave superfluidity. However, we show that for a moderate lattice depth there is still a possibility to create p-wave superfluids with sizable transition temperatures. Due to a long-range character of the dipole-dipole interaction the effect of the suppression of the scattering amplitude is absent for fermionic polar molecules. It is shown that a stable topological $p_x + ip_y$ superfluid of identical microwave-dressed polar molecules may emerge in a 2D lattice. The results of this chapter are based on Refs. [177, 178].

In Chapter 5 we discuss another interesting novel superfluid of fermionic polar molecules. It is expected in a bilayer system, where dipoles are oriented perpendicularly to the layers and in opposite directions in different layers. We demonstrate the emergence of interlayer superfluid pairing. In contrast to the already known s-wave interlayer superfluid, when all dipoles are parallel to each other [152, 154, 156], in our case the s-wave pairing is suppressed and there can be p-wave or higher partial wave superfluids. The results of this chapter are published in Ref. [177].

Chapter 2

Rotonization and stability of 2D Bose gases of tilted dipoles

In this chapter we consider the effect of rotonization (manifestation of a roton-maxon excitation spectrum) and stability for a 2D weakly interacting gas of zero-temperature tilted dipolar bosons in a homogeneous layer. We obtain the conditions for the formation of the roton-maxon excitation spectrum and construct the stability diagram. In contrast to the case of dipoles perpendicular to the layer, in a wide range of tilting angles the condensate depletion remains small even when the roton minimum is extremely close to zero. Predicted effects can be observed in a wide class of dipolar systems. We estimate optimal parameters for observing them with ultracold atoms and polar molecules. The results are published in Ref. [175].

2.1 Background

At zero temperature a 2D system of bosonic dipoles perpendicular to the plane of their translational motion can undergo Bose-Einstein condensation and acquire a roton-maxon excitation spectrum well known in physics of liquid helium [179–181]. For large-spin atoms and polar molecules the height of the roton minimum can be tuned by varying the short-range interaction with the use of Feshbach resonances [182], which looks promising for the observation of novel phenomena.

In particular, a trapped dipolar gas exhibits two kinds of instabilities. When the dipole is oriented along the trap axis, the dipolar interactions have an attractive character and the gas collapses. The collapse is similar to the case of the contact interactions with negative scattering length, but has a different geometrical nature, and different critical scaling behavior. There is, however, another instability mechanism that occurs even in quasi-2D pancake traps for dipoles polarized perpendicularly to the trap plane (along the z-axis). In this case, when the dipolar interactions are sufficiently strong, the gas, despite the quasi-2D trap geometry, feels the 3D nature of the dipolar interactions, i.e. their partially attractive character. This so-called roton instability has been discovered in Ref. [13], and discussed by many authors since then.

Dilute dipolar gases of bosons in 2D may can be made unstable with respect to periodic modulations of the order parameter [13]. However, the non-condensed fraction becomes large before the roton minimum reaches zero [97, 104]. This indicates on the fact that the ordinary condensate disappears before achieving the roton instability.

A subtle question is of how breaking the rotational symmetry, in particular, by tilting

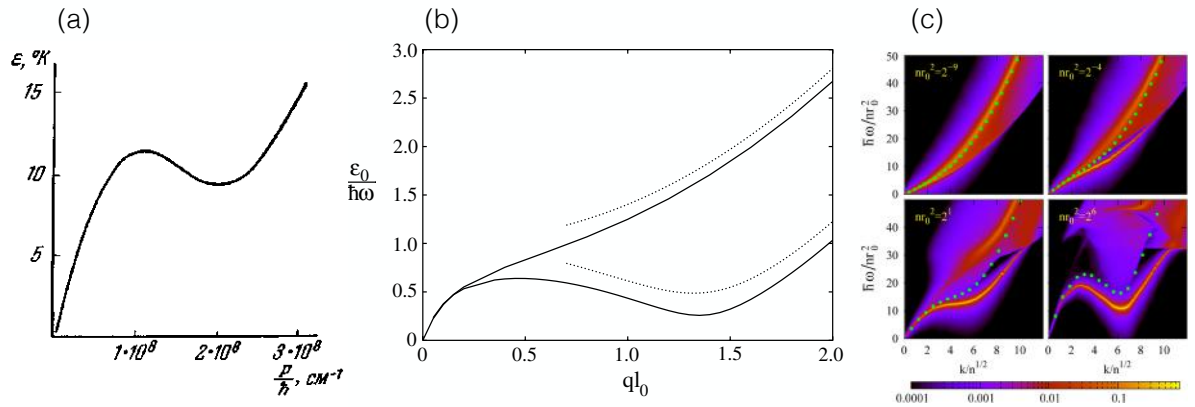

Figure 2.1: Manifestation of the roton-maxon excitation spectrum. In (a) the roton-maxon character of the excitation spectrum in liquid helium (adapted from Ref. [180]). In (b) the prediction of the roton-maxon excitation spectrum for pancaked dipolar bosons (the solid curves show the numerical results, and the dotted curves show the analytical results of Ref. [13]). In (c) the roton-maxon excitation spectrum for 2D dipolar system obtained by the quantum diffusion Monte Carlo algorithm (adapted from Ref. [197]).

the dipoles at a certain angle θ [see Fig. 2.2(a)], may change the situation. The existing studies of tilted dipoles are dedicated to anisotropy of superfluidity [183], sound velocity [184], vortices [185], possibilities of obtaining stripe patterns [186–189], and to the behavior of trapped tilted dipoles [190–193]. Related problems have been considered for systems of dipolar fermions [63, 75, 195, 196].

In the present chapter, we consider a dilute quasi2D BEC gas of dipolar bosons tilted in the x, z plane at an angle θ at zero temperature ($T = 0$) [see Fig. 2.2(a)]. The chapter is organized as follows. In Section 2.2 we demonstrate the emergence of an anisotropic roton-maxon excitation spectrum and calculate the stability diagram. In Section 2.3 we show that the condensate depletion may remain small even when the roton is extremely close to zero. We estimate relevant experimental parameters for ultracold atoms and polar molecules and conclude in Section 2.4.

2.2 Excitation spectrum and stability diagram

We consider a uniform (in the x, y plane) quasi2D weakly-interacting Bose-condensed gas of tilted dipoles and assume that the energy $\hbar\omega_0$ of the tight confinement in the z direction greatly exceeds all other energy scales of the problem. Thus, the motion of particles in the z direction is frozen to zero-point oscillations, and the field operator can be written as

$$\hat{\Psi}(\vec{\mathrm{r}}) \approx \varphi_0(z)\hat{\psi}(\vec{\rho}), \tag{2.1}$$

where $\vec{\rho} = \{x, y\}$ and

$$\varphi_0(z) = \frac{1}{(\pi z_0^2)^{1/4}} \exp\left[-\frac{z^2}{2z_0^2}\right]. \tag{2.2}$$

is the ground-state harmonic oscillator wavefunction of the motion in the z direction, with $z_0 = (\hbar/m\omega_0)^{1/2}$ being the confinement length.

The grand-canonical Hamiltonian of the system reads:

$$\hat{\mathcal{H}} = \hat{H}_0 + \hat{H}_{\mathrm{int}}, \tag{2.3}$$

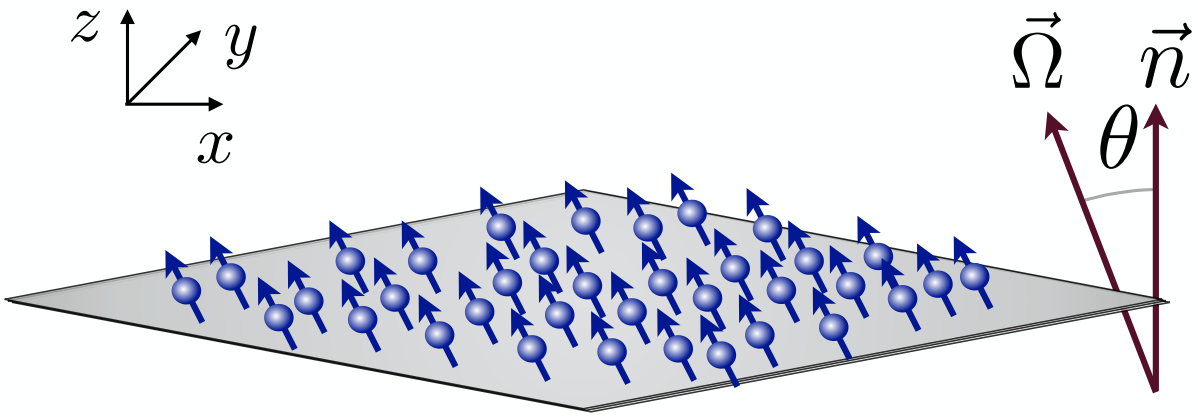

Figure 2.2: BEC gas of dipoles tilted in the x, z plane. The tilting angle θ is controllable by an external (electric or magnetic) field $\vec{\Omega}$.

where

$$\hat{H}_0 = \int d\vec{\mathrm{r}}\, \hat{\Psi}^+(\vec{\mathrm{r}}) \left[-\frac{\hbar^2}{2m}\nabla^2_{\vec{\mathrm{r}}} + \frac{m\omega_0^2 z^2}{2} - \mu_{3D} \right] \hat{\Psi}(\vec{\mathrm{r}}), \tag{2.4}$$

and the binary interaction between particles is described by

$$\hat{H}_{\mathrm{int}} = \frac{1}{2}\int d\vec{\mathrm{r}}\, d\vec{\mathrm{r}}\,' \hat{\Psi}^+(\vec{\mathrm{r}})\hat{\Psi}^+(\vec{\mathrm{r}}')' U(\vec{\mathrm{r}} - \vec{\mathrm{r}}')\hat{\Psi}(\vec{\mathrm{r}}')\hat{\Psi}(\vec{\mathrm{r}}). \tag{2.5}$$

Here $\nabla^2_{\vec{\mathrm{r}}}$ is the 3D Laplacian, μ_{3D} is the chemical potential of the 3D system, and $U(\vec{\mathrm{r}}-\vec{\mathrm{r}}')$ is the potential of interaction between particles.

The potential $U(\vec{\mathrm{r}}-\vec{\mathrm{r}}')$ includes the short-range part $U_s(\vec{\mathrm{r}}-\vec{\mathrm{r}}')$ and the dipole-dipole interaction. For dipoles tilted in the x, z plane the latter is given by

$$V_{dd}(\vec{\mathrm{r}}, \theta) = \frac{d^2}{r^5}\left[\mathrm{r}^2 - 3(x\sin\theta + z\cos\theta)^2\right], \tag{2.6}$$

where d is the dipole moment. In three dimensions in all diagrams the integral

$$\int d\vec{\mathrm{r}}\, d\vec{\mathrm{r}}\,' \hat{\Psi}^+(\vec{\mathrm{r}})\hat{\Psi}^+(\vec{\mathrm{r}}')U_s(\vec{\mathrm{r}} - \vec{\mathrm{r}}')\hat{\Psi}(\vec{\mathrm{r}}')\hat{\Psi}(\vec{\mathrm{r}}) \tag{2.7}$$

is reduced to the short-range coupling constant $g_{3D} = 4\pi\hbar^2 a_{3D}/m$, with a_{3D} being the 3D scattering length. This is equivalent to writing

$$U_s(\vec{\mathrm{r}} - \vec{\mathrm{r}}') = g_{3D}\delta(\vec{\mathrm{r}} - \vec{\mathrm{r}}'). \tag{2.8}$$

For our system we will do the same, assuming that the confinement length z_0 still greatly exceeds the characteristic radius of interaction between particles and omitting the issue of confinement-induced resonances [198]. Thus, we may write

$$U(\vec{\mathrm{r}} - \vec{\mathrm{r}}', \theta) = V_{dd}(\vec{\mathrm{r}} - \vec{\mathrm{r}}', \theta) + g_{3D}\delta(\vec{\mathrm{r}} - \vec{\mathrm{r}}'). \tag{2.9}$$

Strictly speaking, we now have to solve the full scattering problem because there can be a contribution of short interparticle distances to the dipole-dipole scattering caused by the term $V_{dd}(\vec{\mathrm{r}}-\vec{\mathrm{r}}', \theta)$. We, however, omit the related shape resonances [11] and treat the dipole-dipole interaction in the Born approximation [194].

Then, substituting the field operator in the form (2.1) into the Hamiltonian $\hat{\mathcal{H}}$ (2.3) and using relations (2.3)–(2.9), we integrate over z and get an effective 2D grand-canonical Hamiltonian:

$$\begin{aligned}\hat{\mathcal{H}}_{\text{eff}} = &\int d\vec{\rho}\,\hat{\psi}^{+}(\vec{\rho})\left[-\frac{\hbar^2}{2m}\nabla^2_{\vec{\rho}} - \mu\right]\hat{\psi}(\vec{\rho}) \\ &+ \int d\vec{\rho}\,d\vec{\rho}'\hat{\psi}^{+}(\vec{\rho})\,\hat{\psi}^{+}(\vec{\rho}')\,U_{\text{eff}}(\vec{\rho}-\vec{\rho}',\theta)\,\hat{\psi}(\vec{\rho}')\,\hat{\psi}(\vec{\rho}),\end{aligned} \tag{2.10}$$

where $\nabla^2_{\vec{\rho}}$ is the 2D Laplacian, $\mu = \mu_{3D} - \hbar\omega_0/2$ is the chemical potential, and the effective interaction potential has the following form:

$$U_{\text{eff}}(\vec{\rho}-\vec{\rho}',\theta) = \int dz dz'\, U(\vec{\mathrm{r}}-\vec{\mathrm{r}}',\theta)|\varphi_0(z)\varphi_0(z')|^2. \tag{2.11}$$

Transforming this Hamiltonian to the momentum space, we obtain

$$\hat{\mathcal{H}}_{\text{eff}} = \sum_{\mathbf{p}} E_{\mathbf{p}}\hat{a}^{\dagger}_{\mathbf{p}}\hat{a}_{\mathbf{p}} + \frac{1}{2S}\sum_{\mathbf{p},\mathbf{p}',\mathbf{q}} U_{\text{eff}}(\mathbf{q})\hat{a}^{\dagger}_{\mathbf{p}+\mathbf{q}}\hat{a}^{\dagger}_{\mathbf{p}'-\mathbf{q}}\hat{a}_{\mathbf{p}'}\hat{a}_{\mathbf{p}} - \mu\sum_{\mathbf{p}}\hat{a}^{\dagger}_{\mathbf{p}}\hat{a}_{\mathbf{p}} \tag{2.12}$$

where S is the surface area, $E_p = p^2/2m$, $\hat{a}^{\dagger}_{\mathbf{p}}$ and $\hat{a}_{\mathbf{p}}$ are the creation and annihilation operators of particles, and the Fourier transform of the effective interaction potential of 2D tilted dipoles reads

$$U_{\text{eff}}(\mathbf{p},\theta) = g_s + g_d\left(3\cos^2\theta - 1\right) + U_h(\mathbf{p})\sin^2\theta + U_v(\mathbf{p})\cos^2\theta, \tag{2.13}$$

where

$$\begin{aligned}U_h(\mathbf{p}) &= \frac{2d^2}{\hbar}\int_{-\infty}^{+\infty}\frac{p_x^2 dp_z}{p_x^2+p_y^2+p_z^2}\exp\left[-\frac{p_z^2 z_0^2}{2\hbar^2}\right], \\ U_v(\mathbf{p}) &= -\frac{2d^2}{\hbar}\int_{-\infty}^{+\infty}\frac{(p_x^2+p_y^2)dp_z}{p_x^2+p_y^2+p_z^2}\exp\left[-\frac{p_z^2 z_0^2}{2\hbar^2}\right].\end{aligned} \tag{2.14}$$

The first term in the right-hand side of Eq. (2.13) comes from the short-range interaction and the rest from the dipole-dipole interaction. The related coupling constants are

$$g_s = \frac{2\sqrt{2\pi}\hbar^2 a_s}{m z_0} = \frac{g_{3D}}{\sqrt{2\pi}z_0}, \qquad g_d = \frac{2\sqrt{2\pi}\hbar^2 r_*}{3m z_0} = \frac{2\sqrt{2\pi}d^2}{3z_0}, \tag{2.15}$$

where $r_* = md^2/\hbar^2$ is the characteristic dipole-dipole distance.

We then assume that most of the particles are in the condensate, i.e. in the state with momentum $\mathbf{p}$=0. Treating the condensate as a c-number we may write a_0^2=N_0, where N_0 is the number of condensed particles. To zero order the energy of the system is equal to

$$\mathcal{E}_0 = \frac{U_{\text{eff}}(0)}{2S}N_0^2, \tag{2.16}$$

which gives a relation between the condensate density $n_0 = N_0/S$ and the chemical potential μ:

$$\mu = \frac{\partial\mathcal{E}_0}{\partial N} = n_0 U_{\text{eff}}(0). \tag{2.17}$$

The part of the Hamiltonian, which is linear in $\hat{a}_{\mathbf{p}\neq 0}$, vanishes and the bilinear part is given by

$$\hat{\mathcal{H}} = \sum_{\mathbf{p}\neq 0} E_{\mathbf{p}\neq 0} \hat{a}^\dagger_{\mathbf{p}} \hat{a}_{\mathbf{p}} + \frac{n_0}{2} \sum_{\mathbf{p}\neq 0} U_{\text{eff}}(\mathbf{p}) \left(2\hat{a}^\dagger_{\mathbf{p}} \hat{a}_{\mathbf{p}} + \hat{a}^\dagger_{\mathbf{p}} \hat{a}^\dagger_{-\mathbf{p}} + \hat{a}_{\mathbf{p}} \hat{a}_{-\mathbf{p}} \right). \tag{2.18}$$

It can be reduced to the diagonal form

$$\hat{\mathcal{H}}_{\text{eff}} = \sum_{\mathbf{p}\neq 0} \varepsilon_{\mathbf{p}}(\theta)\, \hat{b}^\dagger_{\mathbf{p}} \hat{b}_{\mathbf{p}} + \text{const}, \tag{2.19}$$

by using the Bogoliubov transformation

$$\begin{aligned} \hat{a}_{\mathbf{p}} &= u_{\mathbf{p}} \hat{b}_{\mathbf{p}} - v_{\mathbf{p}} \hat{b}^\dagger_{-\mathbf{p}}, \\ \hat{a}^\dagger_{\mathbf{p}} &= u_{\mathbf{p}} \hat{b}^\dagger_{\mathbf{p}} - v_{\mathbf{p}} \hat{b}_{-\mathbf{p}}, \end{aligned} \tag{2.20}$$

where $\hat{b}^\dagger_{\mathbf{p}}$ and $\hat{b}_{\mathbf{p}}$ are the creation and annihilation operators of elementary excitations. The functions $u_{\mathbf{p}}$, $v_{\mathbf{p}}$ follow from the relation

$$u_{\mathbf{p}}, v_{\mathbf{p}} = \frac{1}{2} \left(\sqrt{\varepsilon_{\mathbf{p}}/E_p} \pm \sqrt{E_p/\varepsilon_{\mathbf{p}}} \right) \tag{2.21}$$

and the excitation energies have the form:

$$\varepsilon_{\mathbf{p}}(\theta) = \sqrt{\frac{p^2}{2m} \left[\frac{p^2}{2m} + 2nU_{\text{eff}}(\mathbf{p}, \theta) \right]}, \tag{2.22}$$

where we replaced n_0 with the total density n.

In general, the system has several controllable dimensionless parameters. The first one is the tilting angle θ (see Fig. 2.2), which is controllable by the polarizing (electric or magnetic) field. The second parameter is the ratio of the coupling constants

$$\alpha = g_s/g_d, \tag{2.23}$$

where g_s is tunable by a Feshbach resonance and g_d for polar molecules can be controlled by an external electric field.

The dynamical stability of the system requires real excitation energies, i.e. one should have:

$$\varepsilon_p^2(\theta) \geq 0. \tag{2.24}$$

In the low-momentum limit, one can use the following expression for the effective potential (2.13):

$$U_{\text{eff}}(\mathbf{p}, \theta) = g_\theta \left[1 - C_\theta \left(p \cos^2\theta - \frac{p_x^2}{p} \sin^2\theta \right) \right] \tag{2.25}$$

where

$$C_\theta = 2\pi d^2/\hbar g_\theta \tag{2.26}$$

and

$$g_\theta = g_s + g_d(3\cos^2\theta - 1). \tag{2.27}$$

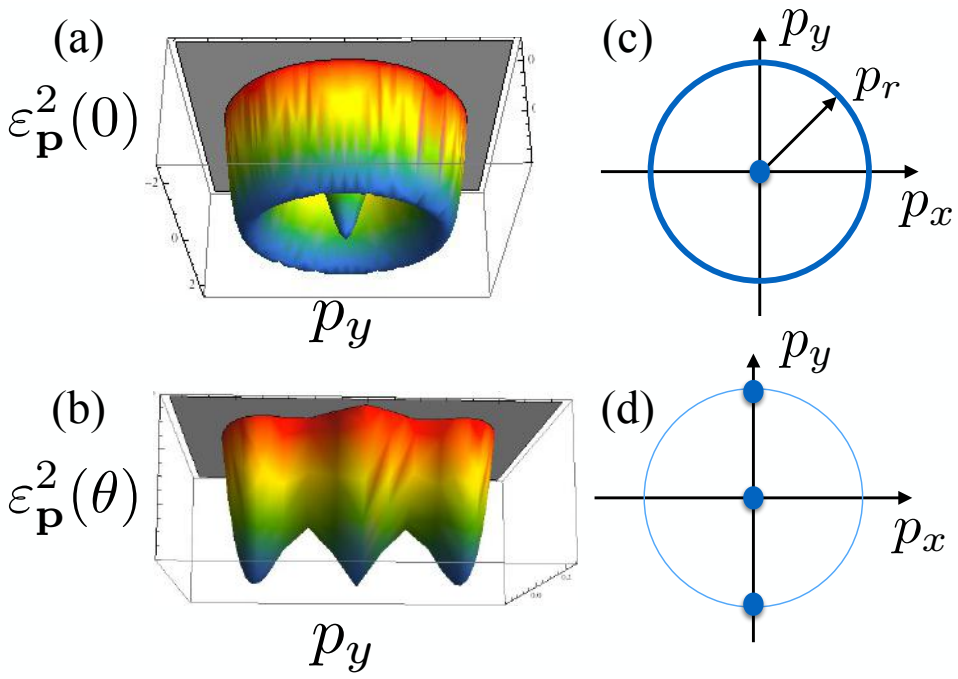

Figure 2.3: The quantity $\varepsilon^2_{\mathbf{p}}(\theta)$ [see Eq. (2.22)] as a function of the 2D momentum $\mathbf{p} = \{p_x, p_y\}$ at the threshold of the instability: In (a) 3D plot at $\theta = 0$ and in (b) 3D plot at a fixed $\theta \neq 0$. It is illustrated in (c) that for at $\theta = 0$ $\varepsilon^2_{\mathbf{p}}$ touches zero at the circumference $|\mathbf{p}| = p_{\rm r}$, whereas if $\theta \neq 0$, $\varepsilon^2_{\mathbf{p}}$ reaches zero in two points $\{0, \pm p_{\rm r}\}$, arising at $x = 0$ as shown in (d).

For $p \to 0$ we have a linear (phonon) dispersion relation

$$\varepsilon_p = \sqrt{\frac{nU_{\rm eff}(0,\theta)}{m}}p, \quad U_{\rm eff}(0,\theta) \equiv g_\theta, \tag{2.28}$$

and using Eq. (2.24) the stability criterion is $U_{\rm eff}(0,\theta) \geq 0$. It can be expressed as

$$\alpha > 1 - 3\cos^2\theta. \tag{2.29}$$

If this condition is not satisfied, then one has a long-wavelength (phonon) instability and related collapse at any density. This type of collapse has been observed in experiments with chromium atoms (the atom spin $S = 3$) [207, 208].

The structure of the spectrum can be characterized in terms of the following dimensionless parameter:

$$\beta(\theta) = \frac{4\pi^2\hbar^2 r_*^2 n_0 \cos^4\theta}{m g_\theta}. \tag{2.30}$$

The excitation energy shows a roton-maxon structure (local maximum and minimum at finite k) for β in the interval $8/9 < \beta < 1$, and for $\beta = 1$ the roton minimum touches zero. An important feature of tilted dipolar gases is that the obtained roton-maxon excitation spectrum is anisotropic (see Fig. 2.2). One can easily put $\theta = 0$ in Eq. (2.30) and reduce this expression to known results for perpendicular dipoles [97, 105]. It is also seen that at $\theta = \pi/2$ the parameter $\beta = 0$, i.e. there are no rotonization and roton instability for in-plane dipoles.

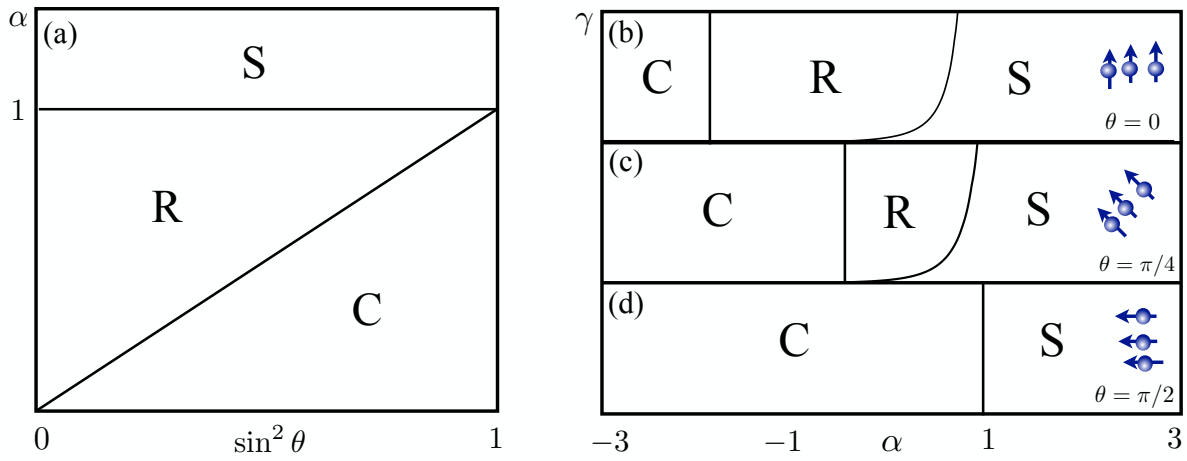

Figure 2.4: The stability diagrams in terms of the ratio of the coupling constants α, tilting angle θ, and dimensionless density γ ($\gamma = 6\sqrt{2\pi} z_0 a_d n_0$). In (a) we present the projection of the diagram in terms of the parameters α and θ. The region S corresponds to the stable homogeneous phase at any γ, the region C stands for the long-wavelength collapse at any γ, and the region R denotes the phase with rotonization at $8/9 < \beta < 1$, and the roton instability at $\beta = 1$. In (b)–(d) we present the stability diagrams in terms of parameters α and β for $\theta = 0$, $\theta = \pi/4$, and $\theta = \pi/2$. The boundaries between different phases are obtained by numerical solution of Eq. (2.36).

Taking into account the anisotropy of the Bogoliubov spectrum (2.24) [see Fig. 2.2(d)], close to the threshold of the instability we obtain

$$\begin{aligned}\varepsilon_{\mathbf{p}}^2(\theta)\big|_{\mathbf{p}\approx\pm\mathbf{p}_\mathrm{r}} &\approx \frac{1}{2}\frac{\partial^2\varepsilon_{\mathbf{p}}^2(\theta)}{\partial p_x^2}p_x^2 + \frac{1}{2}\frac{\partial^2\varepsilon_{\mathbf{p}}^2(\theta)}{\partial p_y^2}(p_y \mp p_\mathrm{r})^2 + \varepsilon_{\mathbf{p}}^2(\theta)\big|_{\mathbf{p}=\pm\mathbf{p}_\mathrm{r}} \\ &= \mathcal{A}(\theta)p_x^2 + \mathcal{B}(\theta)(p_y \mp p_\mathrm{r})^2 + \Delta_r^2(\theta),\end{aligned} \tag{2.31}$$

where Δ_r is the roton gap, and

$$\begin{aligned}\mathcal{A}(\theta) &\equiv \frac{1}{2}\frac{\partial^2\varepsilon_{\mathbf{p}}^2(\theta)}{\partial p_x^2} = \frac{p^2}{2m^2} + \frac{n_0 p^2}{2m}\frac{\partial^2 U_{\mathrm{eff}}(\mathbf{p},\theta)}{\partial p_x^2}, \\ \mathcal{B}(\theta) &\equiv \frac{1}{2}\frac{\partial^2\varepsilon_{\mathbf{p}}^2(\theta)}{\partial p_y^2} = \frac{p^2}{2m^2} + \frac{n_0 p^2}{2m}\frac{\partial^2 U_{\mathrm{eff}}(\mathbf{p},\theta)}{\partial p_y^2}, \quad \frac{\partial^2\varepsilon_{\mathbf{p}}^2(\theta)}{\partial p_x \partial p_y} = 0.\end{aligned} \tag{2.32}$$

Using the low-momentum expression for the interaction potential given by Eq. (2.25), one can obtain the following expression for the roton gap:

$$\Delta_r(\theta) = 2ng_\theta C_\theta \sqrt{\frac{1}{\xi_\theta^2} - \frac{C_\theta^2}{\xi_\theta^4}}, \tag{2.33}$$

where

$$\xi_\theta = \hbar/\sqrt{mng_\theta} \tag{2.34}$$

is the healing length, and the roton is located at the momentum:

$$p_r = 2\hbar\frac{C_\theta}{\xi_\theta^2}. \tag{2.35}$$

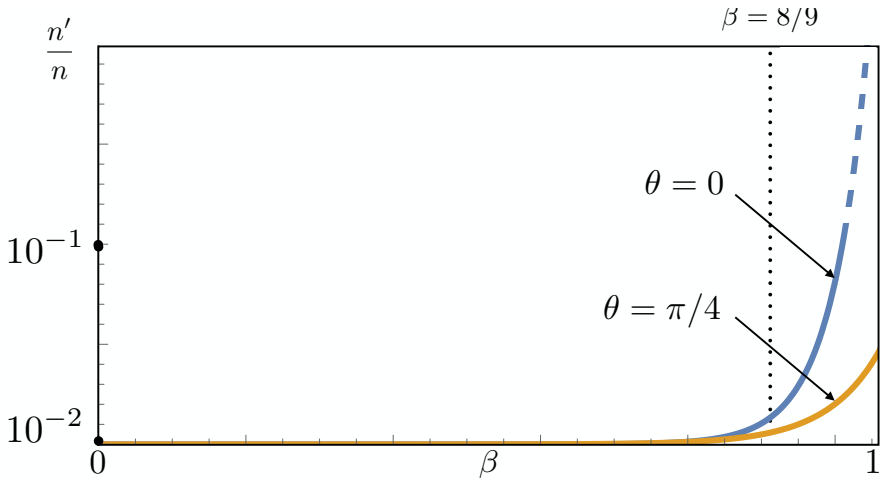

Figure 2.5: The non-condensed fraction (2.39) as a function of the parameter β at $mg_\theta/2\pi\hbar^2 \simeq 10^{-2}$. The non-condensed fraction diverges logarithmically for perpendicular dipoles on approach to the roton instability and, in contrast, it is always small for the selected tilting angle θ. The vertical dotted line corresponds to $\beta = 8/9$ (appearance of the roton).

We find the exact boundaries for the roton instability from the numerical solution of the following equation:

$$\varepsilon^2_{\mathbf{p}}(\theta)\big|_{\mathbf{p}=\pm\mathbf{p}_r} = \frac{d\varepsilon^2_{\mathbf{p}}(\theta)}{dp}\bigg|_{\mathbf{p}=\pm\mathbf{p}_r} = 0. \tag{2.36}$$

The full stability diagram of the system is presented in Fig. 2.4.

2.3 Condensate depletion

Generally, the conditions of the weakly interacting regime [199] for a gas with the dipole-dipole and short-range interactions read:

$$\frac{mg_\theta}{2\pi\hbar^2} \ll 1, \qquad nr_*^2 \ll 1. \tag{2.37}$$

However, these conditions are not sufficient when the roton minimum is close to zero.

Here we consider the growth of the non-condensed fraction of particles when the roton minimum is approaching zero. The non-condensed fraction is given by:

$$\frac{n'}{n} = \frac{1}{n}\int \frac{d\mathbf{p}}{(2\pi\hbar)^2}\left|\langle \hat{a}^\dagger_{\mathbf{p}}\hat{a}_{\mathbf{p}}\rangle\right|^2 = \frac{1}{n}\int \frac{d\mathbf{p}}{(2\pi\hbar)^2}|v_{\mathbf{p}}|^2 = \frac{1}{4n}\int \frac{d\mathbf{p}}{(2\pi\hbar)^2}\left(\sqrt{\frac{\varepsilon_{\mathbf{p}}}{E_p}} - \frac{E_p}{\varepsilon_{\mathbf{p}}}\right)^2. \tag{2.38}$$

where we used Eq (2.21).

Eq. (2.38) is reduced to the following expression:

$$\frac{n'}{n} = \frac{1}{2n}\int \frac{d\mathbf{p}}{(2\pi\hbar)^2}\frac{\left(\varepsilon_{\mathbf{p}} - p^2/2m\right)^2}{\varepsilon_{\mathbf{p}}\, p^2/m} = \frac{1}{2n}\int \frac{d\mathbf{p}}{(2\pi\hbar)^2}\frac{p^2/2m + U_{\text{eff}}(\mathbf{p},\theta)n - \varepsilon_{\mathbf{p}}}{\varepsilon_{\mathbf{p}}}. \tag{2.39}$$

In fact, the non-condensed fraction given by Eq. (2.39), can be presented in the form:

$$\frac{n'}{n} = \frac{mg_\theta}{2\pi\hbar^2} f(\beta, \theta, r_*/z_0). \tag{2.40}$$

In other words, the non-condensed fraction n'/n is proportional to the small parameter $mg_\theta/2\pi\hbar^2$ multiplied by a universal function $f(\beta, \theta, r_*/z_0)$.

The results of numerical solution of Eq. (2.39) are displayed in Fig. 2.5. One sees that for tilted dipoles ($\theta = \pi/4$) the non-condensed fraction remains small even up to the point of the roton instability.

For perpendicular dipoles the excitation energy is an isotropic function of momentum and close to the threshold of the roton instability it can be written as

$$\varepsilon_p^2\big|_{p\approx\pm p_\mathrm{r}} \approx \frac{1}{2}\frac{d\varepsilon_p^2}{dp^2}(p^2 - p_\mathrm{r}^2)^2 + \Delta_r^2. \tag{2.41}$$

Substituting this relation into Eq. (2.39) we find that the integral for the non-condensed fraction diverges logarithmically on the approach to the roton instability. This result has been established in Refs. [96, 104, 105] and it also follows from our numerics.

For tilted dipoles the excitation energy is an anisotropic function of momentum. The roton instability is achieved when ε_p touches zero only at two points $p_x = 0$, $p_y = p_r$ and $p_x = 0$, $p_y = -p_r$. This is the origin of the fact that the integral for n'/n is convergent at the threshold of the roton instability. Moreover, for sufficiently small $mg_\theta/2\pi\hbar^2$ and sufficiently large θ the quantity of n'/n remains small up to the roton instability threshold. This means that, in contrast to the case of perpendicular dipoles, for tilted dipoles the Bogoliubov approach is applicable up to the roton instability.

2.4 Concluding remarks

In conclusion, we have found the effect of rotonization for a 2D uniform weakly interacting gas of tilted dipolar bosons. We have obtained the zero-temperature stability diagram with respect to controllable parameters of the system, in which we find a uniform BEC (with and without the rotonized spectrum), phonon-collapsed regime, and the regime of the roton instability. In contrast to dipoles perpendicular to the plane of their transversal motion, for tilted dipoles the Bogoliubov approach is applicable up to the threshold of the roton instability.

Promising candidates for creating systems with rotonized spectra and roton instabilities are magnetic atoms and polar molecules. For example, ^{164}Dy atoms [38] have magnetic moment $10\mu_B$, which corresponds to the dipole moment $d \simeq 0.1$ D. At the 2D density $n \sim 10^9$ cm^{-2} and confinement frequencies $\omega_0/2\pi$ from 2 kHz up to 5 kHz the rotonization and roton instability are possible in a wide range of tilting angles ($\pi/6 < \theta < 2\pi/3$) with a sufficiently small non-condensed fraction $n'/n \lesssim 0.1$.

For polar molecules it is necessary to select non-reactive ones, i.e. the molecules that do not undergo ultracold chemical reactions. These reactions have been first observed at JILA with KRb molecules [25] (for details, see also Refs. [216–218]):

$$\mathrm{KRb + KRb = K_2 + Rb_2}, \tag{2.42}$$

and they lead to a rapid decay of the gas. In would be interesting to consider non-reactive RbOH molecules, which in the electric field of a few kilovolts per centimeter have dipole moment 0.2D. Then, at the 2D density $n \sim 10^9$ and confinement frequencies $\omega_0/2\pi$ from 2 kHz up to 5 kHz, the rotonization and roton instabilities can be observed in a wide range of angles ($\pi/6 < \theta < 2\pi/3$), and the non-condensed fraction remains small: $n'/n \lesssim 0.05$. We thus see that the observation of rotonization and roton instabilities is feasible.

We have demonstrated the smallness of the non-condensed fraction close the threshold of the roton instability. This makes the system interesting for achieving local density waves with controlled short-range order and supersolidity.

Chapter 3

Roton-maxon spectrum and instability for weakly interacting dipolar excitons

In this chapter we discuss the effect of rotonization for a weakly interacting Bose gas of dipolar excitons in a semiconductor layer at zero temperature. This system is an interesting platform for investigating supersolidity. We calculate the stability diagram. According to our estimates, the threshold of the roton instability for a bose-condensed exciton gas with roton-maxon spectrum is achievable experimentally, e.g. in semiconductor layers of GaAs heterostructures. The results are published in Ref. [176].

3.1 Background

It is known that the BEC critical temperature is inversely proportional to the effective particle mass. For sufficiently light particles the critical temperature can be rather high, which is important for understanding underlying mechanisms of intriguing condensed matter phenomena, such as high-temperature superconductivity [219]. In this context, investigations of collective properties and BEC of excitons, where the effective mass is much smaller than even the electron mass, are highly promising [43, 44, 219–221].

In general, the lifetime of excitons is not long enough to achieve the thermodynamic equilibrium. In order to overcome this difficulty, excitons with spatially separated electrons and holes can be used [222–226]. The electron-hole separation suppresses the recombination processes and the lifetime of excitons significantly increases.

Remarkable progress in creating high-quality 2D semiconductor heterostructures strongly stimulated the work on excitons. Several experimental platforms, including coupled quantum wells (separated by a barrier, see Refs. [42–44]) and single quantum wells in electric fields [227, 228] with long-lived 2D excitons have been realized. Recently, significant attention has been paid to "artificial materials", such as graphene monolayers separated by an insulating barrier [229–232], thin films of topological insulators [233–238], and Van der Waals heterostructures [46–48]. The lifetime of excitons in such systems is of the order of microseconds and there are prospects to increase it by several orders of magnitude.

It is important that the electron-hole separation results in the appearance of the exciton dipole moment. The early theoretical predictions on excitons are related to the Bardeen-Cooper-Schrieffer-type (BCS-type) regime [201, 239], BEC [201], and the BCS-BEC crossover. Presently, there is a growing number of proposals for studying many-body phenomena with excitons (e.g. superfluidity [243–252], Josephson effect [253], and many

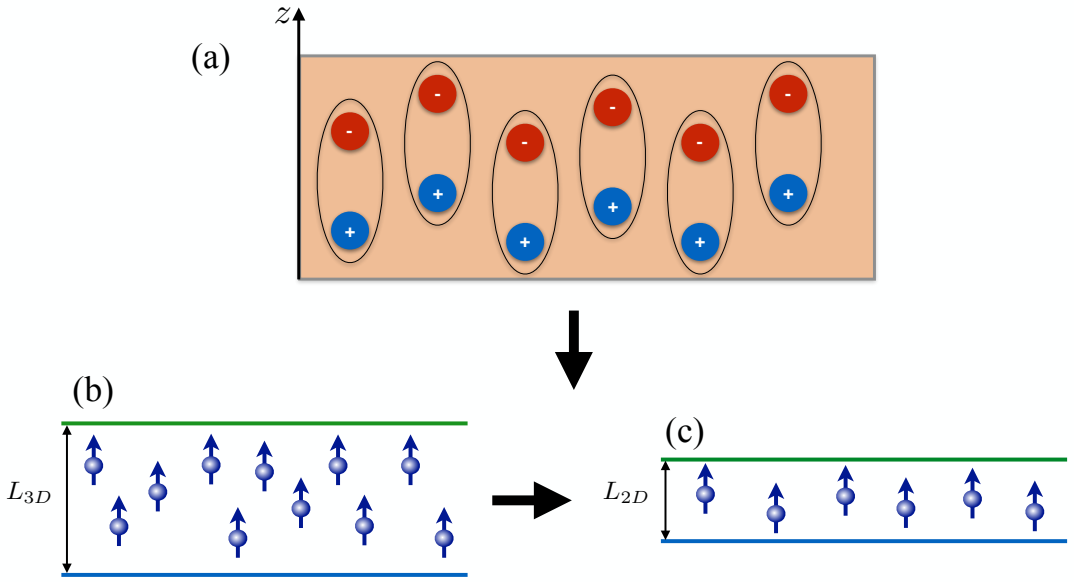

Figure 3.1: Excitons in a semiconductor layer. In (a) direct excitons and their correlated motion in the z direction. This picture is equivalent to a dipolar exciton gas in a layer: in (b) the system where the width of the layer is greater than several interexcitons distances, and in (c) the width of the layer is smaller than the interexciton distance.

others [254–265]). These activities have been accompanied by the intensive work on the observation of collective states of 2D dipolar excitons [41–44, 271–276]

Recently, Monte-Carlo calculations demonstrated that in the strongly interacting regime 2D dipolar excitons can undergo the gas-solid phase transition [54,57,100,277,278]. However, such phases of dipolar excitons require a dense regime with at least several particles within the interaction range, which can be difficult to achieve.

Here we focus on the *weakly* interacting gas of excitons. First of all, such a system allows one to have a transparent physical picture in the framework of the Bogoliubov theory. Furthermore, interesting many-body states in this case can occur due to the anisotropy of the dipole-dipole interaction. In contrast to strongly correlated exciton systems, weakly interacting gases of dipolar excitons are interesting for the consideration in semiconductor layers of heterostructures. Such systems allow one to study excitons in intermediate regimes between 3D and 2D. In particular, if the width of the semiconductor layer is greater than several interexciton distances, excitons with dipole moment aligned "head-to-tail" along the normal direction to the plane of the transversal motion start to attract each other. This can be a reason for a variety of interesting quantum many-body effects, such as rotonization of the excitation spectrum and the roton instability.

The chapter is organized as follows. In Section 3.2 we explain qualitatively the nature of the roton instability for dipolar excitons in a semiconductor layer. In Section 3.3 we calculate the excitation spectrum and zero-temperature stability diagram. In Section 3.4 we present parameters of the system for the observation of the rotonization phenomena in GaAs semiconductor layers, and we give our conclusions.

3.2 Excitons in a layer: 2D *vs.* 3D

We study a weakly interacting exciton gas in an infinite homogeneous semiconductor layer at zero temperature ($T = 0$), and consider the behavior of the system at a crossover between 3D and 2D regimes. This crossover corresponds to the change of the width of the semiconductor layer (see Fig. 3.1).

The dynamical stability criterion requires real excitation energies. For the 3D system with the Bogoliubov spectrum $\varepsilon_{\vec{\mathrm{q}}}$, we have

$$\varepsilon_{\vec{\mathrm{q}}}^2 = \frac{q^4}{4m^2} + V(\vec{\mathrm{q}})\frac{n_0}{m}q^2 \geq 0, \tag{3.1}$$

where $\vec{\mathrm{q}}$ is the momentum, m is the excitons mass, n is the density, and $V(\vec{\mathrm{q}})$ is the Fourier transform of the interaction potential $V(\vec{\mathrm{r}})$. Here $\vec{\mathrm{q}} = \{\mathbf{p}, p_z\}$ and $\vec{\mathrm{r}} = \{\vec{\rho}, z\}$ are 3D vectors, $\mathbf{p}$ and $\vec{\rho} = \{x, y\}$ are 2D vectors (in the semiconductor layer plane).

The dipole-dipole interaction potential of excitons reads:

$$V_d(\vec{\mathrm{r}}) = \frac{d^2}{\epsilon}\frac{\rho^2 - 2z^2}{\mathrm{r}^5}, \tag{3.2}$$

where $d = eD$ is the dipole moment of an exciton, $e > 0$ is the hole charge, D is the effective electron-hole separation, and ϵ is the dielectric constant. The Fourier transform of $V_d(\vec{\mathrm{r}})$ is given by

$$V_d(\vec{\mathrm{q}}) = \frac{4\pi}{3}\frac{d^2}{\epsilon}\frac{2p_z^2 - p^2}{q^2}. \tag{3.3}$$

The key point is the negative sign of the dipole-dipole potential $V_d(\vec{\mathrm{q}})$ for momenta $|p_z| \ll |\mathbf{p}|$ (i.e. at $|z| \gg |\rho|$), which is the result of the dipole-dipole "head-to-tail" attraction. Thus, for the 3D homogeneous system at $|p_z| \ll p$ the square of the spectrum (3.1) is

$$\varepsilon_p^2 = \frac{p^4}{4m^2} - \frac{4\pi}{3}\frac{d^2}{\epsilon}\frac{n}{m}p^2 \tag{3.4}$$

and it is negative for low momenta (see Fig. 3.2). In the "phonon branch", the spectrum possesses a region of imaginary energies, i.e. in 3D the phonon modes are unstable. This regime is known as the instability with respect to the long-wavelength collapse [12, 208].

Let us now consider the system of dipolar excitons confined in the z direction:

$$0 \leq |x|,|y| < \infty, \qquad 0 < z < L, \tag{3.5}$$

where L is the width of the semiconductor layer. For momenta $|p_z| \gg \hbar/L$, the motion of excitons corresponds to the 3D regime. However, for $|p_z| \lesssim \hbar/L$, for example when the semiconductor layer is thin, the motion exhibits the 2D behavior.

It is clear that the 2D regime can be realized for any value of L. However, for the 3D regime the momentum region $|p_z| \gg \hbar/L$ is possible only in fairly wide semiconductor layers, i.e. when the following condition holds for the layer width:

$$L \gg \xi, \qquad \xi = \hbar/\sqrt{2m\mu}. \tag{3.6}$$

Here μ is the chemical potential of dipolar excitons and ξ is the healing length. This is the case of sufficiently wide semiconductor layer (with both 2D and 3D regimes), which corresponds to the layer system with sufficiently large number $\mathcal{N} \sim L^2/\xi^2$ of the occupied energy levels.

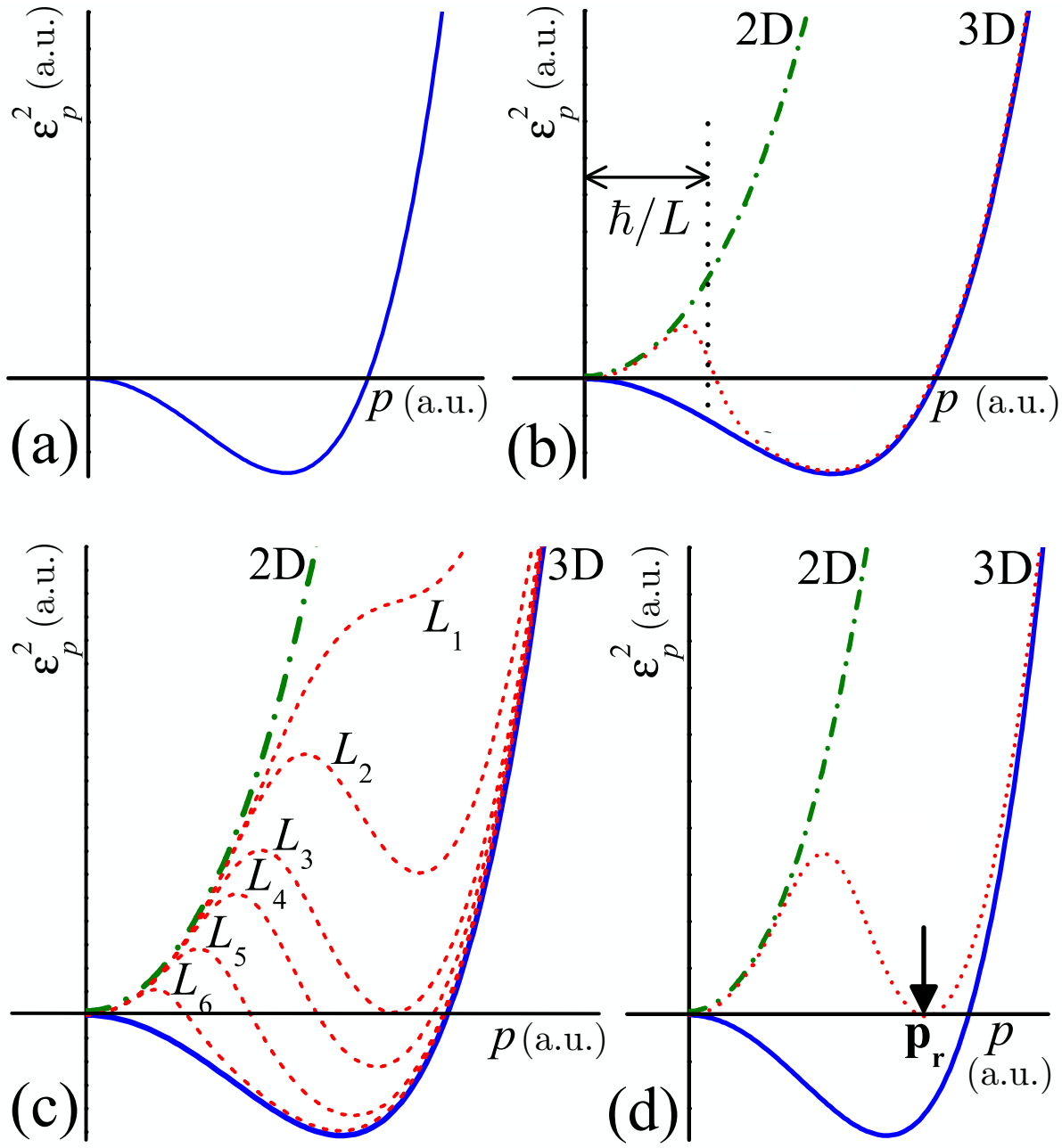

Figure 3.2: Qualitative illustration of the appearance of the roton instability for dipolar system in the layers. The smooth crossover from the 3D (unstable) regime to 2D (stable) one [quantitative examples are presented in Fig. 3.3a]. In (a) and (b) the square of the Bogoliubov spectrum (3.1) of dipolar excitons in 3D (solid), 2D (dot-dashed), and the layer geometry (dashed). In (c) ε_p^2 versus p for various layer widths $L_1 < L_2 < \cdots < L_6$. In (d) the momentum $|\mathbf{p}_r|$ of the unstable mode is indicated.

How does this impact the stability of the system? If the momenta are sufficiently large, $|p_z| \gg \hbar/L$, i.e. when the 3D regime is realized, the excitation spectrum (3.1) is close to the 3D one. This regime is unstable for $|p_z| \ll p$ [see Fig. 3.2a]. *Vice versa*, if the momenta are low, i.e., when the 2D regime is realized, the spectrum is close to that in 2D. The 2D spectrum is stable, because the dipoles repel each other at sufficiently large distances. Therefore, in the momentum interval $|p_z| \sim \hbar/L$, there is a smooth crossover from the 3D (unstable) to the 2D (stable) regime [see Fig. 3.2(b)].

The width of the instability region is determined by the length L. Therefore, for a critical width $L = L_3$ [see Fig. 3.2(c)] the instability region shrinks to the point. If the width L of the semiconductor layer is smaller than the critical one, then the spectrum can have the roton minimum. The critical value of L, at which the roton minimum touches zero, corresponds to the threshold of the roton instability. Immediately after the threshold one gets imaginary energies and dynamical instability.

In summary, the formation of the roton minimum and the roton instability is the result of anisotropy of the dipole-dipole interaction and the layer geometry, which passes through the unstable 3D to stable 2D regime.

3.3 Rotonization and stability diagram

We now consider the stability problem for the exciton gas in an infinite homogeneous semiconductor layer using the following assumptions.

First, the distance at which two excitons can approach each other (of the order of the total scattering length of the excitons) is much larger that their Bohr radius a^*. In this case the overlap of the wavefunctions of electrons and holes belonging to different excitons is exponentially suppressed. The fermionic exchange effects [279] and the composite structure of excitons [280] are then negligible. Thus, we may consider excitons as bosons. One should note that the Zeeman splitting for excitons in magnetic fields [257, 265] is sufficiently larger that other energy scales in many-body exciton systems. Then the system occupies only the lowest spin branch. Thus, excitons have only one spin degree.

Taking into account these assumptions, we obtain the grand-canonical Hamiltonian of the dipolar exciton gas in the following form:

$$\begin{aligned}\hat{\mathcal{H}} = &\int \hat{\Psi}^+(\vec{\mathrm{r}}) \left(-\frac{\hbar^2}{2m}\nabla^2_{\vec{\mathrm{r}}} + V(z) - \mu \right) \hat{\Psi}(\vec{\mathrm{r}}) d\vec{\mathrm{r}} \\ &+ \frac{1}{2}\int \hat{\Psi}^+(\vec{\mathrm{r}})\hat{\Psi}^+(\vec{\mathrm{r}}')U(\vec{\mathrm{r}}-\vec{\mathrm{r}}')\hat{\Psi}(\vec{\mathrm{r}}')\hat{\Psi}(\vec{\mathrm{r}}) d\vec{\mathrm{r}}' d\vec{\mathrm{r}},\end{aligned} \tag{3.7}$$

where $\nabla^2_{\vec{\mathrm{r}}}$ is the 3D Laplace operator, $\hat{\Psi}(\vec{\mathrm{r}})$ is the exciton field operator satisfying standard Bose commutation relations, and

$$U(\vec{\mathrm{r}}-\vec{\mathrm{r}}') = V_d(\vec{\mathrm{r}}-\vec{\mathrm{r}}') + U_s(\vec{\mathrm{r}}-\vec{\mathrm{r}}') \tag{3.8}$$

is the potential of interaction between excitons. In all diagrams the contribution of the short-range potential U_s reduces to the coupling constant g_s ($g_s > 0$ if there are no Feshbach resonances). The confining "box" potential we take in the form:

$$V(z) = \begin{cases} 0, & 0 < z < L, \\ \infty, & z < 0 \text{ or } z > L \end{cases} \tag{3.9}$$

3.3.1 Order parameter in the TF approximation

We consider the Heisenberg equation of motion for the exciton field operator, following form the Hamiltonian (3.7) at $0 < z < L$:

$$i\hbar\frac{\partial\hat{\Psi}(\vec{\mathrm{r}},t)}{\partial t} = \left(-\frac{\hbar^2}{2m}\Delta - \mu\right)\hat{\Psi}(\vec{\mathrm{r}},t), + \int U(\vec{\mathrm{r}}-\vec{\mathrm{r}}')\hat{\Psi}^{+}(\vec{\mathrm{r}}',t)\hat{\Psi}(\vec{\mathrm{r}}',t)d\vec{\mathrm{r}}'\hat{\Psi}(\vec{\mathrm{r}},t). \tag{3.10}$$

where we will consider the exciton condensate as the c-number $\psi(z) \equiv \langle\hat{\Psi}(\vec{\mathrm{r}},t)\rangle$ and it is assumed to be real. In the weakly interacting regime at $T = 0$ the total density of excitons n is close to the condensate density n_0, and the the non-condensed density is small: $n' = (n - n_0) \ll n_0$.

Thus, the product of three fields operators in Eq. (3.10) can be written as:

$$\begin{aligned}&\hat{\Psi}^{+}(\vec{\mathrm{r}}',t)\hat{\Psi}(\vec{\mathrm{r}}',t)\hat{\Psi}(\vec{\mathrm{r}},t) = \psi(z)\psi^2(z')+\\ &\psi^2(z')\hat{\Psi}'(\vec{\mathrm{r}},t) + \psi(z)\psi(z')\{\hat{\Psi}'(\vec{\mathrm{r}}',t) + \hat{\Psi}'^{+}(\vec{\mathrm{r}}',t)\}.\end{aligned} \tag{3.11}$$

Substituting $\psi(z)$ (3.27) into Eq. (3.11) and then the resulting relation into Eq. (3.10), after averaging over the ground state we have:

$$\psi^3\int d\vec{\rho}'\int_0^L dz' U(\vec{\mathrm{r}}-\vec{\mathrm{r}}') = g\psi^3 = \mu\psi, \tag{3.12}$$

where $g = g_s + 2g_d$, with $g_d = (4\pi/3)d^2/\epsilon$. It should be noted that g has a sense of the coupling constant for excitons in the case of both dipole-dipole and van der Waals interactions.

From Eq. (3.12) we can find the chemical potential of excitons in the following form:

$$\mu = gn_0 + \mathcal{O}\left(\mathcal{E}_0\right). \tag{3.13}$$

One can see, that the TF approximation is accurate within a factor of $\mathcal{O}\left(\mathcal{E}_0\right)$. This is in agreement with relation (3.26). This inaccuracy appears as a result of the bending of the order parameter $\psi(z)$ to zero near the boundary of the semiconductor layer $\{z = 0, L\}$, which is ignored in the TF approximation [281].

3.3.2 Bogoliubov–de Gennes equations

By substituting Eq. (3.27) into Eq. (3.11), and then the resulting equation into Eq. (3.10), with the help of Eq. (3.12) we get the following equation for the noncondensed field operator ($0 < z < L$):

$$\begin{aligned}i\hbar\frac{\partial\hat{\Psi}'(\vec{\mathrm{r}},t)}{\partial t} &= \left(-\frac{\hbar^2}{2m}\Delta + gn_0 - \mu\right)\hat{\Psi}'(\vec{\mathrm{r}},t)\\ +n_0\int d\vec{\rho}'\int_0^L dz' U(\vec{\mathrm{r}}-\vec{\mathrm{r}}')&\left(\hat{\Psi}'(\vec{\mathrm{r}}',t)+\hat{\Psi}'^{+}(\vec{\mathrm{r}}',t)\right).\end{aligned} \tag{3.14}$$

To solve Eq. (3.14), we use the Bogoliubov transformation:

$$\hat{\Psi}'(\vec{\mathrm{r}}t) = \frac{1}{\sqrt{S}}\sum\nolimits_{\vec{\mathrm{p}}} e^{\frac{i}{\hbar}\mathbf{pr}}\left(u_{\vec{\mathrm{p}}}(z)\hat{a}_{\vec{\mathrm{p}}}e^{-i\varepsilon_{\vec{\mathrm{p}}}t/\hbar} - v_{\vec{\mathrm{p}}}(z)\hat{a}^{+}_{-\vec{\mathrm{p}}}e^{i\varepsilon_{\vec{\mathrm{p}}}t/\hbar}\right). \tag{3.15}$$

Here, $\hat{a}_{\vec{p}}$ and $\hat{a}^+_{\vec{p}}$ are the operators of Bogoliubov excitations satisfying standard Bose commutation relations,

$$[\hat{a}_{\vec{p}}, \hat{a}_{\vec{p}'}] = 0, \qquad [\hat{a}_{\vec{p}}, \hat{a}^+_{\vec{p}'}] = \delta_{\vec{p}\vec{p}'}, \tag{3.16}$$

$u_{\vec{p}}(z)$ and $v_{\vec{p}}(z)$ are the Bogoliubov uv-functions, which satisfy Eq. (3.19) with the boundary conditions (3.22). The normalization condition and the relation of completeness read:

$$\begin{aligned} \int \frac{d\vec{\rho}}{S} \int_0^L dz e^{-\frac{i}{\hbar}(\mathbf{p}-\mathbf{p}')\mathbf{r}} (u_{\vec{p}}(z) u_{\vec{p}'}(z) - v_{\vec{p}}(z) v_{\vec{p}'}(z)) = \delta_{\vec{p}\vec{p}'}, \\ \int \frac{d\vec{\rho}}{S} \int_0^L dz e^{-\frac{i}{\hbar}(\mathbf{p}-\mathbf{p}')\mathbf{r}} (u_{\vec{p}}(z) v_{\vec{p}'}(z) - v_{\vec{p}}(z) u_{\vec{p}'}(z)) = 0, \end{aligned} \tag{3.17}$$

$$\begin{aligned} \frac{1}{S} \sum\nolimits_{\vec{p}} e^{\frac{i}{\hbar}\mathbf{p}(\mathbf{r}-\mathbf{r}')} (u_{\vec{p}}(z) u_{\vec{p}}(z') - v_{\vec{p}}(z) v_{\vec{p}}(z')) = \delta(\vec{r} - \vec{r}'), \\ \frac{1}{S} \sum\nolimits_{\vec{p}} e^{\frac{i}{\hbar}\mathbf{p}(\mathbf{r}-\mathbf{r}')} (u_{\vec{p}}(z) v_{\vec{p}}(z') - v_{\vec{p}}(z) u_{\vec{p}}(z')) = 0. \end{aligned} \tag{3.18}$$

Substituting $\hat{\Psi}'(\vec{r}, t)$ (3.17) into Eq. (3.14) and commuting both sides of the resulting equation first with $\hat{a}_{\vec{p}}$ and then with $\hat{a}^+_{\vec{p}}$, we obtain the system of Bogoliubov-de Gennes equations [283]:

$$\begin{aligned} \hat{T} u_{\vec{q}}(z) + \hat{U} [u_{\vec{q}}(z) - v_{\vec{q}}(z)] = \varepsilon_{\vec{q}} u_{\vec{q}}(z), \\ \hat{T} v_{\vec{q}}(z) + \hat{U} [v_{\vec{q}}(z) - u_{\vec{q}}(z)] = -\varepsilon_{\vec{q}} v_{\vec{q}}(z), \end{aligned} \tag{3.19}$$

where the operators $\hat{T}$ and $\hat{U}$ are

$$\hat{T} = -\frac{\hbar^2}{2m} \frac{d^2}{dz^2} + \frac{p^2}{2m} + g n_0 - \mu, \tag{3.20}$$

$$\hat{U} f(z) = n_0 \int_0^L \left(g\delta(z - z') - \frac{3 g_d p}{2\hbar} e^{-p|z-z'|/\hbar} \right) f(z') dz', \tag{3.21}$$

and the boundary conditions for the u, v functions read

$$u_{\vec{q}}(0) = v_{\vec{q}}(0) = u_{\vec{q}}(L) = v_{\vec{q}}(L) = 0, \quad p_z = (\pi\hbar/L) l. \tag{3.22}$$

3.3.3 Rotonization

In the weak coupling regime at $T = 0$, we can use the Bogoliubov approximation, considering the Bose-Einstein condensate as a c-number $\psi(z)$ and representing the field operator as

$$\hat{\Psi}(\vec{r}, t) = \psi(z) + \hat{\Psi}'(\vec{r}, t); \quad \psi(z) \equiv \langle \hat{\Psi}(\vec{r}, t) \rangle. \tag{3.23}$$

Here $\langle ... \rangle$ denotes averaging over the ground state. The field operator of the non-condensed fraction is sufficiently small. It has the following representation in the basis of eigenfunctions $\{\chi_j(z)\}$ in the confined direction:

$$\hat{\Psi}'(\vec{r}) = \sum_{j=0}^{\infty} \chi_j(z) \hat{\Psi}'_j(\vec{\rho}), \tag{3.24}$$

where $\hat{\Psi}'(\vec{\rho})$ is the corresponding 2D field operator, and the levels with $j > \mathcal{N}$ are approximately unpopulated. The order parameter is

$$\psi(z) = \sqrt{n_0(z)} > 0, \tag{3.25}$$

and $n_0(z)$ does not depend on $\vec{\rho}$ in the stable phase. It is important to note that the Bogoliubov approximation is applicable for systems in the weakly interacting regime in the semiconductor layer, whereas it is not the case for strongly correlated 2D systems [201].

If the condition (3.6) holds, then the chemical potential μ of excitons is significantly greater than the energy $\mathcal{E}_0$ of the lowest level of transversal quantization:

$$\mu \gg \mathcal{E}_0; \qquad \mathcal{E}_0 = \pi^2\hbar^2/(2mL^2). \tag{3.26}$$

Moreover, if the condition (3.26) holds, then the Thomas-Fermi (TF) regime is realized in the system [281]. In the TF regime one can neglect the kinetic energy term in the Gross-Pitaevskii equation. The order parameter has the form:

$$\psi(z) = \sqrt{n_0(z)} = \begin{cases} \psi \equiv \sqrt{n_0}, & 0 < z < L, \\ 0, & \text{otherwise}\ , \end{cases} \tag{3.27}$$

where $n_0 = \psi^2$ is the 3D BEC density of excitons in the semiconductor layer [282]. The chemical potential μ in the TF regime (3.26) is equal to $\mu \approx gn_0$, where $g = g_s + 2g_d$ with the dipole-dipole coupling constant $g_d = (4\pi/3)d^2/\epsilon$.

In terms of g, we can rewrite the condition of the dilute regime as:

$$\beta \equiv \sqrt{n_0 a^3} \ll 1, \quad a = a_s + 2r_*/3; \quad a_s = \frac{g_s m}{4\pi\hbar^2} \sim a^*; \quad r_* = \frac{md^2}{\hbar^2\varepsilon}, \tag{3.28}$$

where a_s is the scattering length, and r_* is the characteristic dipole-dipole distance for excitons.

The stability of the BEC state is determined by fluctuations related to the non-condensed fraction, which originates from the field operator (3.24) (see Ref. [283]). To identify the threshold of the instability we have to find the excitation spectrum from the Bogoliubov-de Gennes equations (3.19).

This is equivalent to the extremum problem for the following functional:

$$I[u_{\vec{q}}, v_{\vec{q}}] = \frac{1}{2}\int_0^L [u_{\vec{q}}\hat{T}u_{\vec{q}} + v_{\vec{q}}\hat{T}v_{\vec{q}} - \varepsilon_{\vec{q}}(u_{\vec{q}}^2 - v_{\vec{q}}^2) + (u_{\vec{q}} - v_{\vec{q}})\hat{U}(u_{\vec{q}} - v_{\vec{q}})]dz + \varepsilon_{\vec{q}}/2, \tag{3.29}$$

where the dependence of $u_{\vec{q}}$ and $v_{\vec{q}}$ on z is omitted. From the conditions $\delta I/\delta u_{\vec{p}} = 0$ and $\delta I/\delta v_{\vec{p}} = 0$ we can obtain equations (3.19), and by minimization of I with respect to ε_p we can get the normalization condition at $\vec{p} = \vec{p}'$.

The extremum problem for (3.29) is solved numerically by the variational method. In the TF regime (3.26) we can set $\hat{U} \approx U = const$ in Eq. (3.21). This dictates the following form for the trial functions (see Appendix A):

$$u_{\vec{q}}(z) = A\sqrt{\frac{2}{L}}\sin\frac{p_z z}{\hbar}; \quad v_{\vec{q}}(z) = B\sqrt{\frac{2}{L}}\sin\frac{p_z z}{\hbar}, \tag{3.30}$$

with $A, B \neq 0$ being the trial parameters. After substituting Eq. (3.30) into Eq. (3.29), we can find the lowest spectral branch ($p_z = \pi\hbar/L$) in the following form:

$$\bar{\varepsilon}_{\bar{p}} = \sqrt{\frac{\bar{p}^4}{4} + (2 + \alpha - A_{\bar{p}})\gamma\bar{p}^2}. \tag{3.31}$$

In Eq. (3.31), we denote $\bar{p} = pL/\hbar$, $\bar{\varepsilon}_{\bar{p}} = mL^2\varepsilon_p/\hbar^2$, and

$$A_{\bar{p}} = \frac{3\bar{p}^2}{\bar{p}^2 + \pi^2} + \frac{6\pi^2\bar{p}(1 + e^{-\bar{p}})}{(\bar{p}^2 + \pi^2)^2} \approx \begin{cases} \mathcal{O}(\bar{p}), & \bar{p} \ll \pi, \\ 3 & \bar{p} \gg \pi \end{cases} \tag{3.32}$$

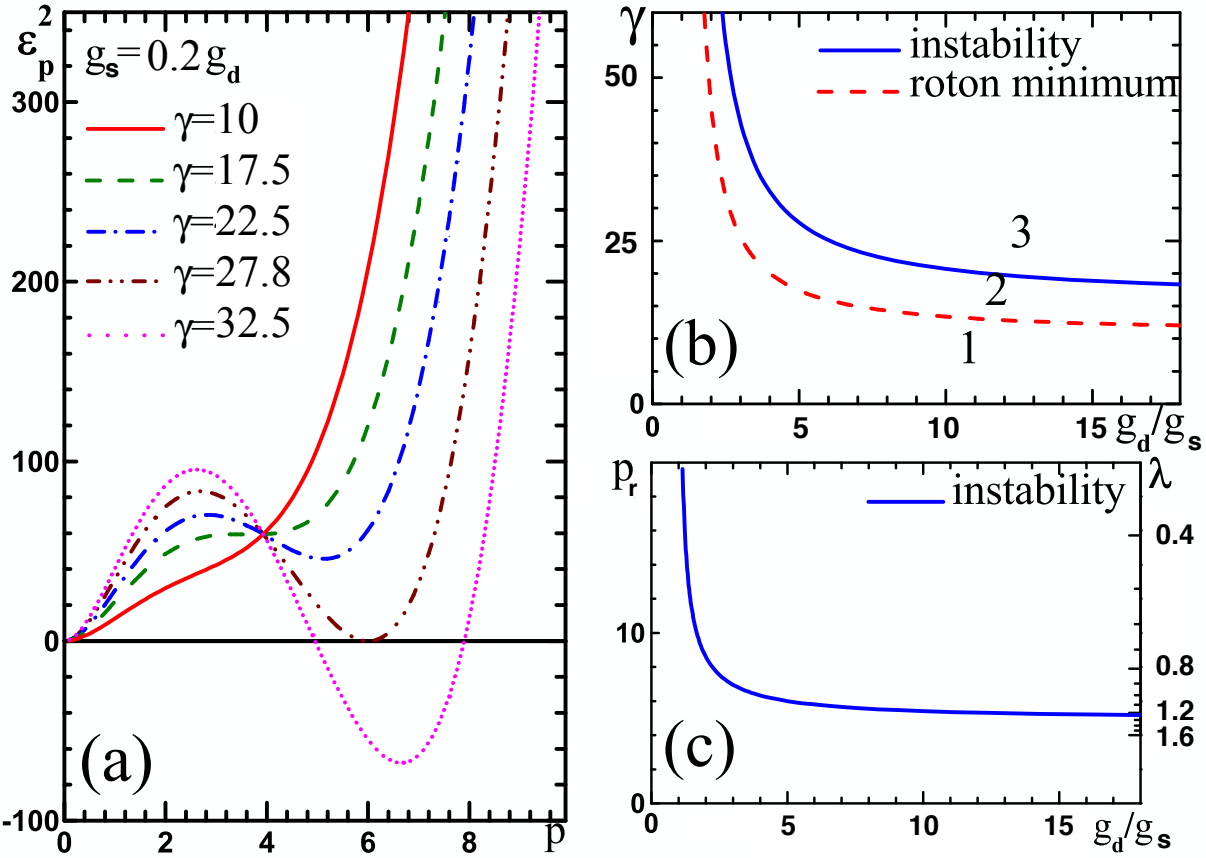

Figure 3.3: (Color online) (a) Calculation of the lowest branches of ε_p^2 at $g_s = 0.2g_d$ and $\gamma = 10$ (solid), $\gamma = 17.5$ (dashed), $\gamma = 22.5$ (dot-dashed), $\gamma = 27.8$ (dot-dot-dashed) and $\gamma = 32.5$ (dotted). (b) Stability diagram in terms of g_d/g_s and γ. The stable phase without the roton minimum (1), with the roton minimum (2), and the unstable phase (3) are shown. (c) Critical momentum value for the threshold of instability and roton wavelength $\lambda = 2\pi/p_{\rm r}$. Units $\hbar = m = L = 1$ are used in (a)–(c).

$$\alpha = \frac{g_s}{g_d}, \qquad \gamma = \frac{m g_d n_0 L^2}{\hbar^2} = \frac{4\pi}{2+\alpha}\left(\frac{\beta L}{a}\right)^2. \tag{3.33}$$

Here the TF regime (3.26) corresponds to $(\beta L/a)^2 \gg 1$, since typically $\alpha \sim 1$ for excitons.

The dynamical instability for the spectral branch (3.31) occurs earlier than that for the other branches (see Appendix A). The exciton chemical potential has the following explicit form:

$$\mu = g n_0 + \frac{\pi^2 \hbar^2}{2mL^2}. \tag{3.34}$$

This expression is justified by the fact that the lowest branch should vanish at $p \to 0$, since the stable 2D gas is superfluid at $T = 0$. Thus, using Eq. (3.13), we find relation (3.34) for the chemical potential of excitons.

It should be noted that with an increase of the density n_0, or the dipole-dipole coupling constant g_d, or the width L of the semiconductor layer, the spectrum ε_p bends down (see Fig. 3.3a). As a result of this bending, the roton minimum is formed. It then touches zero, and the homogeneous phase becomes unstable. The stability diagram is presented in Figs. 3.3b and 3.3c.

The phase boundaries for the formation of the roton minimum and the roton instability are determined from the following conditions, respectively:

$$\left.\frac{d\varepsilon_p^2}{dp}\right|_{p=\pm p_r} = 0; \qquad \left.\varepsilon_p^2\right|_{p=\pm p_r} = 0. \tag{3.35}$$

From the analysis of Eqs. (3.31)–(3.33) and the stability diagram [Fig. 3(b) and 3(c)] we can conclude that there is no phonon instability in contrast to the 3D case. The instability in the system is always the roton one. Accordingly, the unstable phase is possible only if $\alpha < 1$, i.e., when $g_d > g_s$. For purely dipolar interactions ($g_s = 0$) in a sufficiently wide semiconductor layer (γ is large), the system is always unstable. The roton minimum and the roton instability are indeed possible only in the TF regime, i.e., in the layer geometry rather than in the 2D case. In the absence of the Feshbach resonance, the van der Waals interaction of excitons is repulsive: $g_s > 0$. For this case, our numerical solution of Eq. (3.35) with the lowest branch (3.31)–(3.32) shows that the roton minimum exists only if $\mu > 5.26\mathcal{E}_0$, and the roton instability occurs for $\mu > 7.39\mathcal{E}_0$. In both cases $\mu \gg \mathcal{E}_0$. Thus, the TF regime (3.26) is indeed realized. Furthermore, in the limit of a wide semiconductor layer ($L \to \infty$), for the threshold of the instability we have

$$g_d - g_s \approx \frac{\pi\hbar}{L}\sqrt{\frac{3g_d}{mn_0}} = \mathcal{O}\left(\frac{1}{L}\right). \tag{3.36}$$

An important question is about the depletion of the exciton condensate at $T = 0$:

$$\frac{n'}{n_0} = \frac{n - n_0}{n_0} = \frac{1}{N_0}\int \langle \hat{\Psi}'^{+}(\vec{\mathrm{r}})\hat{\Psi}'(\vec{\mathrm{r}})\rangle d\vec{\mathrm{r}} = \frac{1}{N_0}\sum\nolimits_{\vec{\mathrm{q}}} N_{\vec{\mathrm{q}}}, \tag{3.37}$$

where the summation over $\vec{\mathrm{q}}$ excludes the term with $l = 1$ and $p = 0$, $N_{\vec{\mathrm{q}}} = \int_0^L |v_{\vec{\mathrm{q}}}(z)|^2 dz$ is the occupation number of the $\vec{\mathrm{q}}$ mode, $N_0 = n_0 SL$ is the number of condensed particles, and S is the quantization area. Here we take into account both in-plane fluctuations and fluctuations in the z direction.

In our consideration, the lowest spectral branch corresponds to $l = 1$. Other branches do not give a divergent contribution (see Appendix A). Close to the threshold of the

instability, the lowest spectral branch ε_p is close to zero at the roton momentum $p \approx p_{\rm r} \neq 0$. Therefore, the contribution of the lowest branch to the condensate depletion is

$$\frac{n'}{n} = \int_0^\infty \frac{(\varepsilon_p - p^2/2m)^2}{\varepsilon_p p^2/m} \frac{pdp}{4\pi\hbar^2 nL} \tag{3.38}$$

and it diverges logarithmically near the threshold. The divergence of the condensate depletion (3.38) indicates that the condensate vanishes close to the threshold of the roton instability, which is in agreement with Ref. [104].

However, in sufficiently wide semiconductor layers the following hierarchy of parameters takes place:

$$a \ll \xi \ll L \ll \sqrt{S}, \tag{3.39}$$

where the first inequality corresponds to the dilute regime (3.28), the second inequality corresponds to the condition of applicability of the TF regime (3.26), and the third one corresponds to the layer geometry. One can add the following inequality:

$$\sqrt{S} \ll a \exp\left(\frac{3\beta}{2\pi^{3/2}} \frac{L^2}{\xi^2}\right), \tag{3.40}$$

which is satisfied in the deep TF regime [see Eq. (3.6)]. In this case, at $S \to \infty$ the formally divergent term in the non-condensed fraction at sufficiently large L is

$$\frac{n'}{n} \simeq \frac{2\pi^{3/2}}{3} \frac{\beta}{\gamma} \ln \frac{\beta\sqrt{S}}{a\gamma}. \tag{3.41}$$

For small β it can be small (see Appendix IIB). Thus, finite-size effects can make the non-condensed fraction negligible (and Bogoliubov approach applicable) at the threshold of the instability.

3.4 Concluding remarks

We now discuss how the rotonization effect can be realized for dipolar excitons in the semiconductor layer of GaAs heterostructures. This experimental setup allows one to realize 3D and 2D layer regimes for dipolar excitons with direct electrons and holes.

One has two advantages when applying the in-plane magnetic field. First of all, in this case there is no tunneling dissociation of excitons by the polarizing electric field and the bottom of the TF parabola [284] shifts from the radiation zones [285–287]. Therefore, a third particle (phonon, impurity) is needed for the exciton recombination. As a result, the exciton lifetime becomes sufficiently large [285–287] for cooling them down to low temperatures [288]. The second advantage is that in the presence of the in-plane magnetic field all the above-mentioned calculations are relevant [284].

We consider the GaAs semiconductor layer of the width $L = 4$ μm, where the electron mass is $m_e = 0.067m_0$ and the exciton mass is $m = 0.415m_0$ (m_0 is the free electron mass) [284]. Then the Landé g factors [289] are $g_e, g_h \sim 1$. For GaAs semiconductor layer at densities $n \simeq 10^{15}$ cm^{-3} we obtain the gas parameter $n_0 a^3 \simeq 0.2 \ll 1$, which corresponds to $\beta = 0.44$ at the threshold of the instability in the limit $L \to \infty$. The values of external electric and magnetic fields are $E_\perp = 1.5$ kV/cm and $B_\parallel = 4$ T [284]. Therefore, for the dimensionless density we have $\gamma = (4\pi/3)(\beta L/a)^2 \simeq 10^3$, and with $\alpha = 1 - \pi\sqrt{3/\gamma} \approx 1$ we get to the deep TF regime. We then obtain that the exciton gap

in GaAs is $E_g = 1.51$ eV [285–287], which allows us to neglect the anisotropy of the mass and its dependence on $B_\parallel$ and $E_\perp$.

We should point out the following important features of the suggested experimental realization. First of all, in this setup the momentum displacement of the exciton parabola bottom $p_\parallel = 6.1 \times 10^5$ cm$^{-1}\hbar$ is significantly larger than the radiation zone width $q_r = 2.7 \times 10^5$ cm$^{-1}\hbar$ in GaAs. Thus, excitons are actually "dark", i.e., they are long-lived with lifetimes of the order of several tens of milliseconds. Second, the zero-sound velocity in the exciton system $c_s = 6.8 \times 10^5$ cm/s is greater than the velocity of the longitudinal sound $c_{\text{phon}} = 5.36 \times 10^5$ cm/s. This provides a way for efficient cooling of excitons by the GaAs lattice. Finally, the chemical potential of excitons is $\mu = 1.27$ K and it is significantly lower than the Zeeman splitting $\Delta E \sim 5$ K [257, 265]. Therefore, at low temperatures the gas of excitons has only one spin degree.

We note that under these conditions, in the regime of spatially separated cw pump [290–292] and the evaporative cooling [293], the artificially trapped [43, 44, 291–295] excitons are readily cooled to very low temperatures [296], which are lower than the temperature for BEC in the 3D ideal gas, $T_{\text{BEC}}^{\text{IG}} = 650$ mK.

It is important to say that the scattering length of excitons $a = 64$ nm is greater than their Bohr radius $a^* = 11.8$ nm. Then the tunneling transformation of excitons into biexcitons [297] is suppressed. Moreover, the destruction of the BEC [298] and superfluidity [299] by the Fermi exchange effects is exponentially small [300].

The considered exciton density $n \simeq 10^{15}$ cm^{-3} is higher by two orders of magnitude than the concentration of impurities in pure GaAs samples. Their influence is then negligible. Moreover, free carriers [301, 302] can be compensated [227] by the spatially indirect injection [303]. Finally, two-exciton recombination processes were not observed in GaAs heterostructures [304].

We considered the single spin component dipolar gas of excitons. In other words, predicted effects are valid for the lowest spin branch. However, the presence of exchange interaction between excitons could be a reason for a variety of interesting collective phenomena. One can expect to observe transitions between instabilities realized in different spin components and controlled by the detuning of the magnetic field [260–262].

To summarize, in the present work we have considered the system of dipolar excitons with one spin degree of freedom in the weak coupling regime in the layer geometry. For the system in the semiconductor layer, we have predicted the roton-maxon character of the excitation spectrum and the roton instability effect. For the experimental verification of these effects we have suggested layers in GaAs heterostructures.

However, it should be noted that in this work we have focused on the case of the isotropic hole mass. The anisotropy of the hole mass provides an additional symmetry breaking in the system, which can be a reason for interesting structural properties, e.g., density wave phases at the threshold of the roton instability. In order to precisely determine the ground state of the system taking into account this effect, one has to make additional calculations.

Appendix A. Variational approach

I. Trial functions

We have to choose the form of the trial functions $u_{\vec{q}}(z)$ and $v_{\vec{q}}(z)$ for the functional (3.29). We note that in the TF regime the typical momentum of the system, $p \sim \hbar/\xi$, satisfies the inequality $p \gg \pi\hbar/L$. However, the roton instability first appears for the lowest spectral branch $l = 1$ with $p_z = \pi\hbar/L$. Thus, we have

$$p = \sqrt{p^2 - p_z^2} \approx p \gg \pi\hbar/L. \tag{A1}$$

Therefore, the typical scale of variations in Eq. (3.21) is estimated as $|z - z'| \ll L/\pi$. At the same time, the Bogoliubov modes $u_{\vec{q}}(z)$ and $v_{\vec{q}}(z)$ for the spectral branch, obviously, change on the scale $\sim L$, which is larger. As a result, in Eq. (3.21) we can substitute the exponential part $e^{-p|z-z'|/\hbar}$ as

$$(p/\hbar)e^{-p|z-z'|/\hbar} \approx 2\delta(z - z'). \tag{A2}$$

The operator $\hat{U} \approx U = const$ is local.

Therefore, the trial functions $u_{\vec{q}}(z)$ and $v_{\vec{q}}(z)$ are useful in the form (3.30).

II. Variational method and condensate depletion

The extremum for the functional $I(A, B)$ [see Eq. (3.29)] for nontrivial values of A and B ($A, B \neq 0$) is achieved if the condition

$$\varepsilon_{\vec{q}} = \sqrt{C_1(\vec{q})(C_1(\vec{q}) + 2C_2(\vec{q}))} \tag{A3}$$

holds, and the values of A and B at the extremum point have the form:

$$A^2 = \frac{(\varepsilon_{\vec{q}} + C_1(\vec{q}))^2}{4\varepsilon_{\vec{q}} C_1(\vec{q})}, \quad B^2 = \frac{(\varepsilon_{\vec{q}} - C_1(\vec{q}))^2}{4\varepsilon_{\vec{q}} C_1(\vec{q})}. \tag{A4}$$

Here,

$$\begin{aligned} C_1(\vec{q}) &= p^2/2m + gn_0 - \mu, \\ C_2(\vec{q}) &= gn_0 - \frac{3g_d n_0 p}{\hbar L} C(\vec{q}), \end{aligned} \tag{A5}$$

$$\begin{aligned} C(\vec{q}) &= \int\int_0^L \left(\sin\frac{p_z z}{\hbar} \sin\frac{p_z z'}{\hbar} e^{-p|z-z'|/\hbar} \right) dz dz' = \\ &= \frac{\bar{p} L^2}{\pi^2 l^2 + \bar{p}^2} + \frac{2\pi^2 l^2 L^2}{(\pi^2 l^2 + \bar{p}^2)^2} \left(1 - (-1)^l e^{-\bar{p}}\right). \end{aligned} \tag{A6}$$

After substituting Eqs. (A5) and (A6) at $p_z = \pi\hbar/L$ into Eq. (A3) and algebraic transformations, we get Eq. (3.31). Furthermore, by substituting Eqs. (A5) and (A6) into Eq. (A3) one can prove that (i) the lowest spectral branch corresponds to l=1; (ii) the instability for the branch with l=1 occurs earlier than that for other branches; (iii) the divergence of the condensate depletion is possible for the $l = 1$ spectral branch only.

By substituting Eqs. (A5)-(A6) into Eq. (A3) and then Eq. (A3) into Eq. (A4) and integrating this equation over the momentum space, we obtain Eq. (3.37) for the condensate depletion [see Eq. (3.30)].

We note that in the TF regime (3.26) in semiconductor layers we can neglect the last term in Eq. (A6), because it is small as $\mathcal{O}(1/L)$ at $p, p_z \gg \pi\hbar/L$. In this case at sufficiently large L, from Eq. (3.38) we obtain the following expression at the threshold of the roton instability:

$$\frac{n-n_0}{n_0} = \left.\frac{n-n_0}{n_0}\right|_{p,p_z\gg\pi\hbar/L} + \frac{2\pi^{3/2}}{3}\frac{\beta}{\gamma}\ln\frac{\beta\sqrt{S}}{a\gamma}. \tag{A7}$$

Here the first term corresponds to the contribution of all spectral branches, including both in-plane and z-direction fluctuations, and to the convergent part of the lowest spectral branch. Due to condition (3.28), it is small as $2\beta/3\sqrt{\pi}$. The second term comes from the formal divergence of the lowest spectral branch. For small β it can be small.

Chapter 4

Topological p-wave superfluidity of fermionic atoms and polar molecules in a lattice

In this chapter we consider p-wave superfluids of identical fermions in 2D lattices. The optical lattice potential manifests itself in an interplay between an increase in the density of states on the Fermi surface and the modification of the fermion-fermion interaction (scattering) amplitude. The density of states is enhanced due to an increase of the effective mass of atoms. In deep lattices, for short-range interacting atoms the scattering amplitude is strongly reduced compared to free space due to a small overlap of wavefunctions of fermions sitting in the neighboring lattice sites, which suppresses the p-wave superfluidity. However, we show that for a moderate lattice depth there is still a possibility to create atomic p-wave superfluids with sizable transition temperatures. The situation is drastically different for fermionic polar molecules. Being dressed with a microwave field, they acquire a dipole-dipole attractive tail in the interaction potential. Then, due to a long-range character of the dipole-dipole interaction, the effect of the suppression of the scattering amplitude in 2D lattices is absent. This leads to the emergence of a stable topological $p_x + ip_y$ superfluid of identical microwave-dressed polar molecules. The results of this chapter are based on Refs. [177, 178].

4.1 Background

The creation of $p_x + ip_y$ atomic or molecular topological superfluids in 2D optical lattices can be a promising path for quantum information processing, since addressing qubits in the lattice should be much easier than in the gas phase.

For short-range interacting atomic fermions, the effect of the lattice potential on the formation of a superfluid phase of atomic fermions has been actively discussed [305–312]. In particular, for the s-wave pairing of spin-1/2 fermions an increase in the depth of the optical potential results in a stronger atom localization and hence in increasing the on-site interaction. At the same time, the tunneling becomes weaker. The combined effect of these two factors is a strong increase in the critical temperature [305–307]. This has been observed in the MIT experiment [308]. For the lattice filling somewhat smaller than unity, the physical picture can be rephrased as follows. An increase in the lattice

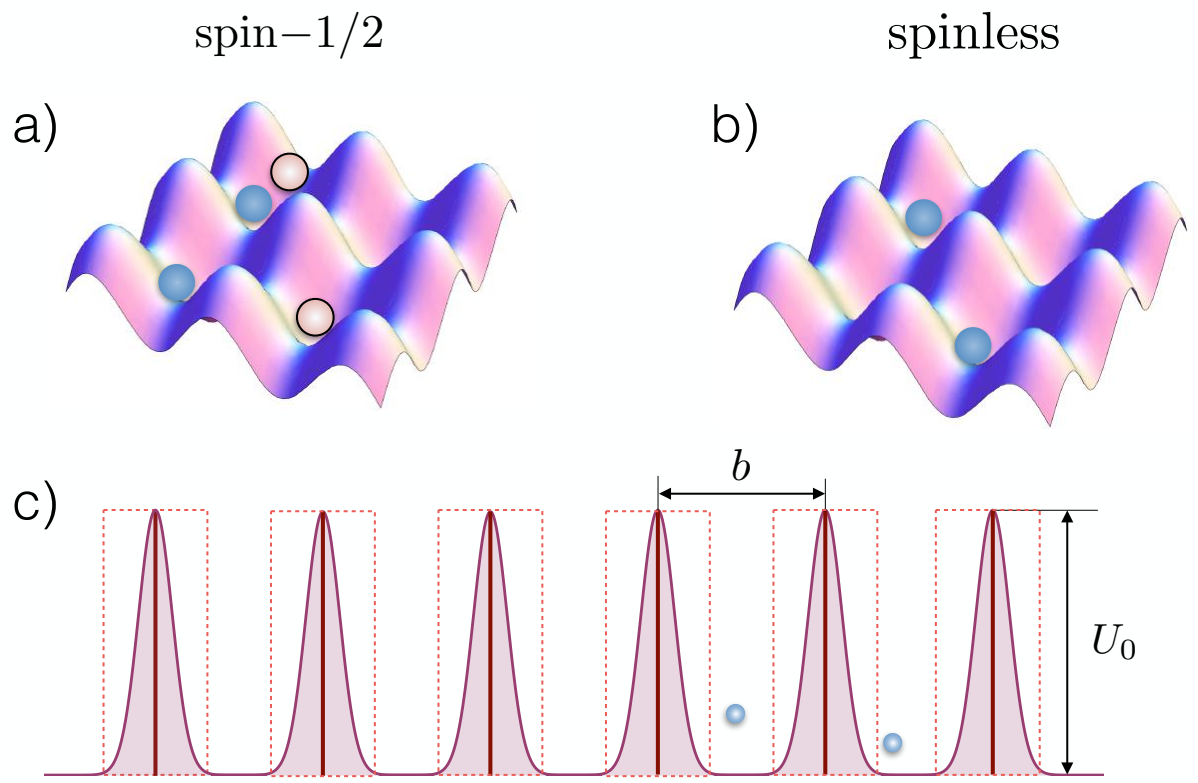

Figure 4.1: Superfluid pairing of short-range interacting lattice fermions in several setups. In (a) two component (spin-1/2) lattice fermions with a short-range interaction. The two spin components are labeled by filled and unfilled circles. In (b) single component (spinless) short-range interacting lattice fermions. In (c) 1D projection of atomic fermions loaded in the 2D Kronig-Penney lattice.

depth increases an effective mass of atoms and, hence, makes the density of states (DOS) larger. The effective fermion-fermion scattering amplitude is also increasing. The critical temperature in the BCS approach is $T_c \propto \exp[-1/\lambda_c]$, where λ_c is proportional to the product of the (modulus of) the scattering amplitude and the DOS on the Fermi surface. Thus, an increase in the lattice potential increases T_c.

On the contrary, for identical fermions in fairly deep lattices (tight-binding model) the fermion-fermion scattering amplitude is strongly reduced (see Fig. 4.1a and Fig. 4.1b). In the lowest band approach two fermions do not occupy the same lattice site, and the amplitude is proportional to a very small overlap of the wavefunctions of fermions sitting in the neighboring sites. This suppresses the p-wave superfluid pairing for fairly small filling factors in deep lattices, which is consistent with numerical calculations of Ref. [307]. Nevertheless, there remains a question about an interplay between an increase of the DOS and the modification of the fermion-fermion scattering amplitude for moderate lattice depths. However, in sinusoidal optical lattices single particle states are described by complicated Mathieu functions, which complicates the analysis. Therefore, we study identical fermionic atoms in a 2D version of the Kronig-Penney model allowing a transparent physical picture for moderate lattice depths (see Fig. 4.1c).

For microwave-dressed polar molecules the long-range character of the acquired attractive dipole-dipole intermolecular interaction strongly changes the situation. The interaction amplitude is not suppressed even in deep lattices, and a collisionally stable $p_x + ip_y$ superfluid may emerge.

The chapter is organized as follows. In Section. 4.2 we discuss superfluidity of identical atomic fermions in a 2D lattice. We first describe a general approach for studying superfluidity of 2D lattice fermions in Subsection 4.2.1. We then show how the ordinary tight-binding optical lattice promotes the s-wave superfluidity of spin-1/2 fermionic atoms and suppresses the p-wave superfluidity of spinless fermions (Subsection 4.2.2). In Subsection 4.2.3, we develop a theory of p-wave superfluidity of spinless fermions in the 2D Kronig-Penney lattice and discuss inelastic decay processes. In Section 4.3, we discuss p-wave superfluidity of identical microwave-dressed polar molecules and show that the long-range character of the dipole-dipole attraction leads to similar results regarding the critical temperature as in free space. In Section 4.4 we conclude.

4.2 Superfluidity of identical fermionic atoms in a 2D lattice

4.2.1 General relations and qualitative arguments

Let us first present a general framework for the investigation of superfluid pairing of weakly interacting lattice fermions. We will do this for 2D identical (spinless) fermions, having in mind that the approach for spin-1/2 fermions is very similar. The grand-canonical Hamiltonian of the system is $\hat{\mathcal{H}} = \hat{H}_0 + \hat{H}_{\rm int}$, and the single particle part is given by (hereinafter in this Section we put $\hbar = 1$ and set the normalization volume (surface) equal to unity):

$$\hat{H}_0 = \int d^2\mathbf{r}\, \hat{\psi}^\dagger(\mathbf{r}\,) \left[-\frac{\nabla^2}{2m} + U(\mathbf{r}) - \mu \right] \hat{\psi}(\mathbf{r}), \tag{4.1}$$

with μ being the chemical potential, m the particle mass, $U(\mathbf{r})$ the 2D periodic lattice potential, and $\hat{\psi}(\mathbf{r})$ the fermionic field operator.

The term $\hat{H}_{\rm int}$ describes the interaction between particles:

$$\hat{H}_{\rm int} = \frac{1}{2} \int d^2r d^2r'\, \hat{\psi}^\dagger(\mathbf{r})\hat{\psi}^\dagger(\mathbf{r}')V(\mathbf{r}-\mathbf{r}')\hat{\psi}(\mathbf{r}')\hat{\psi}(\mathbf{r}), \tag{4.2}$$

where $V(\mathbf{r}-\mathbf{r}')$ is the potential of interparticle interaction of radius r_0.

In the absence of interactions, fermions in the periodic potential $U(\mathbf{r})$ fill single particle energy levels $\varepsilon_\nu(\mathbf{k})$ determined by the Schrödinger equation:

$$\left[-\frac{\nabla^2}{2m} + U(\mathbf{r}) \right] \chi_{\nu\mathbf{k}}(\mathbf{r}) = \varepsilon_\nu(\mathbf{k})\chi_{\nu\mathbf{k}}(\mathbf{r}). \tag{4.3}$$

Here $\nu = 0, 1, 2, \ldots$ numerates energy bands, the wave vector $\mathbf{k} = \{k_x, k_y\}$ takes values within the Brillouin zone:

$$\{-\pi/b < k_i < \pi/b; i = x, y\}, \tag{4.4}$$

and b is the lattice period. The eigenfunctions $\chi_{\nu\mathbf{k}}(\mathbf{r})$ obey the periodicity condition

$$\chi_{\nu\mathbf{k}}(\mathbf{r} + \mathbf{R}_n) = \chi_{\nu\mathbf{k}}(\mathbf{r}) \exp\left[i\mathbf{k}\mathbf{R}_n\right], \tag{4.5}$$

where $n = (n_x, n_y)$ is the index of the lattice site, with integer n_x, n_y. In the described Bloch basis the field operator reads:

$$\hat{\psi}(\mathbf{r}) = \sum\nolimits_{\nu,\mathbf{k}} \hat{a}_{\nu\mathbf{k}} \chi_{\nu\mathbf{k}}(\mathbf{r}), \tag{4.6}$$

with $\hat{a}_{\nu\mathbf{k}}$ being the annihilation operator of fermions with quasimomentum $\mathbf{k}$ in the energy band ν.

We assume a dilute regime where the 2D density n is such that $nb^2 \lesssim 1$, and all fermions are in the lowest Brillouin zone (hereinafter we omit the corresponding index $\nu = 0$). In the low momentum limit (small filling factor) that we consider, their Fermi energy E_F is small compared to the energy bandwidth E_B. The lattice potential amplitude U_0 is assumed to be sufficiently large, so that both E_F and E_B are smaller than the gap between the first and second lattice bands. The single particle dispersion relation then takes the form:

$$E_k = \frac{k^2}{2m^*}, \tag{4.7}$$

where $m^* > m$ is the effective mass.

In 2D the transition of a Fermi gas from the normal to superfluid state is set by the Kosterlitz-Thouless mechanism. However, in the weakly interacting regime the Kosterlitz-Thouless transition temperature is very close to T_c calculated in the Bardeen-Cooper-Schrieffer (BCS) approach [313]. We then reduce the Hamiltonian given by Eqs. (4.1) and (4.2) to the standard BCS form:

$$\hat{\mathcal{H}}_{\mathrm{BCS}} = \sum\nolimits_{\mathbf{k}} \left\{ (E_k - \mu) \hat{a}^\dagger_{\mathbf{k}} \hat{a}_{\mathbf{k}} + \frac{1}{2} \left[\hat{a}^\dagger_{\mathbf{k}} \hat{a}^\dagger_{-\mathbf{k}} \Delta(\mathbf{k}) + \mathrm{h.c.} \right] \right\}, \tag{4.8}$$

where the momentum-space order parameter $\Delta(\mathbf{k})$ is given by

$$\Delta(\mathbf{k}) = \sum\nolimits_{\mathbf{k}'} V(\mathbf{k}, \mathbf{k}') \langle \hat{a}_{-\mathbf{k}'} \hat{a}_{\mathbf{k}'} \rangle, \;\; \Delta(\mathbf{k}) = -\Delta(-\mathbf{k}), \tag{4.9}$$

with $V(\mathbf{k}, \mathbf{k}')$ being the matrix element of the interaction potential between the corresponding states.

The Hamiltonian (4.8) is then decomposed in a set of independent quadratic Hamiltonians and the anomalous averages are determined by the standard BCS expressions:

$$\langle \hat{a}_{-\mathbf{k}} \hat{a}_{\mathbf{k}} \rangle = -\Delta(\mathbf{k}) \mathcal{K}(k), \tag{4.10}$$

where $\mathcal{K}(k) = \tanh[\mathcal{E}(k)/2T]/2\mathcal{E}(k)$, and

$$\mathcal{E}(k) = \sqrt{(E_k - \mu)^2 + |\Delta_\nu(\vec{k})|^2} \tag{4.11}$$

is the energy of excitation with quasimomentum $\mathbf{k}$. From Eqs. (4.9) and (4.10) we have an equation for $\Delta(\mathbf{k})$ (gap equation):

$$\Delta(\mathbf{k}) = -\sum\nolimits_{\mathbf{k}'} V(\mathbf{k}, \mathbf{k}') \mathcal{K}(k') \Delta(\mathbf{k}'). \tag{4.12}$$

Eq. (4.12) can be expressed [122,123] in terms of the effective off-shell scattering amplitude $f(\mathbf{k}', \mathbf{k})$ of a fermion pair with momenta $\mathbf{k}$ and $-\mathbf{k}$ defined as

$$f(\mathbf{k}', \mathbf{k}) = \int d^2 r_1 d^2 r_2 \, \Phi^{(0)*}_{\mathbf{k}'}(\mathbf{r}_1, \mathbf{r}_2) V(\mathbf{r}_1 - \mathbf{r}_2) \Phi_{\mathbf{k}}(\mathbf{r}_1, \mathbf{r}_2). \tag{4.13}$$

Here

$$\Phi_{\mathbf{k}}^{(0)}(\mathbf{r}_1,\mathbf{r}_2)=\chi_{\mathbf{k}}(\mathbf{r}_1)\chi_{-\mathbf{k}}(\mathbf{r}_2), \tag{4.14}$$

is the wavefunction of a pair of non-interacting fermions with quasimomenta $\mathbf{k}$ and $-\mathbf{k}$. The quantity $\Phi_{\mathbf{k}}(\mathbf{r}_1,\mathbf{r}_2)$ is the true (i.e., accounting for the interaction) wavefunction, which develops from the incident wavefunction $\Phi_{\mathbf{k}}^{(0)}(\mathbf{r}_1,\mathbf{r}_2)$ of a free pair. The wavefunction $\Phi_{\mathbf{k}}(\mathbf{r}_1,\mathbf{r}_2)$ satisfies the Schrödinger equation

$$[\hat{H}_{12}-2E_k]\Phi_{\mathbf{k}}(\mathbf{r}_1,\mathbf{r}_2)=0, \tag{4.15}$$

with the two-particle Hamiltonian:

$$\hat{H}_{12}=-\frac{\nabla_1^2+\nabla_2^2}{2m}+U(\mathbf{r}_1)+U(\mathbf{r}_2)+V(\mathbf{r}_1-\mathbf{r}_2). \tag{4.16}$$

The renormalized gap equation for the function $\Delta(\mathbf{k})$ then takes the form similar to that in free space (see Refs. [122, 123] and references therein):

$$\Delta(\mathbf{k})=\int\frac{d^2k'}{(2\pi)^2}f(\mathbf{k}',\mathbf{k})\Delta(\mathbf{k}')\left\{\mathcal{K}(k')-\frac{1}{2(E_{k'}-E_k)}\right\}. \tag{4.17}$$

In the weakly interacting regime the chemical potential coincides with the Fermi energy $E_F=k_F^2/2m^*$, where $k_F=\sqrt{4\pi n}$ is the Fermi momentum. Note that here we omit a correction to the bare interparticle interaction due to polarization of the medium by colliding particles [314].

We will see below that the scattering amplitude and the corresponding critical temperature of the superfluid transition of lattice fermions depend drastically on the presence or absence of spin and on the pairing angular momentum. Before analyzing various regimes, we discuss the situation in general.

The efficiency of superfluid pairing first of all depends on the symmetry of the order parameter. For the pairing with orbital angular momentum l we have

$$\Delta(\mathbf{k})\to\Delta_l(k)\exp\left[il\phi_{\mathbf{k}}\right], \tag{4.18}$$

where $\phi_{\mathbf{k}}$ is the angle of the vector $\mathbf{k}$ with respect to the quantization axis. Integrating Eq. (4.17) over $\phi_{\mathbf{k}}$ and $\phi_{\mathbf{k}'}$ we obtain the same equation in which $\Delta(\mathbf{k})$ and $\Delta(\mathbf{k}')$ are replaced with $\Delta_l(k)$ and $\Delta_l(k')$, and $f(\mathbf{k}',\mathbf{k})$ is replaced with its l-wave part

$$f_l(k',k)=\int\frac{d\phi_{\mathbf{k}}d\phi_{\mathbf{k}'}}{(2\pi)^2}f(\mathbf{k}',\mathbf{k})\exp\left[il\phi_{\mathbf{k}}-il\phi_{\mathbf{k}'}\right]. \tag{4.19}$$

Alternatively, we can write

$$f_l(k',k)=\int d^2r_1d^2r_2\Phi_{lk'}^{(0)*}(\mathbf{r}_1,\mathbf{r}_2)V(|\mathbf{r}_1-\mathbf{r}_2|)\Phi_{lk}(\mathbf{r}_1,\mathbf{r}_2). \tag{4.20}$$

where the l-wave parts of the wavefunctions, $\Phi_{lk'}^{(0)}$ and Φ_{lk}, are given by

$$\Phi_{lk'}^{(0)}(\mathbf{r}_1,\mathbf{r}_2)=\int\frac{d\phi_{\mathbf{k}'}}{2\pi}\Phi_{\mathbf{k}'}^{(0)}(\mathbf{r}_1,\mathbf{r}_2)\exp\left[il\phi_{\mathbf{k}'}\right], \tag{4.21}$$

$$\Phi_{lk}(\mathbf{r}_1,\mathbf{r}_2)=\int\frac{d\phi_{\mathbf{k}}}{2\pi}\Phi_{\mathbf{k}}(\mathbf{r}_1,\mathbf{r}_2)\exp\left[il\phi_{\mathbf{k}}\right]. \tag{4.22}$$

As well as in free space (see Ref. [122,123]), we turn from $f_l(k',k)$ to the (real) function

$$\tilde{f}_l(k',k) = f_l(k',k)\left[1 - i\tan\delta(k)\right], \tag{4.23}$$

where $\delta(k)$ is the scattering phase shift. This leads to the gap equation:

$$\Delta_l(k) = -P\int \frac{d^2k'}{(2\pi)^2}\tilde{f}_l(k',k)\Delta_l(k')\left\{\mathcal{K}(k') - \frac{1}{E_{k'} - E_k}\right\}, \tag{4.24}$$

where the symbol P denotes the principal value of the integral.

In order to estimate the critical temperature T_c, we first put $k = k_F$ and notice that the main contribution to the integral over k' in Eq. (4.24) comes from k' close to k_F. At temperatures T tending to the critical temperature T_c from below, we put $\mathcal{E}(k') = |E_{k'} - E_F|$ in $\mathcal{K}(k')$. Then for the pairing channel related to the interaction with orbital angular momentum l, we have the following estimate:

$$T_c \sim E_F \exp\left[-\frac{1}{\lambda_c}\right], \quad \lambda_c = \rho(k_F)|f_l(k_F)|. \tag{4.25}$$

The quantity $\rho(k_F)=m^*/2\pi$ is the effective density of states on the Fermi surface, and $f_l(k_F)$ is the on-shell l-wave scattering amplitude of lattice fermions. The derivation for spin-1/2 fermions with attractive intercomponent interaction leads to the same gap equations (4.17), (4.24) and estimate (4.25) in which

$$\Delta(\mathbf{k}) = \sum_{\mathbf{k}'} V(\mathbf{k},\mathbf{k}')\langle \hat{a}_{\downarrow -\mathbf{k}'}\hat{a}_{\uparrow \mathbf{k}'}\rangle \tag{4.26}$$

and $f(\mathbf{k}',\mathbf{k})$, $f_l(k',k)$ are the amplitudes of the intercomponent interaction.

Eq. (4.25) shows that compared to free space we have an additional pre-exponential factor $m/m^* < 1$. Assuming that the lattice amplitude $f_l(k_F)$ and the free-space amplitude $f_l^0(k_F)$ are related to each other as

$$f_l(k_F) = \mathcal{R}_l f_l^0(k_F), \tag{4.27}$$

we see that the exponential factor λ_c in Eq. (4.25) becomes

$$\lambda_c = \mathcal{R}_l \frac{m^*}{m}\lambda_c^0, \tag{4.28}$$

where $1/\lambda_c^0$ is the BCS exponent in free space. Below we compare T_c in various lattice setups with the critical temperature in free space.

4.2.2 Short-range interacting atomic fermions in a deep 2D lattice

We start with the analysis of superfluid pairing in deep 2D lattices. As an example, we consider a quadratic lattice with the lattice potential of the form:

$$U(\mathbf{r}) = U_0\left[\cos\left(\frac{2\pi}{b}x\right) + \cos\left(\frac{2\pi}{b}y\right)\right]. \tag{4.29}$$

For sufficiently deep lattices, the single particle wavefunction has the Wannier form:

$$\chi_{\mathbf{k}}(\mathbf{r}) = \frac{1}{\sqrt{\mathcal{N}}} \sum_j \phi_0(\mathbf{r} - \mathbf{R}_j) \exp[i\mathbf{k}\mathbf{R}_j], \tag{4.30}$$

where the ground state wavefunction in the lattice cell has an extention ξ_0 and is given by

$$\phi_0(\mathbf{r}) = \frac{1}{\sqrt{\pi}\xi_0} \exp\left[-\frac{r^2}{2\xi_0^2}\right]. \tag{4.31}$$

Using a general formula for the effective mass from Ref. [317], for a deep potential of the form (4.29) one obtains:

$$\frac{m^*}{m} \simeq \pi \frac{\xi_0^2}{b^2} \exp\left[\frac{2}{\pi^2}\frac{b^2}{\xi_0^2}\right]. \tag{4.32}$$

We will consider fermionic atoms interacting with each other via a short-range potential $V(\mathbf{r})$ of radius r_0 and assume the following hierarchy of length scales:

$$r_0 \ll \xi_0 < b < 1/k_F. \tag{4.33}$$

We first discuss the s-wave pairing of spin-1/2 fermions with attractive intercomponent interaction ($l = 0$).

Turning to Eq. (4.20) for $l = 0$, we notice that the main contribution to the s-wave scattering amplitude in the lattice comes from the interaction between spin-up and spin-down fermions sitting in one and the same lattice site. The wavefunctions $\Phi^{(0)}_{0k'}$ and Φ_{0k} can be written as

$$\Phi^{(0)}_{0k'}(\mathbf{r}_1, \mathbf{r}_2) = \chi_0(\mathbf{r}_1)\chi_0(\mathbf{r}_2), \tag{4.34}$$

$$\Phi_{0k}(\mathbf{r}_1, \mathbf{r}_2) = \chi_0(\mathbf{r}_1)\chi_0(\mathbf{r}_2)\zeta_0(|\mathbf{r}_1 - \mathbf{r}_2|), \tag{4.35}$$

where the function $\zeta_0(|\mathbf{r}_1 - \mathbf{r}_2|)$ is a solution of the Schrödinger equation for the s-wave relative motion of two particles in free space at zero energy, and it is tending to unity for interatomic separations greatly exceeding r_0. We put $l = 0$ in Eq. (4.20) and integrate over $\mathbf{r} = \mathbf{r}_1 - \mathbf{r}_2$ and $\mathbf{r}_+ = (\mathbf{r}_1 + \mathbf{r}_2)/2$. Then, owing to the inequality $r_0 \ll \xi_0$, this equation is reduced to

$$f_0(k', k) = \int d^2r\, V(r)\zeta(r) \int d^2r_+ |\chi_0(r_+)|^4. \tag{4.36}$$

Recalling that in the low momentum limit the free space scattering amplitude is given by

$$f_0^0 = \int V(r)\zeta(r) d^2r \tag{4.37}$$

and using Eq. (4.30) for the function $\chi_0(r)$, we obtain for the ratio of the lattice to free space amplitude:

$$\mathcal{R}_{l=0} = \frac{1}{2\pi}\frac{b^2}{\xi_0^2}. \tag{4.38}$$

Therefore, according to Eqs. (4.28) and (4.32) the BCS exponent λ_c^{-1} becomes smaller than in free space by the following factor:

$$\mathcal{R}_{l=0}\frac{m^*}{m} \simeq \frac{1}{2} \exp\left[\frac{2}{\pi^2}\frac{b^2}{\xi_0^2}\right]. \tag{4.39}$$

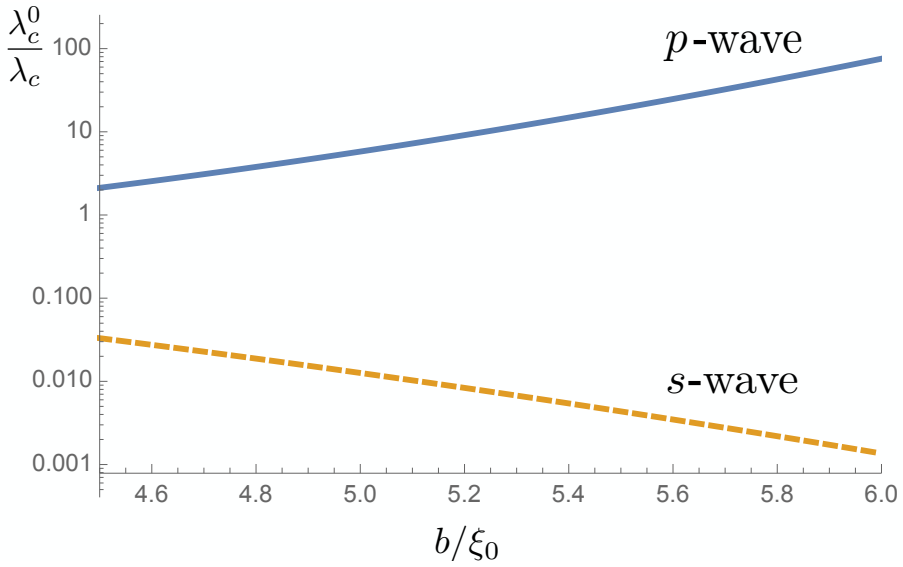

Figure 4.2: The ratio of the BCS exponent in the tight–binding sinusoidal lattice to the BCS exponent in free space, λ_c^0/λ_c, at the same density and short-range coupling strength. The dashed curve shows λ_c^0/λ_c as a function of the lattice period (in units of the harmonic oscillator length ξ_0) for the s-wave pairing of spin-1/2 fermions, and the solid curve is λ_c^0/λ_c for the p-wave pairing of identical fermions.

For example, taking $b/\xi_0 = 4$ the BCS exponent λ_c^{-1} decreases by a factor of 0.08, whereas the effective mass becomes higher by a factor of 5 compared to the bare mass m (see Fig. 4.2). Then, for ^{6}Li atoms at density 10^8 cm^{-2} ($b \simeq 250$ nm, $k_F b \simeq 0.5$) we have the Fermi energy ~ 40 nK. Assuming that the free space BCS exponent is about 30 and the related critical temperature is practically zero, in the lattice we obtain $T_c \sim 3$ nK. We thus see that the lattice setup may strongly promote the s-wave superfluidity of spin-1/2 fermions.

The situation with p-wave superfluidity of identical fermions is drastically different. In the single band approximation (tight binding model) two such fermions can not occupy one and the same lattice site. This is clearly seen using the functions $\chi_{\mathbf{k}}(\mathbf{r}_1)$ and $\chi_{-\mathbf{k}}(\mathbf{r}_2)$ from Eq. (4.30) at the same $\mathbf{R}_j$, so that the wavefunction $\Phi^{(0)}_{\mathbf{k}'}(\mathbf{r}_1, \mathbf{r}_2)$ becomes independent of $\mathbf{k}'$. Therefore, the p-wave part of this wavefunction $\Phi^{(0)}_{1k'}$ and the p-wave scattering amplitude $f_1(k', k)$ following from Eqs. (4.21) and (4.20) at $l = 1$ are equal to zero.

The main contribution to the interaction amplitude then comes from the overlap of the wavefunctions of fermions sitting in the neighbouring sites. We then use Eqs. (4.30) and (4.31) and write:

$$\begin{aligned}\Phi^{(0)}_{\mathbf{k}'}(\mathbf{r}_1, \mathbf{r}_2) &= \chi_{\mathbf{k}'}(\mathbf{r}_1)\chi_{-\mathbf{k}'}(\mathbf{r}_2) \\ &= \frac{1}{\mathcal{N}\pi\xi_0^2} \sum_{i,j} \exp\left\{ -\frac{(\mathbf{r}_1 - \mathbf{R}_i)^2}{2\xi_0^2} - \frac{(\mathbf{r}_2 - \mathbf{R}_j)^2}{2\xi_0^2} - i\mathbf{k}'\mathbf{b}_j \right\},\end{aligned} \tag{4.40}$$

with $\mathbf{b}_j = \mathbf{R}_j - \mathbf{R}_i$ and $\mathbf{R}_i, \mathbf{R}_j$ being the coordinates of the sites i and j. For the short-range interaction between particles the main contribution to the scattering amplitude comes from distances $\mathbf{r}_1, \mathbf{r}_2$ that are very close to each other, and for given i, j both coordinates should be close to $(\mathbf{R}_j + \mathbf{R}_i)/2$. Therefore, Eq. (4.40) is conveniently rewritten

as

$$\Phi^{(0)}_{\mathbf{k}'}(\mathbf{r}_1,\mathbf{r}_2)=\frac{1}{\mathcal{N}\pi\xi_0^2}\sum_{i,j}\exp\Big\{-i\mathbf{k}'\mathbf{b}_j-\frac{r_{+j}^2}{\xi_0^2}-\frac{r^2}{4\xi_0^2}-\frac{b^2}{4\xi_0^2}-\frac{\mathbf{r}\mathbf{b}_j}{2\xi_0^2}\Big\}, \tag{4.41}$$

where $\mathbf{r}=\mathbf{r}_1-\mathbf{r}_2$, $\mathbf{r}_{+j}=\mathbf{r}_+-(\mathbf{R}_i+\mathbf{R}_j/2$, $\mathbf{r}_+=(\mathbf{r}_1+\mathbf{r}_2)/2$, and the summation is performed over the sites j that are nearest neighbours of the site i. Assuming the conditions $k'b\ll 1$ and $r\sim r_0\ll\xi_0^2/b\ll\xi_0$, for the p-wave part of this wavefunction equation (4.21) at $l=1$ gives:

$$\begin{aligned}\Phi^{(0)}_{1k'}(r,r_+,\phi_{\mathbf{r}})=\frac{k'rb^2}{\mathcal{N}8\pi\xi_0^4}\sum_{i,j}\exp\left\{-\frac{r_{+j}^2}{\xi_0^2}-\frac{b^2}{4\xi_0^2}\right\}\\ \times[\exp(i\phi_{\mathbf{r}})+\exp(-i\phi_{\mathbf{r}}+2i\phi_j)],\end{aligned} \tag{4.42}$$

where $\phi_{\mathbf{r}}$ and ϕ_j are the angles of the vectors $\mathbf{r}$ and $\mathbf{b}$ with respect to the quantization axis. The p-wave part of the true relative-motion wavefunction $\Phi_{\mathbf{k}}(\mathbf{r}_1,\mathbf{r}_2)$ under the same conditions is given by

$$\begin{aligned}\Phi_{1k}(r,r_+,\phi_{\mathbf{r}})=\frac{b^2}{\mathcal{N}4\pi\xi_0^4}\zeta_1(r)\sum_{i',j'}\exp\left\{-\frac{r_{+j'}^2}{\xi_0^2}-\frac{b^2}{4\xi_0^2}\right\}\\ \times[\exp(i\phi_{\mathbf{r}})+\exp(-i\phi_{\mathbf{r}}+2i\phi_j)].\end{aligned} \tag{4.43}$$

The function $\zeta_1(r)$ is a solution of the Schrödinger equation for the p-wave relative motion of two particles at energy tending to zero in free space. Sufficiently far from resonance, where the on-shell scattering amplitude satisfies the inequality $m|f_1(k)|\ll 1$, the function $\zeta_1(r)$ becomes $kr/2$ at distances $r\gg r_0$.

Looking at the product of the free and true relative-motion wavefunctions we notice that the main contribution to the scattering amplitude (4.20) comes from the terms in which $\mathbf{R}_i+\mathbf{R}_j=\mathbf{R}_{i'}+\mathbf{R}_{j'}$, i.e. $\mathbf{r}_{+j}=\mathbf{r}_{+j'}$. This is realized for $i=i'$, $j=j'$ or $i'=j$, $j'=i$. Then, recalling that for $k'r_0\ll 1$ and $kr_0\ll 1$ the free space off-shell scattering amplitude is

$$f_1^0(k',k)=\int V(r)(k'r/2)\zeta_1(r)d^2r, \tag{4.44}$$

we first integrate each term of the sum over $i,j,i'j'$ in the product $\Phi^{(0)*}_{1k'}\Phi_{1k}$ over d^2r and d^2r_+ in Eq. (4.20). After that we make a summation over the neighbouring sites j and over the sites i and take into account that $\mathcal{N}=1/b^2$. Eventually, this gives for the ratio of the lattice to free space p-wave amplitude:

$$\mathcal{R}_{l=1}=\frac{1}{2\pi}\left(\frac{b}{\xi_0}\right)^6\exp\left[-\frac{b^2}{2\xi_0^2}\right]. \tag{4.45}$$

Thus, with the help of Eq. (4.32) the inverse BCS exponent in the lattice becomes:

$$\lambda_c=\mathcal{R}_{l=1}\frac{m^*}{m}\lambda_c^0=\frac{\lambda_c^0}{2}\left(\frac{b}{\xi_0}\right)^4\exp\left[-\frac{cb^2}{\xi_0^2}\right], \tag{4.46}$$

where $c\simeq 0.3$.

We now clearly see that the inverse BCS exponent λ_c in the lattice is exponentially small compared to its value in free space. In particular, already for $b/\xi_0=5$ the ratio λ_c^0/λ_c it is about 6, which practically suppresses p-wave superfluidity of identical fermions (see Fig. 4.2). However, this ratio rapidly reduces with decreasing the ratio b/ξ_0 and becomes ~ 1 for $b/\xi_0=4$. It is therefore interesting to analyze more carefully the case of moderate lattice depths.

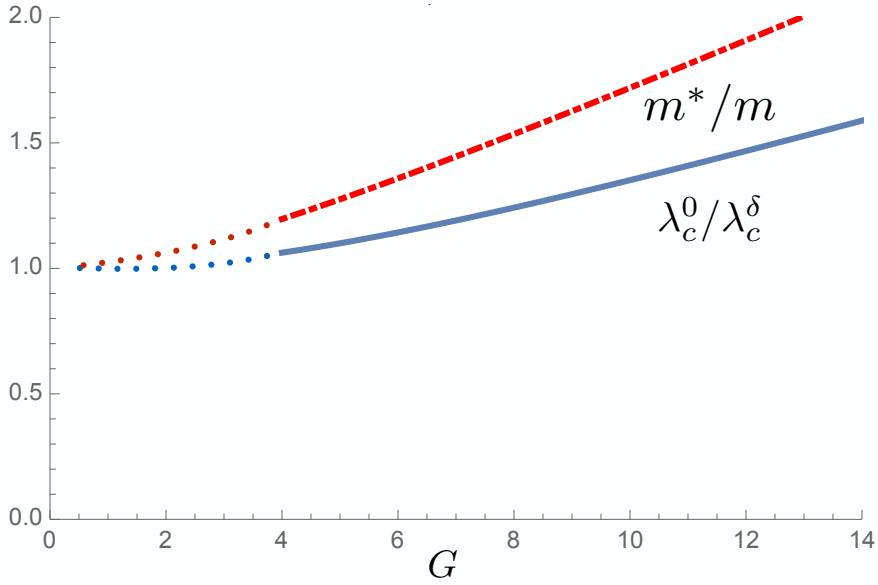

Figure 4.3: The ratio of the BCS exponent in the 2D δ-functional Kronig-Penney lattice to the BCS exponent in free space, $\lambda_c^0/\lambda_c^\delta$, at the same density and short-range coupling strength. The solid blue curve shows $\lambda_c^0/\lambda_c^\delta$ as a function of the lattice depth G, and the dashed red curve the effective mass m^*/m versus G. The dotted parts of these curves show our expectation at $G \lesssim 1$, where the single-band approximation used in our calculations does not work.

4.2.3 Superfluid p-wave pairing in the 2D Kronig-Penney lattice

We will do so using a 2D version of the Kronig-Penney model, namely a superposition of two 1D Kronig-Penney lattices (in the x and y directions, respectively), with a δ-functional form of potential barriers:

$$U(x,y) = U_0 b \sum_{j=-\infty}^{+\infty} \left[\delta(x - jb) + \delta(y - jb)\right]. \tag{4.47}$$

With the eigenfunctions being piecewise plane waves, the 1D Kronig-Penney potential is used in ultracold atom theory (see, e.g. [173,174,315,316]) to mimic sinusoidal potentials. The model (4.47) catches the key physics and allows for transparent calculations. The latter circumstance is a great advantage compared to sinusoidal lattices where single particle states are described by complicated Mathieu functions. The considered model allows us to investigate two important questions. The first question is about an interplay between an increase of the DOS and the modification of the fermion-fermion interaction for moderate lattice depths. The second one is the stability of the system with respect to collisional losses.

Single-particle energies in the periodic potential (4.47) are represented as

$$E_{\mathbf{k}} = E(k_x) + E(k_y), \tag{4.48}$$

where $E(k_{x,y}) > 0$ is the dispersion relation for the 1D Kronig–Penney model. It follows from the equation (see, e.g., Ref. [317]):

$$\cos(qb) + G\frac{\sin(qb)}{qb} = \cos(kb), \tag{4.49}$$

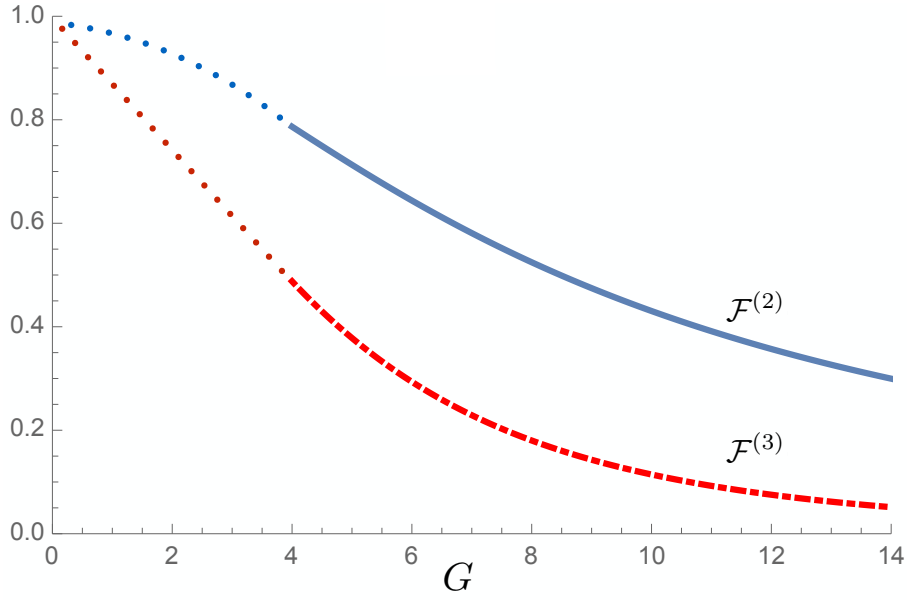

Figure 4.4: Coefficients $\mathcal{F}^{(2)}$ and $\mathcal{F}^{(3)}$ as functions of the lattice depth G. The dotted parts of the curves show our expectation at $G \lesssim 1$, where the single-band approximation used in our calculations does not work.

where $q{=}\sqrt{2mE(k)} > 0$, and $G = mU_0b^2$. As well as in the previous section, we consider a dilute regime where the filling factor is $\nu = nb^2{\lesssim}1$ and the fermions fill only a small energy interval near the bottom of the lowest Brillouin zone. Then the energy counted from the bottom of the zone is given by Eq. (4.7) and for the effective mass Eq. (4.49) yields:

$$\frac{m^*}{m} \approx \frac{\tan(\eta/2)}{\eta}\left[1+\frac{\sin\eta}{\eta}\right], \tag{4.50}$$

with η being the smallest root of the equation:

$$\eta\tan(\eta/2) = G. \tag{4.51}$$

Actually, $\eta = q_0b$ where q_0 follows from Eq. (4.49) at $k = 0$.

For $m^* \gg m$ we have $m^*/m = G/\pi^2$, which means that the quantity G should be very large. Then the width of the lowest Brillouin zone is $E_B = 2/m^*b^2$ and it is much larger than the Fermi energy $E_F = k^2/2m^*$ for $k_Fb < 0.5$. The gap between the lowest and second zones is $E_G = 3\pi^2/2mb^2$ and it greatly exceeds E_B and E_F. Note that even for $m^* \simeq 1.3m$ ($G \simeq 5$) we have E_G close to $4E_B$, and the ratio E_F/E_B is significantly smaller than unity if $k_Fb < 0.5$. This justifies the single-band approximation and the use of the quadratic dispersion relation (4.7).

Single-particle wavefunctions $\chi_{\mathbf{k}}(\mathbf{r})$ are of the form $\chi_{\mathbf{k}}(\mathbf{r}) = \chi_{k_x}(x)\chi_{k_y}(y)$, where

$$\chi_{k_x}(x){=}\frac{\sqrt{2}\sin(\eta/2)}{\sqrt{1+\sin\eta/\eta}}\sum_{j=-\infty}^{j=+\infty}A_j(x)\exp\left[ik_xjb\right]\left\{\frac{e^{iqb}e^{iq(x-jb)}}{e^{iqb}-e^{ik_xb}}-\frac{e^{-iqb}e^{-iq(x-jb)}}{e^{-iqb}-e^{ik_xb}}\right\} \tag{4.52}$$

is the exact eigenfunction of the 1D Kronig-Penney model, with $A_j(x) = 1$ for $(j-1)b < x < jb$ and zero otherwise. The function $\chi_{k_y}(y)$ has a similar form. For $k'b \ll 1$ and $kb \ll 1$ the p-wave parts of the wavefunctions, $\Phi^{(0)}_{1k'}$ and Φ_{1k}, following from Eqs. (4.14),

(4.21), and (4.22) at $l = 1$ turn out to be

$$\Phi^{(0)}_{1k'} = ik'r\frac{\eta\cot(\eta/2)}{[1+\sin\eta/\eta]^2}\sum_{j_x,j_y=-\infty}^{\infty} A_{j_x}(x_+)A_{j_y}(y_+) \tag{4.53}$$
$$\times\left\{\cos\phi_{\mathbf{r}}\cos^2\left(q_0y_+ - j_yb + \frac{b}{2}\right) + i\sin\phi_{\mathbf{r}}\cos^2\left(q_0x_+ - j_xb + \frac{b}{2}\right)\right\};$$
$$\Phi_{1k} = 2i\zeta_1(r)\frac{\eta\cot(\eta/2)}{[1+\sin\eta/\eta]^2}\sum_{j_x,j_y=-\infty}^{\infty} A_{j_x}(x_+)A_{j_y}(y_+) \tag{4.54}$$
$$\times\left\{\cos\phi_{\mathbf{r}}\cos^2\left(q_0y_+ - j_yb + \frac{b}{2}\right) + i\sin\phi_{\mathbf{r}}\cos^2\left(q_0x_+ - j_xb + \frac{b}{2}\right)\right\},$$

where the function $\zeta_1(r)$ is defined after equation (4.43). For the ratio of the lattice to free space scattering amplitude we then obtain:

$$\mathcal{R}_{l=1} = \frac{\eta^2\cot^2(\eta/2)}{[1+\sin\eta/\eta]^4}\left[\frac{3}{2} + \frac{2\sin\eta}{\eta} + \frac{\sin 2\eta}{4\eta}\right], \tag{4.55}$$

and using Eq. (4.50) the inverse BCS exponent in the lattice is expressed through the inverse BCS exponent in free space as

$$\lambda_c^\delta = \mathcal{R}_{l=1}\frac{m^*}{m}\lambda_c^0 = \frac{\eta\cot(\eta/2)}{[1+\sin\eta/\eta]^3}\left[\frac{3}{2} + \frac{2\sin\eta}{\eta} + \frac{\sin 2\eta}{4\eta}\right]\lambda_c^0. \tag{4.56}$$

In the extreme limit of $G \gg 1$ we have $\eta \simeq (\pi - 2\pi/G)$, so that $\mathcal{R}_{l=1} \simeq \pi^4/G^2$ and $\lambda_c^\delta/\lambda_c^0 \simeq \pi^2/G \ll 1$. We thus arrive at the same conclusion as in the previous section for sinusoidal lattices: in a very deep lattice the p-wave pairing of identical fermions is suppressed. However, even for $G \simeq 20$ the BCS exponent in the lattice exceeds the exponent in free space only by a factor of 1.7 at the same density and short-range coupling strength (see Fig. 4.3). It is thus crucial to understand what happens with the rates of inelastic decay processes in the lattice setup.

A detailed derivation of the rates of two-body inelastic relaxation and three-body recombination is given in Appendix B. We obtain that in the lattice the two-body inelastic relaxation is reduced by a factor of $\mathcal{F}_2$ compared to free space:

$$W_2^{\text{lat}} = \mathcal{F}_2(\eta)W_2^{\text{free}}. \tag{4.57}$$

The function $\mathcal{F}_2(\eta)$ follows from Eq. (B25) and is displayed in Fig. 4.4 versus the lattice depth G, which is related to η by Eq. (4.51).

The relation between the three-body recombination decay rate in free space and the one in the 2D lattice reads:

$$W_3^{\text{lat}} = W_3^{\text{free}}\mathcal{F}_3(\eta). \tag{4.58}$$

The function $\mathcal{F}_3$ is shown in Fig. 4.4 versus the lattice depth G related to η by Eq. (4.51). The results of this Section indicate that both two-body and three-body inelastic collisions are significantly suppressed in the lattice setup even at moderate depths.

The obtained results indicate that there are possibilities to create the superfluid topological $p_x + ip_y$ phase of atomic lattice fermions. In deep lattices the p-wave superfluid pairing is suppressed and even for moderate lattice depths the BCS exponent is larger than in free space at the same density and short-range coupling strength. However, the

lattice setup significantly reduces the inelastic collisional losses, so that one can get closer to the p-wave Feshbach resonance and increase the interaction strength without inducing a rapid decay of the system.

For ultracold ^{6}Li the p-wave resonance is observed for atoms in the lowest hyperfine state $(1/2, 1/2)$ [137–143], and the only decay channel is three-body recombination. In the 2D Kronig-Penney lattice with the depth $G \simeq 12$ and the period $b \simeq 200$ nm ($m^*/m \simeq 2$ and $\mathcal{R}_{l=1}m^*/m \approx 0.7$), at $k_F b \simeq 0.5$ the Fermi energy is close to 100 nK and the 2D density is about 0.5×10^8 cm^{-2}. Slightly away from the Feshbach resonance (at the scattering volume $V_{sc} \simeq 8 \times 10^{-15}$ cm^3) we are still in the weakly interacting regime, and the 3D recombination rate constant is $\alpha_{rec}^{3D} \sim 10^{-24}$ cm^6/s [137]. Then, using Eq. (4.25) and the quasi2D scattering amplitude expressed through V_{sc} and the tight confinement length $l_0 = \sqrt{1/m\omega_0}$ [320], for the confinement frequency $\omega_0 \simeq 100$ kHz we obtain the BCS critical temperature $T_c \simeq 5$ nK. The 2D recombination rate constant is $\alpha_{rec}^{2D} \approx \mathcal{F}_3 \alpha_{rec}^{3D}/\sqrt{3}\pi l_0^2$ and with $\mathcal{F}_3 \simeq 0.05$ at $G \simeq 12$ we arrive at the decay time $\tau_{rec} \sim 1/\alpha_{rec}^{2D} n^2$ approaching 1 second.

The p-wave Feshbach resonance for ^{40}K occurs between atoms in the excited hyperfine state $(9/2, -7/2)$. Therefore, there is also a decay due to two-body relaxation. For the same parameters as in the discussed Li case (G, V_{sc}, l_0, b, n) we then have the Fermi energy $E_F \simeq 20$ nK, and the BCS transition temperature approaches 1 nK. Using experimental values for the relaxation and recombination rate constants in 3D [134] and retransforming them to the 2D lattice case, we obtain the relaxation and recombination times of the order of seconds.

4.3 P-wave superfluids of fermionic polar molecules in a 2D lattice

4.3.1 Scattering problem for microwave-dressed polar molecules in 2D lattices

We will consider identical fermionic polar molecules in a 2D lattice of period b (see Fig. 4.5). Being dressed with a microwave field, they acquire an attractive dipole-dipole tail in the interaction potential [122, 123, 318, 319]:

$$V(r) = -d^2/r^3. \tag{4.59}$$

Here d is an effective dipole moment, and we assume that Eq. (4.59) is valid at intermolecular distances $r \gtrsim b$.

In the low momentum limit at a small filling factor the system of lattice polar molecules is equivalent to that of molecules with effective mass m^* in free space. We now demonstrate this explicitly by the calculation of the off-shell scattering amplitude $f(\mathbf{k}', \mathbf{k})$. For our problem the main part of the scattering amplitude can be obtained in the Born approximation [122, 123].

In the lattice the scattering amplitude is, strictly speaking, the function of both incoming quasimomenta $\mathbf{q}_1, \mathbf{q}_2$ and outgoing quasimomenta $\mathbf{q}_1', \mathbf{q}_2'$. However, in the low-momentum limit where $qb \ll 1$, taking into account the momentum conservation law the amplitude becomes the function of only relative momenta $\mathbf{k}=(\mathbf{q}_1 - \mathbf{q}_2)/2$ and $\mathbf{k}'=(\mathbf{q}_1' -$

$\mathbf{q}_2')/2$. For the off-shell scattering amplitude the first Born approximation gives:

$$\begin{aligned} f(\mathbf{k}',\mathbf{k}) &= S\int \chi^*_{\mathbf{q}_1'}(\mathbf{r}_1)\chi^*_{\mathbf{q}_2'}(\mathbf{r}_2)V(\mathbf{r}_1-\mathbf{r}_2)\chi_{\mathbf{q}_1}(\mathbf{r}_1)\chi_{\mathbf{q}_2}(\mathbf{r}_2)d^2r_1d^2r_2 \\ &= -\frac{d^2b^4}{S}\sum_{\mathbf{r}_j,\mathbf{r}_j'}\frac{\exp[i(\mathbf{q}_1-\mathbf{q}_1')\mathbf{r}_j+i(\mathbf{q}_2\mathbf{q}_2')\mathbf{r}_j']}{|\mathbf{r}_j-\mathbf{r}_j'|^3}, \end{aligned} \tag{4.60}$$

where $V(\mathbf{r}_1-\mathbf{r}_2)$ is given by Eq. (4.59), and S is the surface area. The last line of Eq. (4.60) is obtained assuming the tight-binding regime, where the single particle wavefunction is

$$\chi_{\mathbf{q}}(\mathbf{r}) = \frac{1}{\sqrt{N}}\sum_j \Phi_0(\mathbf{r}-\mathbf{r}_j)\exp\left[i\mathbf{q}\mathbf{r}_j\right]. \tag{4.61}$$

Here, the index j labels the lattice sites located at the points $\mathbf{r}_j$, and $N = S/b^2$ is the total number of sites. The particle wavefunction in a given site j has extension ξ_0 and is expressed as

$$\Phi_0(\mathbf{r}-\mathbf{r}_j) = (1/\sqrt{\pi}\xi_0)\exp[-(\mathbf{r}-\mathbf{r}_j)^2/2\xi_0^2]. \tag{4.62}$$

In the low-momentum limit we may replace the summation over j and j' by the integration over d^2r_j and d^2r_j' taking into account that $b^2\sum_j$ transforms into $\int d^2r_j$. This immediately yields

$$f(\mathbf{k}',\mathbf{k}) = -d^2\int \exp[i(\mathbf{k}-\mathbf{k}')\mathbf{r}]\frac{d^2r}{r^3}, \tag{4.63}$$

and the p-wave part of the scattering amplitude is obtained multiplying Eq. (4.63) by $\exp(-i\phi)$ and integrating over $d\phi/2\pi$, where ϕ is the angle between the vectors $\mathbf{k}$ and $\mathbf{k}'$. This is the same result as in free space (see, e.g., Refs. [122,123]). The on-shell amplitude ($k = k'$) can be written as

$$f(k) = -(8\hbar^2/3m^*)kr^*_{\text{eff}}, \tag{4.64}$$

where $r^*_{\text{eff}} = m^*d^2/\hbar^2$ is the effective dipole-dipole distance in the lattice. The applicability of the Born approximation assumes that $kr^*_{\text{eff}} \ll 1$, which is clearly seen by calculating the second order correction to the scattering amplitude.

Up to the terms $\sim (kr^*_{\text{eff}})^2$, the on-shell scattering amplitude following form the solution of the scattering problem for particles with mass m^*, is given by [122,123]:

$$f(k) = -\frac{8}{3}\frac{\hbar^2}{m}kr^* + \frac{\pi}{2}\frac{\hbar^2}{m}(kr^*)^2\ln\left(Bkr^*\right), \tag{4.65}$$

where the numerical coefficient B comes form short-range physics. For calculating B we introduce a perfectly reflecting wall at intermolecular distances $r \sim b$, which takes into account that two fermions practically can not get to one and the same lattice site. The coefficient B depends on the ratio r^*_{eff}/b, and we show this dependence in Fig. 4.6a.

4.3.2 *P*-wave pairing of microwave-dressed polar molecules in a 2D lattice

Being dressed with a microwave field, polar molecules acquire an attractive dipole-dipole tail in the interaction potential. This leads to superfluid p-wave pairing of identical molecules. In free space the emerging ground state is the topological $p_x + ip_y$ superfluid,

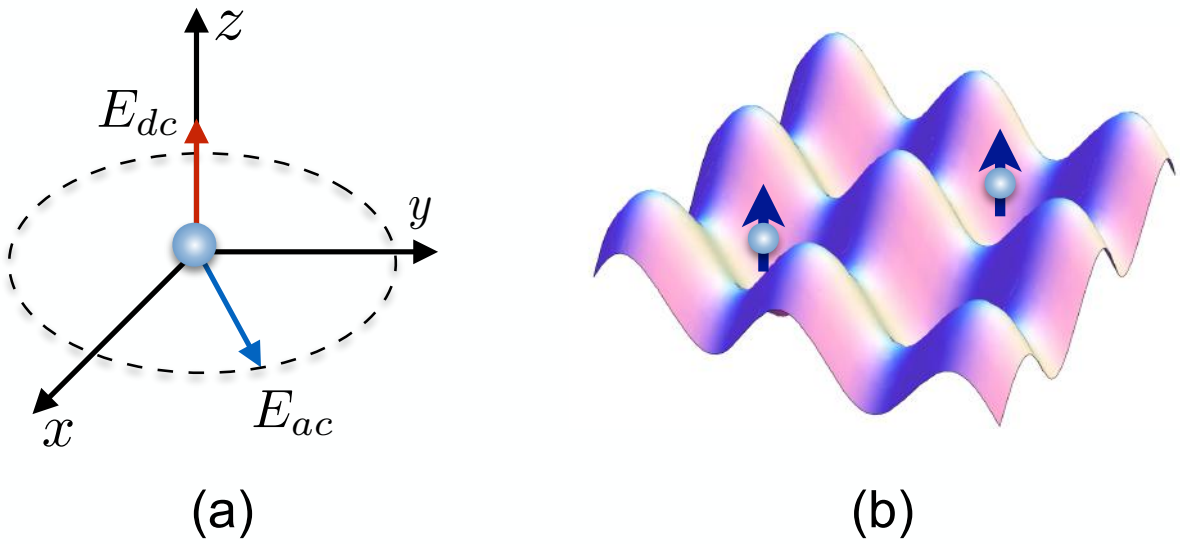

Figure 4.5: In (a) polar molecule in an external microwave field E_{ac} rotating in the plane perpendicular to the stationary field E_{dc} (upper part), and in (b) microwave-dressed polar molecules loaded in a 2D lattice.

and the leading part of the scattering amplitude can be obtained in the first Born approximation [122, 123]. We assume the weakly interacting regime at a small filling factor in the lattice, $k_F b \ll 1$.

The Hamiltonian of the system is $\hat{\mathcal{H}} = \hat{H}_0 + \hat{H}_{\rm int}$, with

$$\hat{H}_0 = \sum\nolimits_{\mathbf{q}} \varepsilon_{\mathbf{q}} \hat{a}^\dagger_{\mathbf{q}} \hat{a}_{\mathbf{q}}, \tag{4.66}$$

where $\hat{a}_{\mathbf{q}}$, $\hat{a}^\dagger_{\mathbf{q}}$ are the annihilation and creation operators of a molecule with quasimomentum $\mathbf{q}$, and $\varepsilon_{\mathbf{q}}$ is the single particle energy. In the low momentum limit we have $\varepsilon_{\mathbf{q}} = \hbar^2 q^2/2m^*$, where $m^* > m$ is the effective mass in the lowest Bloch band. The quantity $\hat{H}_{\rm int}$ describes the interaction between the molecules and is given by

$$\hat{H}_{\rm int} = -\frac{1}{2} \sum_{\mathbf{r}_j \neq \mathbf{r}'_j} \hat{\psi}^\dagger(\mathbf{r}_j) \hat{\psi}^\dagger(\mathbf{r}'_j) \frac{d^2}{|\mathbf{r}_j - \mathbf{r}'_j|^3} \hat{\psi}(\mathbf{r}'_j) \hat{\psi}(\mathbf{r}_j), \tag{4.67}$$

where $\hat{\psi}(\mathbf{r}_j)$ is the field operator of a particle in the lattice site j located at $\mathbf{r}_j$ in the coordinate space. At a small filling factor in the low momentum limit, the main contribution to the matrix elements of $\hat{H}_{\rm int}$ comes from intermolecular distances $|\mathbf{r}_j - \mathbf{r}'_j| \gg b$. Therefore, we may replace the summation over $\mathbf{r}_j$ and $\mathbf{r}'_j$ by the integration over $d^2\mathbf{r}_j$ and $d^2\mathbf{r}'_j$. As a result the Hamiltonian of the system reduces to

$$\hat{H} = -\int \frac{\hbar^2}{2m^*} \hat{\psi}^\dagger(\mathbf{r}) \nabla^2 \hat{\psi}(\mathbf{r}) d^2 r - \frac{d^2}{2} \int \frac{d^2 r d^2 r'}{|\mathbf{r} - \mathbf{r}'|^3} \hat{\psi}^\dagger(\mathbf{r}) \hat{\psi}^\dagger(\mathbf{r}') \hat{\psi}(\mathbf{r}') \hat{\psi}(\mathbf{r}), \tag{4.68}$$

where the first term in the right hand side is $\hat{H}_0$ (4.66) rewritten in the coordinate space. We thus see that the problem becomes equivalent to that of particles with mass m^* in free space.

The scattering amplitude at $k = k_F$ is obtained from the solution of the scattering problem in the lattice (see Subsection 4.3.1). For particles that have mass m^*, the

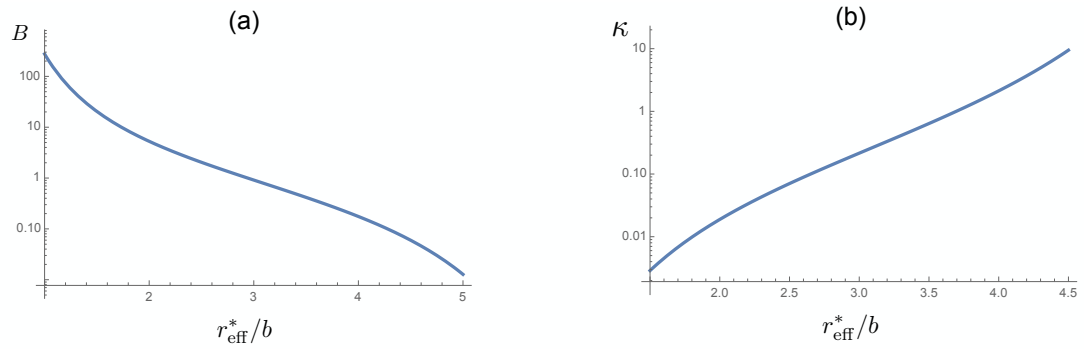

Figure 4.6: Coefficients B and κ as functions of $r^*_{\rm eff}/b$.

amplitude is written as follows:

$$f(k_F) = -\frac{8}{3}\frac{\hbar^2}{m^*}k_F r^*_{\rm eff} + \frac{\pi}{2}\frac{\hbar^2}{m^*}(k_F r^*_{\rm eff})^2 \ln\left(B k_F r^*_{\rm eff}\right), \tag{4.69}$$

where $k_F r^*_{\rm eff} \ll 1$, and B is a numerical coefficient coming from short-range physics. Since for weak interactions two fermions practically do not get to the same lattice site, for calculating B we may introduce a perfectly reflecting wall at intermolecular distances $r \sim b$. For the superfluid pairing the most important are particle momenta $\sim k_F$. Therefore, the low-momentum limit requires the inequality $k_F b \ll 1$. The the coefficient B as the of function $r^*_{\rm eff}/b$ is shown in Fig. 4.6.

The treatment of the superfluid pairing is the same as in Ref. [122], including the Gor'kov-Melik-Barhudarov correction [314]. We should only replace the mass m with m^*. The expression for the critical temperature then becomes:

$$T_c = E_F \frac{\kappa}{(k_F r^*_{\rm eff})^{9\pi^2/64}} \exp\left[-\frac{3\pi}{4 k_F r^*_{\rm eff}}\right], \tag{4.70}$$

where $\kappa \simeq 0.19 B^{-9\pi^2/64}$. The coefficient κ is displayed in Fig. 4.6b as a function of $r^*_{\rm eff}/b$. There are two important differences of equation (4.70) from a similar equation in free space obtained in Ref. [122]. First, the Fermi energy E_F is smaller by a factor of m/m^*, and the effective dipole-dipole distance $r^*_{\rm eff}$ is larger than the dipole-dipole distance in free space by m^*/m. Second, the coefficient B and, hence, κ in free space is obtained from the solution of the Schrödinger equation in the full microwave-induced potential of interaction between two molecules, whereas here B follows from the fact that the relative wavefunction is zero for $r \leq b$ (perfectly reflecting wall).

It is clear that for the same 2D density n (and k_F) the critical temperature in the lattice is larger than in free space because the BCS exponent in Eq. (4.70) is smaller. However, in ordinary optical lattices one has the lattice constant $b \gtrsim 200$ nm. In this case, for $m^*/m \approx 2$ (still the tight binding case with $b/\xi_0 \approx 3$, where ξ_0 is the extension of the particle wavefunction in the lattice site) and at a fairly small filling factor (let say, $k_F b = 0.35$) the Fermi energy for the lightest alkaline polar molecules NaLi is about 10 nK ($n \approx 2 \times 10^7$ cm^{-2}). Then, for $k_F r^*_{\rm eff}$ approaching unity the critical temperature is of the order of a nanokelvin (for $k_F b = 0.35$ and $r^*_{\rm eff}/b \approx 3$ Fig. 4.6 gives $\kappa \sim 1$).

4.4 Concluding remarks

The critical temperature of proposed p-wave lattice superfluids was estimated on the level of a few nanokelvins, which is fairly low. The situation is quite different in

recently introduced subwavelength lattices, where the lattice constant can be as small as $b \simeq 50$ nm [163–174]. This strongly increases all energy scales. Then, in the case of fermionic atoms for $k_F b = 0.5$ the density and the Fermi energy will be higher by an order of magnitude. Hence, departing from the Feshbach resonance one gets the same BCS exponent as in the ordinary lattice, and the critical temperature for ^{6}Li will be ∼50 nK. The recombination time is again on the level of a second.

Note that there is a (second-order) process, in which the interaction between two identical fermions belonging to the lowest Bloch band provides a virtual transfer of one of them to a higher band. Then, the two fermions may get to the same lattice site and undergo the inelastic process of collisional relaxation. The rate constant of this second-order process is roughly equal to the rate constant in free space, multiplied by the ratio of the scattering amplitude (divided by the elementary cell area) to the frequency of the potential well in a given lattice site (the difference in the energies of the Bloch bands). This ratio originates from the virtual transfer of one of the fermions to a higher band and does not exceed $(\xi/b)^2$. Even in not a deep lattice, where m^*/m is 2 or 3, we have $(\xi/b)^2 < 0.1$. Typical values of the rate constant of inelastic relaxation in free space are $\sim 10^{-8}$–10^{-9} cm^2/s [122], and hence in the lattice it will be lower than 10^{-9} or even 10^{-10} cm^2/s. Thus, the rate of this process is rather low and for densities approaching 10^9 cm^{-2} the decay time will be on the level of seconds or even tens of seconds.

For NaLi molecules taking $b = 50$ nm and $k_F b = 0.35$, the Fermi energy exceeds 200 nK ($n \approx 4 \times 10^8$ cm^{-2}). Then, for the same $\kappa \sim 1$ and $k_F r^*_{\rm eff}$ approaching unity we have $T_c \sim 20$ nK, which is twice as high as in free space. An additional advantage of the lattice system is the foreseen quantum information processing, since addressing qubits in the lattice is much easier than in free space.

Superfluidity itself can be detected in the same way as in the case of s-wave superfluids [8,321]. Rotating the $p_x + ip_y$ superfluid and inducing the appearance of vortices one can find signatures of Majorana modes on the vortex cores in the RF absorption spectrum [322]. Eventually, one can think of revealing the structure of the order parameter by visualizing vortex-related dips in the density profile on the approach to the strongly interacting regime, where these dips should be pronounced at least in time-of-flight experiments.

Appendix B. Inelastic decay processes

We first consider the two-body relaxation, assuming that both colliding atoms are in an excited (internal energy E_0) hyperfine state and they relax to the ground state. The released hyperfine-state energy $2E_0$ goes to the kinetic energy of the atoms. It greatly exceeds the Fermi energy and the lattice potential depth, so that the relative motion of the atoms in the final state is described by a 3D plane wave with a high momentum and they escape from the system. Then the number of relaxation events per unit time can be written in the form (see, e.g. Ref. [325]):

$$W_2 = \int_{-\infty}^{\infty} dt \sum_i \rho_i \langle |\hat{H}'(0)\hat{H}'(t)| \rangle, \tag{B1}$$

where ρ_i is the equilibrium density matrix, and $\hat{H}'$ is the Hamiltonian responsible for the relaxation process:

$$\hat{H}'(t) = \exp\{i\hat{H}_0 t\}\hat{H}'(0)\exp\{-i\hat{H}_0 t\}, \tag{B2}$$

with $\hat{H}_0$ being the Hamiltonian of elastic interaction, and

$$\hat{H}'(0) = \int d\vec{\mathbf{r}}_1 d\vec{\mathbf{r}}_2 V_r(\vec{\mathbf{r}}_1 - \vec{\mathbf{r}}_2) \left[\hat{\Phi}^\dagger(\vec{\mathbf{r}}_2)\hat{\Phi}^\dagger(\vec{\mathbf{r}}_1)\hat{\psi}(\vec{\mathbf{r}}_1)\hat{\psi}(\vec{\mathbf{r}}_2) + \text{h.c.}\right]. \tag{B3}$$

Here $\vec{\mathbf{r}}_1$ and $\vec{\mathbf{r}}_2$ are the 3D coordinates of the atoms, $\hat{\psi}(\vec{\mathbf{r}})$ is the field operator of the initial-state atoms, and $V_r(\vec{\mathbf{r}}_1 - \vec{\mathbf{r}}_2)$ is the interaction potential causing the inelastic relaxation. The field operator of atoms in the final (ground) internal state is

$$\Phi(\vec{\mathbf{r}}) = \sum\nolimits_{\vec{\mathbf{q}}} \hat{a}_{\vec{\mathbf{q}}} \exp(i\vec{\mathbf{q}}\vec{\mathbf{r}}), \tag{B4}$$

and initially these states are not occupied. We thus have:

$$\begin{aligned} W_2 = \int_{-\infty}^{\infty} dt \int d\vec{\mathbf{r}}_1 d\vec{\mathbf{r}}_2 d\vec{\mathbf{r}'}_1 d\vec{\mathbf{r}'}_2 V_r(\vec{\mathbf{r}}_1 - \vec{\mathbf{r}}_2) V_r(\vec{\mathbf{r}'}_1 - \vec{\mathbf{r}'}_2) \\ \times \exp\{i\vec{\mathbf{q}}_1(\vec{\mathbf{r}}_1 - \vec{\mathbf{r}'}_1) + i\vec{\mathbf{q}}_2(\vec{\mathbf{r}}_2 - \vec{\mathbf{r}'}_2) - i[2E_0 - \hbar^2(q_1^2 + q_2^2)/2m]t\} \\ \times \langle \hat{\psi}^\dagger(\vec{\mathbf{r}}_1, 0)\hat{\psi}^\dagger(\vec{\mathbf{r}}_2, 0)\hat{\psi}(\vec{\mathbf{r}'}_2, t)\hat{\psi}(\vec{\mathbf{r}'}_1, t)\rangle. \end{aligned} \tag{B5}$$

The momenta q_1 and q_2 are large but the center of mass momentum $|\vec{\mathbf{q}}_1 + \vec{\mathbf{q}}_2|$ is almost zero. The energy conservation law then reads:

$$2E_0 = \frac{p^2}{m}, \tag{B6}$$

where $\vec{\mathbf{p}} = (\vec{\mathbf{q}}_1 - \vec{\mathbf{q}}_2)/2$ is the relative momentum. From the summation over $\vec{\mathbf{q}}_1, \vec{\mathbf{q}}_2$ we turn to the integration over $\vec{\mathbf{p}}$ and $(\vec{\mathbf{q}}_1 + \vec{\mathbf{q}}_2)$. The coordinate-dependent part of the exponent in Eq. (B5) takes the form:

$$\exp\{i\vec{\mathbf{q}}_1(\vec{\mathbf{r}}_1 - \vec{\mathbf{r}'}_1) + i\vec{\mathbf{q}}_2(\vec{\mathbf{r}}_2 - \vec{\mathbf{r}'}_2)\} = \exp\{i(\vec{\mathbf{q}}_1 + \vec{\mathbf{q}}_2)(\vec{\mathbf{R}} - \vec{\mathbf{R}'}) + i\vec{\mathbf{p}}(\vec{\mathbf{r}} - \vec{\mathbf{r}'})\}, \tag{B7}$$

where $\vec{\mathbf{R}} = (\vec{\mathbf{r}}_1 + \vec{\mathbf{r}}_2)/2$, $\vec{\mathbf{R}'} = (\vec{\mathbf{r}'}_1 + \vec{\mathbf{r}'}_2)/2$, $\vec{\mathbf{r}} = \vec{\mathbf{r}}_1 - \vec{\mathbf{r}}_2$, and $\vec{\mathbf{r}'} = \vec{\mathbf{r}'}_1 - \vec{\mathbf{r}'}_2$. The integration over $(\vec{\mathbf{q}}_1 + \vec{\mathbf{q}}_2)$ yields:

$$\int \frac{d(\vec{\mathbf{q}}_1 + \vec{\mathbf{q}}_2)}{(2\pi)^3} \exp\{i(\vec{\mathbf{q}}_1 + \vec{\mathbf{q}}_2)(\vec{\mathbf{R}} - \vec{\mathbf{R}'})\} = \delta(\vec{\mathbf{R}} - \vec{\mathbf{R}'}), \tag{B8}$$

and the correlation function becomes:

$$\langle\hat{\psi}^\dagger(\vec{\mathbf{r}}_1,0)\hat{\psi}^\dagger(\vec{\mathbf{r}}_2,0)\hat{\psi}(\vec{\mathbf{r}'}_2,t)\hat{\psi}(\vec{\mathbf{r}'}_1,t)\rangle =$$
$$\langle\hat{\psi}^\dagger(\vec{\mathbf{R}}+\vec{\mathbf{r}'}/2)\hat{\psi}^\dagger(\vec{\mathbf{R}}-\vec{\mathbf{r}'}/2)\hat{\psi}(\vec{\mathbf{R}}-\vec{\mathbf{r}}/2,t)\hat{\psi}(\vec{\mathbf{R}}+\vec{\mathbf{r}}/2,t)\rangle.$$

Characteristic times t on which the correlation function changes are of the order of the inverse Fermi energy or even larger. They are much longer than the times $\sim E_0^{-1}$ that dominate the integral over dt in Eq. (B5). Therefore, we may put $t=0$ in the correlation function, which reduces Eq. (B5) to

$$W_2 = \int \tilde{W}_2(\vec{\mathbf{r}},\vec{\mathbf{r}'})d\vec{\mathbf{R}}d\vec{\mathbf{r}}d\vec{\mathbf{r}'}\langle\hat{\psi}^\dagger(\vec{\mathbf{R}}+\vec{\mathbf{r}}'/2)\hat{\psi}^\dagger(\vec{\mathbf{R}}-\vec{\mathbf{r}}'/2)\hat{\psi}(\vec{\mathbf{R}}-\vec{\mathbf{r}}/2)\hat{\psi}(\vec{\mathbf{R}}+\vec{\mathbf{r}}/2)\rangle, \quad \text{(B9)}$$

with

$$\tilde{W}_2 = \int V_r(\vec{\mathbf{r}})V_r(\vec{\mathbf{r}'})\exp\{i\vec{\mathbf{p}}(\vec{\mathbf{r}}-\vec{\mathbf{r}'})\}\delta\left(2E_0-\frac{p^2}{m}\right)\frac{d\vec{\mathbf{p}}}{(2\pi)^2}. \quad \text{(B10)}$$

In the quasi-2D geometry the field operator can be written as

$$\hat{\psi}(\vec{\mathbf{r}}_{1,2}) = \psi_0(z_{1,2})\psi(\mathbf{r}_{1,2}), \quad \text{(B11)}$$

where $\mathbf{r}_{1,2}$ is the 2D vector in the x,y plane, and

$$\psi_0(z_{1,2}) = \frac{1}{(\pi l_0^2)^{1/4}}\exp\left[-\frac{z_{1,2}^2}{2l_0^2}\right] \quad \text{(B12)}$$

is the wavefunction in the tightly confined z-direction. Strictly speaking, the use of this relation in the correlation function

$$\langle\hat{\psi}^\dagger(\vec{\mathbf{R}}+\vec{\mathbf{r}'}/2)\hat{\psi}^\dagger(\vec{\mathbf{R}}-\vec{\mathbf{r}'}/2)\hat{\psi}(\vec{\mathbf{R}}+\vec{\mathbf{r}}/2)\hat{\psi}(\vec{\mathbf{R}}-\vec{\mathbf{r}'}/2)\rangle \quad \text{(B13)}$$

requires interparticle distances r, r' exceeding the interaction radius r_0 (but under the condition $r_0 \ll l_0$ they can still be much smaller than the confinement length l_0). This leads to renormalization of the integrand in the expression for $\tilde{W}_2(\vec{\mathbf{r}},\vec{\mathbf{r}'})$, which in the lattice occurs in the same way as in free space. As the inelastic relaxation occurs at interparticle distances much smaller than the confinement length l_0, the product of four field operators in Eq. (B9) becomes

$$\hat{\psi}^\dagger(\mathbf{R}+\mathbf{r}'/2)\hat{\psi}^\dagger(\mathbf{R}-\mathbf{r}'/2)\hat{\psi}(\mathbf{R}-\mathbf{r}/2)\hat{\psi}(\mathbf{R}+\mathbf{r}/2)\psi_0^4(Z), \quad \text{(B14)}$$

where $\mathbf{R},\mathbf{r}$ and $\mathbf{r}'$ are 2D vectors in the x,y plane, and $Z=(z_1+z_2)/2$. Integrating over Z in Eq. (B9) we then have:

$$W_2 = \int \tilde{w}_2(\mathbf{r},\mathbf{r}')d\mathbf{R}d\mathbf{r}d\mathbf{r}'\langle\hat{\psi}^\dagger(\mathbf{R}+\mathbf{r}'/2)\hat{\psi}^\dagger(\mathbf{R}-\mathbf{r}'/2)\hat{\psi}(\mathbf{R}-\mathbf{r}/2)\hat{\psi}(\mathbf{R}+\mathbf{r}/2)\rangle, \quad \text{(B15)}$$

where

$$\tilde{w}_2(\mathbf{r},\mathbf{r}') = \int \tilde{W}_2(\vec{\mathbf{r}},\vec{\mathbf{r}'})\frac{dzdz'}{\sqrt{2\pi}l_0}, \quad \text{(B16)}$$

with $z=z_1-z_2$ and $z'=z_1'-z_2'$.

Using expansion (4.6) one can express the averaged product of four 2D field operators in terms of the standard Slater determinants $\mathcal{D}(\mathbf{r},\mathbf{R};\mathbf{k}_1,\mathbf{k}_2)$:

$$\begin{aligned}&\langle\hat{\psi}^\dagger(\mathbf{R}+\mathbf{r}'/2)\hat{\psi}^\dagger(\mathbf{R}-\mathbf{r}'/2)\hat{\psi}(\mathbf{R}-\mathbf{r}/2)\hat{\psi}(\mathbf{R}+\mathbf{r}/2)\rangle\\&=\frac{1}{2!}\sum_{\mathbf{k}_1,\mathbf{k}_2}N_{k_1}N_{k_2}\mathcal{D}^*(\mathbf{r}',\mathbf{R};\mathbf{k}_1,\mathbf{k}_2)\mathcal{D}(\mathbf{r},\mathbf{R};\mathbf{k}_1,\mathbf{k}_2),\end{aligned}\tag{B17}$$

where N_k is the Fermi distribution function, and

$$\mathcal{D}(\mathbf{r},\mathbf{R};\mathbf{k}_1,\mathbf{k}_2)=\mathrm{Det}\begin{pmatrix}\chi_{\mathbf{k}_1}(\mathbf{R}+\mathbf{r}/2) & \chi_{\mathbf{k}_1}(\mathbf{R}-\mathbf{r}/2)\\ \chi_{\mathbf{k}_2}(\mathbf{R}+\mathbf{r}/2) & \chi_{\mathbf{k}_2}(\mathbf{R}-\mathbf{r}/2)\end{pmatrix}.\tag{B18}$$

The distance $\mathbf{r}$ between relaxing particles is small compared to the lattice period and particle wavelengths. Therefore, all the wave functions entering Eq. (B18) should be taken within the same lattice cell (n,m) of the considered 2D lattice, so that Eq. (B15) will contain only one double lattice summation over n and m. The Slater determinant (B18) within a given cell (n,m) contains a factor $\exp\left[i(k_{1x}+k_{2x})bn+i(k_{1y}+k_{2y})bm\right]$ [see Eq. (4.52)], which does not contribute to the product $\mathcal{D}^*\mathcal{D}$. Below we will imply that the corresponding exponential factors have been already extracted from the wave functions. In the leading (linear) order in small $\mathbf{r}$ we have:

$$\chi_{\mathbf{k}}\left(\mathbf{R}\pm\frac{\mathbf{r}}{2}\right)\approx\chi_{\mathbf{k}}(\mathbf{R})\left\{1\pm\frac{1}{2}\mathbf{r}\cdot\nabla_{\mathbf{R}}\ln\left[\chi_{\mathbf{k}}(\mathbf{R})\right]\right\},\tag{B19}$$

and the Slater determinant takes the form:

$$\mathcal{D}(\mathbf{r},\mathbf{r};\mathbf{k}_1,\mathbf{k}_2)=\chi_{\mathbf{k}_1}(\mathbf{R})\chi_{\mathbf{k}_2}(\mathbf{R})\mathbf{r}\cdot\nabla_{\mathbf{R}}\left\{\ln\left[\chi_{\mathbf{k}_1}(\mathbf{R})\right]-\ln\left[\chi_{\mathbf{k}_2}(\mathbf{R})\right]\right\}.\tag{B20}$$

As the leading contribution to the scattering of slow identical fermions comes from the p-wave scattering channel, the expression in the curly brackets in Eq. (B20) is linear (in the leading order) in the difference $(\mathbf{k}_1-\mathbf{k}_2)$. For instance, the "$x$-component" of this expression has the form:

$$\ln\left[\chi_{k_{1x}}(X)\right]-\ln\left[\chi_{k_{2x}}(X)\right]=\frac{i(k_{1x}-k_{2x})b}{2\sin(\eta/2)}\frac{\sin\left[q(X-nb)\right]}{\cos\left[q(X-nb)+b/2)\right]},\tag{B21}$$

where X varies from $(n-1)b$ to nb (see Eq. (4.52)). In the considered low density limit $(kb\ll 1)$ we may put $\mathbf{k}_1=0=\mathbf{k}_2$ in the product $\chi_{\mathbf{k}_1}(\mathbf{r}_1)\chi_{\mathbf{k}_2}(\mathbf{r}_1)$ in Eq. (B20). As a result we transform Eq. (B15) to

$$W_2=\frac{\mathcal{F}_2(\eta)}{2}\int\mathbf{r}\mathbf{r}'w_2(\mathbf{r},\mathbf{r}')d\mathbf{r}d\mathbf{r}'\int N_{k_1}N_{k_2}(k_1^2+k_2^2)\frac{d\mathbf{k}_1d\mathbf{k}_2}{(2\pi)^4}.\tag{B22}$$

The quantity $\mathcal{F}_2$ is determined by the integral over the 2D lattice:

$$\mathcal{F}_2=\frac{1}{8\sin^2\eta/2}\sum_{n,m}^{\infty}\int_{-\infty}^{\infty}\int_{-\infty}^{\infty}dxdyA_n(x)A_m(y)|\chi_0(x)|^4|\chi_0(y)|^4\left[P^2(x)+P^2(y)\right],\tag{B23}$$

where the functions $A_j(x)$ are defined below Eq. (4.52), and the function P results from the differentiation of the curly brackets in Eq. (B20) with the use of Eq. (B21):

$$P(u)\equiv\frac{d}{du}\frac{\sin\left[qu\right]}{\cos\left[q(u+b/2)\right]}.\tag{B24}$$

Performing the integration in Eq. (B23) we find

$$\mathcal{F}_2(\eta) = \mathcal{R}_{l=1}(\eta), \tag{B25}$$

with the lattice factor $\mathcal{R}_{l=1}$ given by Eq. (4.55).

In the absence of the 2D lattice (i.e. in free 2D space) we also arrive at Eq. (B15). Then, using $\chi_{\mathbf{k}}(\mathbf{r}) = \exp(i\mathbf{kr})$, the Slater determinant becomes:

$$\mathcal{D}(\mathbf{r}, \mathbf{R}; \mathbf{k}_1, \mathbf{k}_2) \simeq i(\mathbf{k}_1 - \mathbf{k}_2)\mathbf{r} \exp\left[i(\mathbf{k}_1 + \mathbf{k}_2)\mathbf{R}\right]. \tag{B26}$$

Performing integrations we get Eq. (B22) with $\mathcal{F}_2$ replaced by unity. Thus, we obtain that in the lattice the two-body inelastic relaxation is reduced by a factor of $\mathcal{F}_2$ compared to free space:

$$W_2^{\text{lat}} = \mathcal{F}_2(\eta) W_2^{\text{free}}. \tag{B27}$$

The function $\mathcal{F}_2(\eta)$ following from Eqs. (4.55) and (B25) is displayed in Fig. 4.4 versus the lattice depth G, which is related to η by Eq. (4.51).

We complete this Appendix with the discussion of three-body recombination, assuming that the binding energy of the molecule formed in this process greatly exceeds the Fermi energy and the lattice depth. In this case the kinetic energy of the molecule and atom in the output channel of the recombination is very high and they escape from the system. The results for the ratio of the three-body recombination rate in the lattice to the rate in free space are obtained in a way similar to that for the two-body relaxation. The number of recombination events per unit time, W_3, is given by Eq. (B1) in which $\hat{H}'(t)$ follows from Eq. (B2), and the Hamiltonian $\hat{H}'(0)$ is

$$\hat{H}'(0) = \int d\vec{\mathbf{r}}_1 d\vec{\mathbf{r}}_2 \vec{\mathbf{r}}_3 V(\vec{\mathbf{r}}_1, \vec{\mathbf{r}}_2, \vec{\mathbf{r}}_3) \left[\hat{B}^\dagger(\vec{\mathbf{r}}_1, \vec{\mathbf{r}}_2)\hat{\psi}^\dagger(\vec{\mathbf{r}}_3)\hat{\psi}(\vec{\mathbf{r}}_3)\hat{\psi}(\vec{\mathbf{r}}_2)\hat{\psi}(\vec{\mathbf{r}}_1) + \text{h.c.}\right] \tag{B28}$$

with $V(\vec{\mathbf{r}}_1, \vec{\mathbf{r}}_2, \vec{\mathbf{r}}_3)$ being the sum of three pair interaction potentials, and $\hat{B}^\dagger(\vec{\mathbf{r}}_1, \vec{\mathbf{r}}_2)$ the field operator of the molecules. The latter can be written as

$$\hat{B}^\dagger(\vec{\mathbf{r}}_1, \vec{\mathbf{r}}_2) = \sum\nolimits_{\vec{\mathbf{q}}, s} \exp^{-i\vec{\mathbf{q}}\vec{\mathbf{R}}} \chi_s^*(\vec{\mathbf{r}}) \hat{b}^\dagger_{\vec{\mathbf{q}}s}, \tag{B29}$$

where $\hat{b}^\dagger_{\vec{\mathbf{q}}s}$ is the creation operator of the molecule with momentum $\vec{\mathbf{q}}$ in the internal state s, $\chi_s(\vec{\mathbf{r}})$ is the wavefunction of this state, and the notations for coordinates are the same as in the above discussion of two-body relaxation.

Initially molecules are not present in the system and, hence, for the average of the molecular field operators we have:

$$\begin{aligned}\langle \hat{B}(\vec{\mathbf{r}'}_1, \vec{\mathbf{r}'}_2, 0)\hat{B}^\dagger(\vec{\mathbf{r}}_1, \vec{\mathbf{r}}_2, t)\rangle = \chi_s(\vec{\mathbf{r}}')\chi_s^*(\vec{\mathbf{r}}) \\ \times \sum_{\vec{\mathbf{q}}, s} \exp\left\{-i\vec{\mathbf{q}}(\vec{\mathbf{R}} - \vec{\mathbf{R}}') + i\left(\frac{q^2}{4m} - E_s\right)t\right\},\end{aligned} \tag{B30}$$

with E_s being the binding energy of the molecule in the state s; $\vec{\mathbf{R}} = (\vec{\mathbf{r}}_1 + \vec{\mathbf{r}}_2)/2$; $\vec{\mathbf{r}} = \vec{\mathbf{r}}_1 - \vec{\mathbf{r}}_2$ (and similarly for $\vec{\mathbf{R}}'$ and $\vec{\mathbf{r}}'$). The momentum p of the atom in the outgoing recombination channel is very high, and the states with such momenta are not initially occupied. Therefore, we get

$$\langle \hat{\psi}(\vec{\mathbf{r}}'_3, 0)\hat{\psi}^\dagger(\vec{\mathbf{r}}_3, t)\rangle = \sum_{\vec{\mathbf{p}}} \exp\left\{-i\vec{\mathbf{p}}(\vec{\mathbf{r}}_3 - \vec{\mathbf{r}}'_3) + i\frac{p^2}{2m}t\right\}. \tag{B31}$$

Thus, the initial expression for W_3 (Eq. (B1) with $\hat{H}'(t)$ (B2) and $\hat{H}'(0)$ (B28)) takes the form:

$$\begin{aligned} W_3 = & \int_{-\infty}^{\infty} dt \int d\vec{\mathbf{R}} d\vec{\mathbf{R}}' d\vec{\mathbf{r}} d\vec{\mathbf{r}}' d\vec{\mathbf{u}} d\vec{\mathbf{u}}' V(\vec{\mathbf{r}}', \vec{\mathbf{u}}') V(\vec{\mathbf{r}}, \vec{\mathbf{u}}) \\ & \sum_{\vec{\mathbf{p}}, \vec{\mathbf{q}}, s} \exp\left\{-i\left[\vec{\mathbf{p}}(\vec{\mathbf{R}} - \vec{\mathbf{R}}' + \vec{\mathbf{u}} - \vec{\mathbf{u}}') + \vec{\mathbf{q}}(\vec{\mathbf{R}} - \vec{\mathbf{R}}')\right]\right\} \chi_s(\vec{\mathbf{r}}') \chi_s^*(\vec{\mathbf{r}}) \\ & \exp\left[i\left(\frac{p^2}{2m} + \frac{q^2}{4m} - E_s\right) t\right] \times \langle \hat{\psi}^\dagger(\vec{\mathbf{R}}' + \vec{\mathbf{r}}'/2, 0) \hat{\psi}^\dagger(\vec{\mathbf{R}}' - \vec{\mathbf{r}}'/2, 0) \hat{\psi}^\dagger(\vec{\mathbf{R}}' + \vec{\mathbf{u}}', 0) \\ & \times \hat{\psi}^\dagger(\vec{\mathbf{R}} + \vec{\mathbf{u}}, t) \hat{\psi}(\vec{\mathbf{R}} - \vec{\mathbf{r}}/2, t) \hat{\psi}(\vec{\mathbf{R}} + \vec{\mathbf{r}}/2, t) \rangle, \end{aligned} \tag{B32}$$

where

$$V(\vec{\mathbf{r}'}, \vec{\mathbf{u}'}) \equiv V(\vec{\mathbf{R}} + \vec{\mathbf{r}}/2, \vec{\mathbf{R}} - \vec{\mathbf{r}}/2, \vec{\mathbf{R}} + \vec{\mathbf{u}}) \tag{B33}$$

and $\vec{\mathbf{u}} = \vec{\mathbf{r}}_3 - \vec{\mathbf{R}}$. Omitting a small difference between q and p in the time-dependent exponent transforms it to $\exp[i(3p^2/4m - E_s)t]$ and after putting $t = 0$ in the correlation function the integration over t yields $\delta(3p^2/4m - E_s)$. The summation over $\vec{\mathbf{q}}$ gives $\delta(\vec{\mathbf{R}} - \vec{\mathbf{R}}')$. As a result, Eq. (B32) reduces to

$$\begin{aligned} W_3 = & \int \tilde{W}_3(\vec{\mathbf{r}}, \vec{\mathbf{r}}', \vec{\mathbf{u}}, \vec{\mathbf{u}}') d\vec{\mathbf{R}} d\vec{\mathbf{r}} d\vec{\mathbf{r}}' d\vec{\mathbf{u}} d\vec{\mathbf{u}}' \langle \hat{\psi}^\dagger(\vec{\mathbf{R}} + \vec{\mathbf{r}}'/2) \hat{\psi}^\dagger(\vec{\mathbf{R}} - \vec{\mathbf{r}}'/2) \hat{\psi}^\dagger(\vec{\mathbf{R}} + \vec{\mathbf{u}}') \\ & \times \hat{\psi}(\vec{\mathbf{R}} + \vec{\mathbf{u}}) \hat{\psi}(\vec{\mathbf{R}} - \vec{\mathbf{r}}/2) \hat{\psi}(\vec{\mathbf{R}} + \vec{\mathbf{r}}/2) \rangle, \end{aligned} \tag{B34}$$

with

$$\begin{aligned} \tilde{W}_3(\vec{\mathbf{r}}, \vec{\mathbf{r}}', \vec{\mathbf{u}}, \vec{\mathbf{u}}') = & V(\vec{\mathbf{r}}, \vec{\mathbf{u}}) V(\vec{\mathbf{r}}', \vec{\mathbf{u}}') \int \frac{d\vec{\mathbf{p}}}{(2\pi)^2} \\ & \times \exp\left[i\vec{\mathbf{p}}(\vec{\mathbf{u}} - \vec{\mathbf{u}}')\right] \sum_s \delta\left(\frac{3p^2}{4m} - E_s\right) \chi_s^*(\vec{\mathbf{r}}) \chi_s(\vec{\mathbf{r}}'). \end{aligned} \tag{B35}$$

Integrating out the motion of particles in the tightly confined z-direction in a way similar to that for the two-body relaxation, we transform Eq. (B34) to

$$\begin{aligned} W_3 = & \int d\mathbf{R} d\mathbf{r} d\mathbf{r}' d\mathbf{u} d\mathbf{u}' \tilde{w}_3(\mathbf{r}, \mathbf{r}', \mathbf{u}, \mathbf{u}') \langle \hat{\psi}^\dagger(\mathbf{R} + \mathbf{r}'/2) \hat{\psi}^\dagger(\mathbf{R} - \mathbf{r}'/2) \\ & \times \hat{\psi}^\dagger(\mathbf{R} + \mathbf{u}') \hat{\psi}(\mathbf{R} + \mathbf{u}) \hat{\psi}(\mathbf{R} - \mathbf{r}/2) \hat{\psi}(\mathbf{R} + \mathbf{r}/2) \rangle, \end{aligned} \tag{B36}$$

where $\mathbf{R}, \mathbf{r}, \mathbf{u}$ and $\mathbf{R}', \mathbf{r}', \mathbf{u}'$ are 2D vectors in the x, y plane and

$$\tilde{w}_3(\mathbf{r}, \mathbf{r}', \mathbf{u}, \mathbf{u}') = \int \tilde{W}_3(\vec{\mathbf{r}}, \vec{\mathbf{r}}', \vec{\mathbf{u}}, \vec{\mathbf{u}}') \frac{dz dz' du_z du_z'}{\sqrt{3}\pi l_0^2}. \tag{B37}$$

Similarly to Eq. (B17), the averaged product of six fermionic field operators is represented as

$$\begin{aligned} S_3 \quad & \equiv \langle \hat{\psi}^\dagger(\mathbf{r}_1') \hat{\psi}^\dagger(\mathbf{r}_2') \hat{\psi}^\dagger(\mathbf{r}_3') \hat{\psi}(\mathbf{r}_3) \hat{\psi}(\mathbf{r}_2) \hat{\psi}(\mathbf{r}_1) \rangle \\ & = \frac{1}{3!} \sum_{\mathbf{k}_1, \mathbf{k}_2, \mathbf{k}_1} N_{k_1} N_{k_2} N_{k_3} \mathcal{D}^*(\mathbf{r}_1', \mathbf{r}_2', \mathbf{r}_3'; \mathbf{k}_1, \mathbf{k}_2, \mathbf{k}_3) \mathcal{D}(\mathbf{r}_1, \mathbf{r}_2, \mathbf{r}_3; \mathbf{k}_1, \mathbf{k}_2, \mathbf{k}_3), \end{aligned}$$

where $\mathcal{D}(\mathbf{r}_1,\mathbf{r}_2,\mathbf{r}_3;\mathbf{k}_1,\mathbf{k}_2,\mathbf{k}_3)$ is the (Slater) determinant of the 3×3 matrix $\{\chi_{\mathbf{k}_i}(\mathbf{r}_j)\}$. Using the expansion of the wavefunctions in (small) relative coordinates $\mathbf{r}=\mathbf{r}_1-\mathbf{r}_2$ and $\mathbf{u}=\mathbf{r}_3-(\mathbf{r}_1+\mathbf{r}_2)/2$ we find that $\mathcal{D}$ is bilinear in the components of these quantities:

$$\begin{aligned}&\mathcal{D}(\mathbf{R}+\mathbf{r}/2,\mathbf{R}-\mathbf{r}/2,\mathbf{R}+\mathbf{u};\mathbf{k}_1,\mathbf{k}_2,\mathbf{k}_3)\\&=\frac{1}{2}\chi_{\mathbf{k}_1}(\mathbf{R})\chi_{\mathbf{k}_2}(\mathbf{R})\chi_{\mathbf{k}_3}(\mathbf{R})\sum_{\alpha,\beta}(r_\alpha u_\beta-r_\beta u_\alpha)\\&\times\{\nabla_\alpha[\ln\chi_{\mathbf{k}_1}(\mathbf{R})-\ln\chi_{\mathbf{k}_2}(\mathbf{R})]\nabla_\beta[\ln\chi_{\mathbf{k}_2}(\mathbf{R})-\ln\chi_{\mathbf{k}_3}(\mathbf{R})]\\&-\nabla_\beta[\ln\chi_{\mathbf{k}_1}(\mathbf{R})-\ln\chi_{\mathbf{k}_2}(\mathbf{R})]\nabla_\alpha[\ln\chi_{\mathbf{k}_2}(\mathbf{R})-\ln\chi_{\mathbf{k}_3}(\mathbf{R})]\},\end{aligned}\tag{B38}$$

where $\alpha,\beta=\{x,y\}$. Using Eqs. (B21) and (B24), to the leading order in small relative wavevectors equation (B38) takes the form:

$$\begin{aligned}&\mathcal{D}(\mathbf{R}+\mathbf{r}/2,\mathbf{R}-\mathbf{r}/2,\mathbf{R}+\mathbf{u};\mathbf{k}_1,\mathbf{k}_2,\mathbf{k}_3)\simeq\frac{[\chi_0(\mathbf{R})]^3b^2}{4\sin^2(\eta/2)}\\&\times\sum_{\alpha,\beta}(r_\alpha u_\beta-r_\beta u_\alpha)(k_1-k_2)_\alpha(k_3-k_2)_\beta P(R_\alpha)P(R_\beta).\end{aligned}\tag{B39}$$

Substituting the result of Eq. (B39) into equation (B38) we find for the correlation function:

$$\begin{aligned}S_3=&\frac{|\chi_0(\mathbf{R})|^6b^4}{2^7\sin^4(\eta/2)}\frac{1}{3}\int N_{k_1}N_{k_2}N_{k_3}[k_1^2k_2^2+k_1^2k_3^2+k_1^2k_3^2]\frac{d^2k_1d^2k_2d^2k_3}{(2\pi)^6}\\&\times\sum_{\alpha,\beta}(r_\alpha u_\beta-r_\beta u_\alpha)(r'_\alpha u'_\beta-r'_\beta u'_\alpha)P^2(R_\alpha)P^2(R_\beta).\end{aligned}\tag{B40}$$

Having in mind that only the terms with $\beta\neq\alpha$ contribute to the summation over 2D Cartesian indices, from Eq. (B36) we obtain for the decay rate:

$$\begin{aligned}W_3=&\frac{\mathcal{F}_3(\eta)}{12}\int d\mathbf{r}d\mathbf{r}'d\mathbf{u}d\mathbf{u}'\tilde{w}_3(\mathbf{r},\mathbf{r}',\mathbf{u},\mathbf{u}')[\vec{\mathbf{r}}\times\vec{\mathbf{u}}]_z[\vec{\mathbf{r}}'\times\vec{\mathbf{u}}']_z\\&\times\int N_{k_1}N_{k_2}N_{k_3}[k_1^2k_2^2+k_2^2k_3^2+k_1^2k_3^2]\frac{d^2k_1d^2k_2d^2k_3}{(2\pi)^6},\end{aligned}\tag{B41}$$

where we expressed the combination $r_1u_2-r_2u_1$ in terms of 3D vectors $\vec{\mathbf{r}}$ and $\vec{\mathbf{u}}$. The quantity $\mathcal{F}_3(\eta)$ in Eq. (B41) is given by

$$\mathcal{F}_3(\eta)=\frac{b^2}{16\sin^4(\eta/2)}\int d\mathbf{R}|\chi_0(\mathbf{R})|^6P^2(X)P^2(Y).\tag{B42}$$

Here the integration over $\mathbf{R}$ is only in the 2D lattice cell, while the summation over all lattice cells resulted in the multiplication of the result by the cell number $1/b^2$. Performing the integration we obtain:

$$\mathcal{F}_3(\eta)=\eta^4\cot^4(\eta/2)\left[1+\frac{\sin\eta}{\eta}\right]^{-4}.\tag{B43}$$

Let us now compare the result of Eq. (B41) with that in free space. Taking the wavefunction $\chi_{\mathbf{k}}=\exp(i\mathbf{kr})$ the expression for $\mathcal{D}$ becomes:

$$\begin{aligned}&\mathcal{D}(\mathbf{R}+\mathbf{r}/2,\mathbf{R}-\mathbf{r}/2,\mathbf{R}+\mathbf{u};\mathbf{k}_1,\mathbf{k}_2,\mathbf{k}_3)\\&=\exp[i(\mathbf{k}_1+\mathbf{k}_2+\mathbf{k}_3)\mathbf{R}]i\sum_{\alpha,\beta}(r_\alpha u_\beta-r_\beta u_\alpha)(k_1-k_2)_\alpha(k_3-k_2)_\beta.\end{aligned}\tag{B44}$$

Using $\mathcal{D}$ (B44) in Eqs. (B38) and (B36) we arrive at the recombination rate given by Eq. (B41) without the factor $\mathcal{F}_3$ in the right hand side. Thus, the relation between the recombination decay rate in free space and the one in the 2D lattice reads:

$$W_3^{\rm lat} = W_3^{\rm free}\mathcal{F}_3(\eta). \tag{B45}$$

The function $\mathcal{F}_3$ is shown in Fig. 4.4 versus the lattice depth G related to η by Eq. (4.51). From Fig. 4.4 we see that there is a significant suppression of both 2-body and 3-body decay processes.

For usual sinusoidal optical lattices used in experiments with ultracold atoms, one can proceed along the same lines as in the case of the 2D Kronig-Penney model. For the two-body relaxation, Eqs. (B1)-(B18) remain the same. Then, for fairly deep lattices ($b/\xi_0 \gtrsim 4$) where the function $\chi_{\mathbf{k}}(\mathbf{r})$ can be still used in the form (4.30), we obtain the ratio of the lattice to free space relaxation rate $W_2^{\rm sl}/W_2^{\rm free} \simeq \mathcal{R}_{l=1}$, with the factor $\mathcal{R}_{l=1}$ given by Eq. (4.45). The calculations for the three-body recombination are more involved. The estimate using an analogy with the Kronig-Penney model at large G, leads to the ratio of the lattice to free space recombination rate $W_3^{\rm sl}/W_3^{\rm free}\sim\mathcal{R}_{l=1}^2$. In particular, for $b/\xi_0 = 4$ ($m^*/m \simeq 5$) the two-body relaxation is suppressed by a factor of 5 and the three-body recombination by about a factor of 25.

Chapter 5

Interlayer p-wave superfluidity of polar molecules

In Chapter 5 we discuss another interesting novel superfluid of fermionic polar molecules. It is expected in a bilayer system, where dipoles are oriented perpendicularly to the layers and in opposite directions in different layers. Such a system can be a quantum simulator of superconductivity in layered condensed matter systems. We demonstrate the emergence of interlayer superfluid pairing, where Cooper pairs are formed by dipoles of different layers. In contrast to the already known s-wave interlayer superfluid, where all dipoles are parallel to each other [152, 154, 156], in our case the s-wave pairing is suppressed and there can be p-wave or higher partial wave superfluids. The results of this chapter are published in Ref. [177].

5.1 Background

Dipolar systems in bilayer [63, 152–154, 156–158, 162] and multilayer [60, 63, 159–162] configurations with all dipoles oriented in the same direction have been actively discussed. The picture of interlayer superfluid pairing is different for the dipoles of one layer that are opposite to the dipoles of the other. The s-wave pairing is practically impossible, and the system may form p-wave and higher partial wave superfluids.

This type of bilayer systems can be created by putting polar molecules with rotational moment $J = 0$ in one layer, and molecules with $J = 1$ in the other (see Fig. 5.1). Then, applying an electric field (perpendicular to the layers) one gets a field-induced average dipole moment of $J = 0$ molecules parallel to the field, and the dipole moment of $J = 1$ molecules oriented in the opposite direction. One should also prevent a flip-flop process in which the dipole-dipole interaction between given $J = 1$ and $J = 0$ molecules reverses their dipoles, thus inducing a rapid three-body decay in collisions of a dipole-reversed molecule with two original ones. This can be done by making the electric field inhomogeneous, so that it is larger in the layer with $J = 0$ molecules and the flip-flop process requires an increase in the Stark energy. This process will be suppressed if the difference in the Stark energies of molecules in the layers significantly exceeds the Fermi energy, which is a typical kinetic energy of the molecules ($\sim$ 100 nK for the example considered below). This is realistic for present facilities.

As we will see below, promising superfluid transition temperatures may require bilayer

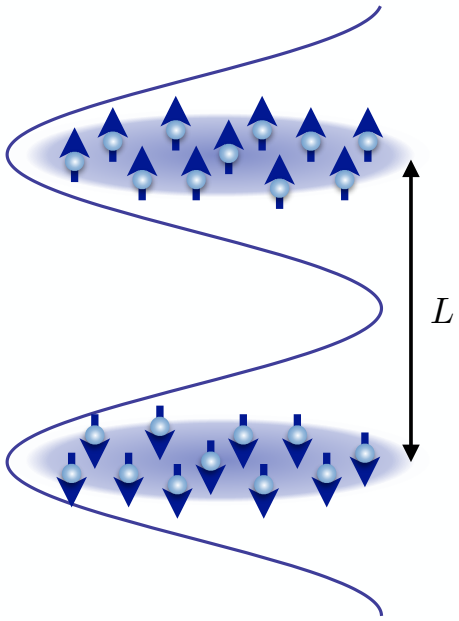

Figure 5.1: Bilayer system of polar molecules with dipole moments in the upper and lower layers, oriented opposite to each other.

systems based on the subwavelength lattices, so that the interlayer spacing is ~ 50 nm. For the dipole moment close to 1 Debye and the interlayer spacing of 50 nm, one thus should have the field gradient (perpendicularly to the layers) significantly exceeding 0.5 kV/cm^2. This could be done by using electrodes consisting of four rods, and even a higher gradient ~ 30 kV/cm^2 should be achievable [323, 324]. By changing the positions of the rods one can obtain the field gradient exceeding 0.5 kV/cm^2 in the direction perpendicular to the layers of the bilayer system. The field itself will not be exactly perpendicular to the layers and there will also be the field gradient parallel to the layers. This, however, does not essentially influence the physics.

5.2 Interlayer interaction

The potential of interaction between two molecules belonging to different layers has the form:

$$V_L(r) = -d^2 \frac{r^2 - 2L^2}{(r^2 + L^2)^{5/2}}, \tag{5.1}$$

where L is the interlayer spacing, r is the in-layer separation between the molecules, and $-d^2$ is the scalar product of the average dipole moments of these molecules. The potential $V_L(r)$ is repulsive for $r < \sqrt{2}L$ and attractive at larger r (see Fig. 5.2). The potential well is much more shallow than in the case of all dipoles oriented in the same direction, which were considered in Refs. [152, 156, 157, 162].

We have checked that s-wave interlayer dimers, which exist at any r_*/L, are weakly bound even for $r_*/L \approx 3$. Their binding energy at $r_*/L \lesssim 3$ is much smaller than the Fermi energy at least for $k_F L > 0.1$. For such r_*/L, interlayer dimers with orbital angular momenta $|l| \geq 1$ do not exist. We thus are dealing with purely fermionic physics.

For the analysis of the superfluid pairing we are interested in particle momenta $k \sim k_F$. As well as in the case of all dipoles oriented in the same direction [152, 156, 157, 162],

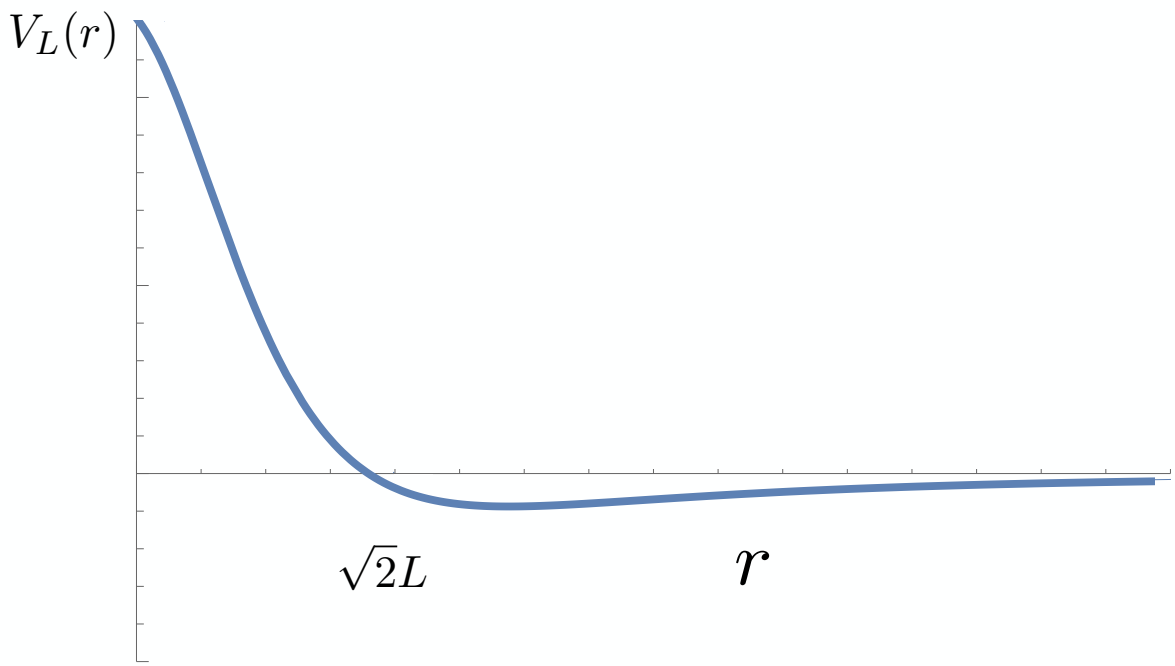

Figure 5.2: The interaction potential between two molecules belonging to different layers.

under the condition $k_F r^* \ll 1$ (where $r^* = md^2/\hbar^2$) the amplitude of interlayer interaction is obtained in the Born approximation. The Fourier transform of the potential (5.1) is

$$V_L(\mathbf{k}', \mathbf{k}) = (2\pi\hbar^2/m) r^* |\mathbf{k} - \mathbf{k}'| \exp\left[-|\mathbf{k} - \mathbf{k}'| L\right], \tag{5.2}$$

and in the first Born approximation the on-shell amplitude of the l-wave scattering at $k = k_F$ reads:

$$f_l(k_F) = \frac{2\hbar^2 k_F r^*}{m} \int_0^{2\pi} d\phi \cos(l\phi) |\sin(\phi/2)| \exp\left[-2k_F L |\sin(\phi/2)|\right]. \tag{5.3}$$

The s-wave amplitude is positive, i.e. the s-wave channel corresponds to repulsion. Note that for extremely low collision energies comparable with the dimer binding energy, where the Born approximation is not accurate, the s-wave scattering amplitude can be negative. This, however, does not lead to superfluid s-wave pairing.

The channels with $|l| \geq 1$ correspond to attraction. A straightforward calculation shows that for $k_F L \lesssim 0.7$ the largest is the p-wave amplitude and, hence, at sufficiently low temperatures the system will be an interlayer p-wave superfluid. As for d-wave and higher partial wave superfluids, they are possible only at extremely low temperatures. Thus, we confine ourselves to the p-wave pairing.

For the interlayer interaction potential $V_L(r)$ given by equation (5.1), the scattering amplitude for $k_F r^* \ll 1$ can be calculated in the Born approximation [152]. The p-wave part of the first order contribution to the off-shell amplitude is

$$f_1(k', k) = \int \frac{d\varphi_k' d\varphi_k}{(2\pi)^2} e^{i(\varphi_k' - \varphi_k)} V_L(r) e^{i(\mathbf{k}' - \mathbf{k})r} = -\frac{2\pi\hbar^2}{m} (kr^*) \mathcal{F}_1(k', k, L), \tag{5.4}$$

where

$$\mathcal{F}_1(k'L, kL) = \frac{1}{kL} \int_0^\infty x dx \, J_1(k'Lx) J_1(kLx) \frac{x^2 - 2}{(x^2 + 1)^{5/2}}, \tag{5.5}$$

and J_1 is the Bessel function. Regarding the second order contribution, for the solution of the gap equation we only need the on-shell p-wave part, which is given by

$$f_2(k) = \frac{2\pi\hbar^2}{m}(kr^*)^2\mathcal{F}_2(kL), \tag{5.6}$$

where

$$\mathcal{F}_2(kL) = \frac{\pi}{(kL)^2}\int_0^\infty xdx\, J_1^2(kLx)\frac{x^2-2}{(x^2+1)^{5/2}}\int_x^\infty ydy\, J_1(kLy)N_1(kLy)\frac{y^2-2}{(y^2+1)^{5/2}}. \tag{5.7}$$

In fact, the true p-wave scattering amplitude follows from the exact relation

$$f(k',k) = \int_0^\infty J_1(k'r)V_L(r)\psi(k,r)2\pi r dr, \tag{5.8}$$

where $\psi(k,r)$ is the true wavefunction of the p-wave relative motion with momentum k, normalized such that for $r\to\infty$ we have

$$\psi(k,r) = J_1(kr) - (imf(k)/4\hbar^2)H_1^{(1)}(kr) \tag{5.9}$$

with $H_1^{(1)}$ being the Hankel function. This amplitude is complex and it is related to the real amplitude $\tilde{f} = f_1 + f_2$ given by equations (5.4)–(5.7) as

$$f(k',k) = \frac{\tilde{f}(k',k)}{1+im\tilde{f}(k)/4\hbar^2}. \tag{5.10}$$

5.3 Superfluid pairing of fermionic polar molecules in a bilayer system

In order to calculate the superfluid transition temperature we use the BCS approach along the lines of Refs. [122,123]. We consider temperatures T tending to T_c from below and rely on the renormalized gap equation of the following form:

$$\begin{aligned}\Delta_{\mathbf{k}} = &-\int\frac{d^2k'}{(2\pi)^2}f(\mathbf{k}',\mathbf{k})\Delta_{\mathbf{k}'}\left\{\mathcal{K}(k') - \frac{1}{2(E_{k'}-E_k-i0)}\right\}\\ &-\int\frac{d^2k'}{(2\pi)^2}\delta V(\mathbf{k}',\mathbf{k})\Delta_{\mathbf{k}'}\mathcal{K}(k'),\end{aligned} \tag{5.11}$$

where $\mathcal{K}(k) = \tanh(\epsilon_k/2T)/2\epsilon_k$, with

$$\epsilon_k = \sqrt{(E_k-\mu)^2 + |\Delta(k)|^2} \tag{5.12}$$

being the excitation energy, and $E_k = \hbar^2k^2/2m$. The quantity $\delta V(\mathbf{k}',\mathbf{k})$ is a correction to the bare interparticle interaction due to polarization of the medium by colliding particles. The leading terms of this quantity introduced by Gor'kov and Melik-Barkhudarov [314], are second order in the bare interaction.

For the p-wave pairing the order parameter is $\Delta_{\mathbf{k}} = \Delta(k)e^{i\varphi_k}$, and we then multiply Eq. (5.11) by $e^{-i\varphi_k}$ and integrate over $d\varphi_{k'}$ and $d\varphi_k$. As a result, we obtain the same

equation (5.11) in which $\Delta_{\mathbf{k}}$ and $\Delta_{\mathbf{k}'}$ are replaced with $\Delta(k)$ and $\Delta(k')$, the off-shell scattering amplitude $f(\mathbf{k}', \mathbf{k})$ with its p-wave part, and $\delta V(\mathbf{k}', \mathbf{k})$ with its p-wave part

$$\delta V(k', k) = \int \frac{d\varphi_{k'} d\varphi_k}{4\pi^2} \, \delta V(\mathbf{k}', \mathbf{k}) \exp\left[i(\varphi_{k'} - \varphi_k)\right]. \tag{5.13}$$

Calculating the contribution of the pole in the second term in square brackets and using Eq. (5.10) we obtain

$$\begin{aligned} \Delta(k) = -P \int \frac{m dE_{k'}}{2\pi\hbar^2} \tilde{f}(k', k) \Delta(k') \left[\mathcal{K}(k') - \frac{1}{2(E_{k'} - E_k)} \right] \\ - \int \frac{m dE_{k'}}{2\pi\hbar^2} \delta V(k', k) \Delta(k') \mathcal{K}(k'), \end{aligned} \tag{5.14}$$

where the symbol P stands for the principal value of the integral. In the first term in the right hand side of Eq. (5.14) we divide the region of integration into two parts: $|E_{k'} - E_F| < \omega$ and $|E_{k'} - E_F| > \omega$, where $\Delta(k_F), T_c \ll \omega \ll E_F$. The contribution to the p-wave order parameter from the first region we denote as $\Delta^{(1)}(k)$, and the contribution from the second region as $\Delta^{(2)}(k)$. The contribution of the second term in the right hand side of equation (5.14) is denoted as $\Delta^{(3)}(k)$.

We first notice that the main contribution to $\Delta(k)$ comes from k' close to k_F. Retaining only f_1, which is proportional to kr^*, in the off-shell scattering amplitude and omitting the second term in the right hand side of Eq. (5.14) (which is proportional to $(kr^*)^2$) we obtain

$$\Delta(k) = \Delta(k_F) f_1(k_F, k)/f_1(k_F). \tag{5.15}$$

Putting $k = k_F$ and performing the integration in the first region in the first term of Eq (5.14), where $E_F - \omega < E_{k'} < E_F + \omega$, we may put $\Delta(k') = \Delta(k_F)$ and $\tilde{f}(k', k) = \tilde{f}(k_F) = f_1(k_F) + f_2(k_F)$. Then, putting $\epsilon_{k'} = |\xi_{k'}|$ in $\mathcal{K}(k')$ and taking into account that the contribution of the second term in square brackets is zero, we obtain:

$$\Delta^{(1)}(k_F) = -\Delta(k_F) \rho(k_F) \tilde{f}(k_F) \ln\left(\frac{2e^C \omega}{\pi T_c}\right), \tag{5.16}$$

with C=0.577 being the Euler constant, and $\rho(k_F) = m/2\pi\hbar^2$ the density of states.

In the second region, where $E_{k'} > E_F + \omega$ or $E_{k'} < E_F - \omega$, we put $\mathcal{K} = 1/2|\xi_{k'}|$ and keep only f_1 in the scattering amplitude. For $k = k_F$ the integral over $E_{k'}$ from $E_F + \omega$ to ∞ vanishes. In the integral from 0 to $E_F - \omega$ we use $\Delta(k')$ from Eq. (5.15) and find

$$\Delta^{(2)}(k_F) = -\Delta(k_F) \rho(k_F) f_1(k_F) \left[\ln\left(\frac{E_F}{\omega}\right) - \eta(k_F L) \right], \tag{5.17}$$

where

$$\begin{aligned} \eta(k_F L) &= -2 \int_0^{E_F - \omega} \frac{k' dk'}{(k_F^2 - k'^2)} \left[\frac{f_1^2(k_F, k)}{f_1^2(k_F)} - 1 \right] \\ &= -2 \int_0^1 \frac{y dy}{1 - y^2} \left\{ \left[\frac{\mathcal{F}_1(k_F L, k_F L y)}{\mathcal{F}_1(k_F L)} \right]^2 - 1 \right\}, \end{aligned} \tag{5.18}$$

and $\mathcal{F}_1(k_F L) \equiv \mathcal{F}_1(k_F L, k_F L)$.

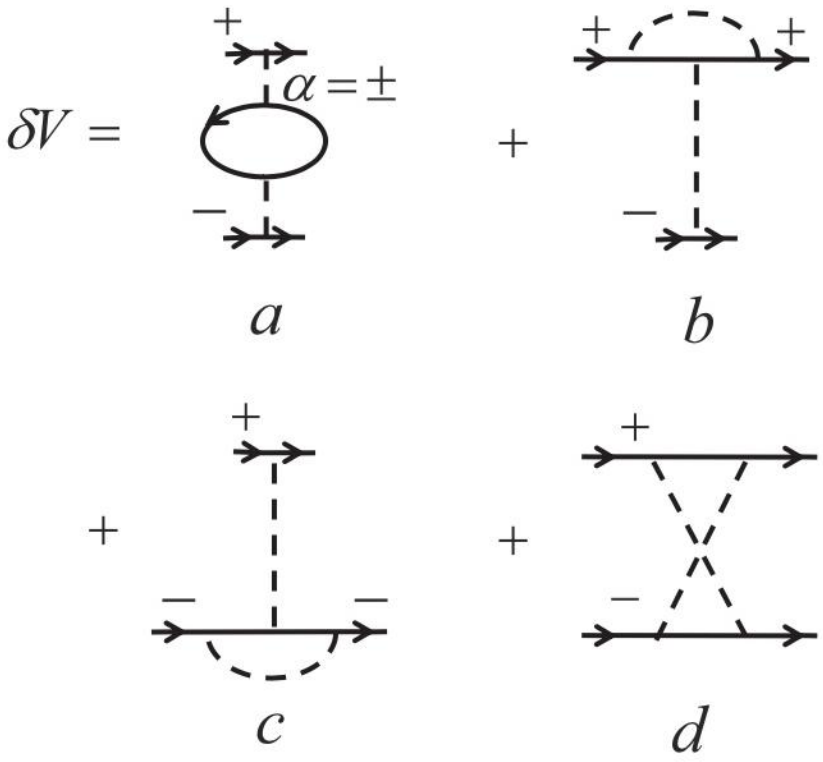

Figure 5.3: The second-order contributions to the effective interlayer interaction. Solid lines correspond to particles from different layers (labeled by + and −), and the dashed lines correspond to the dipole-dipole interactions.

Then, we consider the Gor'kov-Melik-Barkhudarov corrections to the bare interaction of the molecules in the bilayer. These many-body corrections are second order in $(k_F r^*)$ and are described by four diagrams (for details, see [123, 156, 314] and Fig. 5.3). For the case of p-wave superfluidity of identical fermionic polar molecules they have been considered in Ref. [123]. They have been also studied for the interlayer s-wave superfluidity of dipoles oriented in the same direction in Ref. [156].

We are interested in the case of sufficiently small $k_F L$. Following the same treatment as in Refs. [123, 156], in the limit of $k_F L \to 0$ we obtain:

$$\delta V(k_F, k_F) = -\alpha \frac{\hbar^2}{m} (k_F r^*)^2, \tag{5.19}$$

where $\alpha \simeq 10.57$. The dominant contribution to this result comes from the diagram containing a bubble in the interaction line (diagram a) in Refs. [123, 156]). This contribution strongly decreases with increasing $k_F L$. In particular, for $k_F L \simeq 0.15$ we have $\alpha \simeq 2.8$, and $\alpha \simeq 2.2$ when increasing $k_F L$ to 0.2. Comparing δV with the scattering amplitude $f_1(k_F)$ we see that for not very small $k_F r^*$ the perturbative treatment of the Gor'kov-Melik-Barkhudarov corrections is adequate for $k_F L \gtrsim 0.15$. We therefore confine ourselves to these values of $k_F L$.

Performing the integration in the second term of Eq. (5.14) we obtain the contribution of the Gor'kov-Melik-Barkhudarov corrections to the order parameter:

$$\Delta^{(3)}(k_F) = \Delta(k_F) \frac{\alpha(k_F L)}{2\pi} (k_F r^*)^2 \ln\left(\frac{E_F}{T_c}\right), \tag{5.20}$$

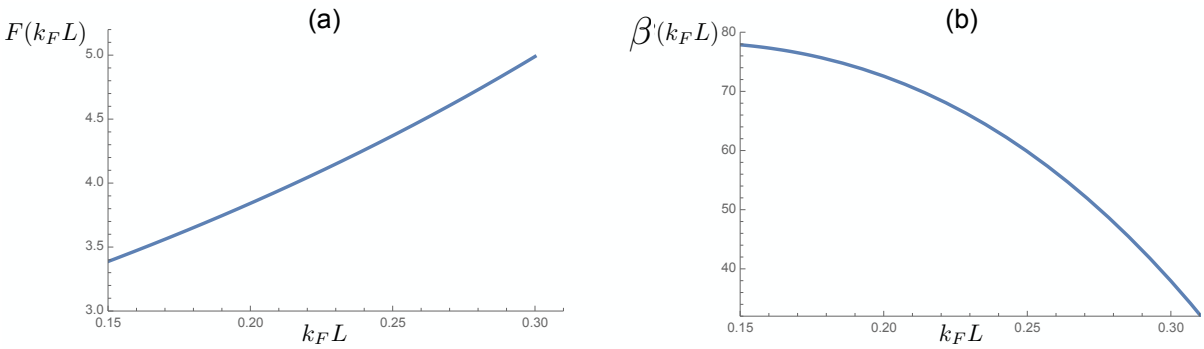

Figure 5.4: The dependence of F and β on k_FL.

The sum of Eqs. (5.16), (5.17) and (5.20) yields

$$\Delta(k_F) = \Delta(k_F)\left[\left\{(k_Fr^*)\mathcal{F}_1(k_FL)\ln\left(\frac{2e^{C-\eta(k_FL)}}{\pi}\frac{E_F}{T_c}\right)\right\} - \left\{\left(\mathcal{F}_2(k_FL) - \frac{\alpha(k_FL)}{2\pi}\right)(k_Fr^*)^2\ln\left(\frac{E_F}{T_c}\right)\right\}\right], \tag{5.21}$$

where we put $\omega \sim E_F$ in the terms proportional to $(k_Fr^*)^2$. We should also recall that the bare mass m should be replaced with the effective mass

$$m^* = m[1 - (4/3\pi)k_Fr^*], \tag{5.22}$$

which has been found in Refs. [73, 156]. Since the relative difference between m^* and m is small as k_Fr^*, it is sufficient to replace m with m^* only in the multiple $r^* \sim m$ in the first term of Eq. (5.21). This leads to the appearance of a new term

$$-\Delta(k_F)\frac{4}{3\pi}\mathcal{F}_1(k_FL)(k_Fr^*)^2\ln\left(\frac{E_F}{T_c}\right) \tag{5.23}$$

in the right hand side of equation (5.21). Then, dividing both sides of Eq. (5.21) by $\Delta(k_F)$ we obtain for the critical temperature:

$$T_c = E_F\beta(k_FL)\exp\left[-\frac{F(k_FL)}{k_Fr^*}\right], \tag{5.24}$$

where

$$F(k_FL) = [\mathcal{F}_1(k_FL)]^{-1} \tag{5.25}$$

and

$$\beta(k_FL) = \exp\left[C + \ln\left(\frac{2}{\pi}\right) - \eta(k_FL) - \frac{\mathcal{F}_2(k_FL)}{\mathcal{F}_1^2(k_FL)} - \frac{4}{3\pi}\frac{1}{\mathcal{F}_1(k_FL)} + \frac{\alpha(k_FL)}{2\pi}F^2(k_FL)\right]. \tag{5.26}$$

The dependence of F and β on k_FL is shown in Fig. 5.4. We stop at $k_FL = 0.3$ because for larger values of this parameter the function F is so large that the critical temperature will be negligible.

For not very small k_Fr^* the validity of the perturbative treatment of the Gor'kov-Melik-Barkhudarov corrections requires $k_FL \gtrsim 0.15$. The functions $F(k_FL)$ and $\beta(k_FL)$ are given by expressions (5.25) and (5.26), respectively. For k_FL ranging from 0.15 to 0.3 the function F increases from 3.4 to 5, and the coefficient β is fairly large, being about 80 at $k_FL = 0.15$ (see Fig. 5.4).

For $L \approx 50$ nm and $k_FL \simeq 0.15$, the Fermi energy of NaLi molecules is close to 100 nK, and the critical temperature for k_Fr^* approaching 0.5 is about 10 nK.

5.4 Strongly interacting regime

For completeness, we also consider the regime of strong interactions within a single layer. Assuming that the coupling between the layers is still fairly weak, we have superfluid (interlayer) pairing between *quasiparticles*. Related problems have been discussed for coupled 2D Fermi liquids as models for layered superconductors [113]. In this case, we replace the bare mass m by the effective mass m^* and account for renormalization of the fermionic Green functions by a factor $Z < 1$ [209]. Then, the expression for the transition temperature takes the form:

$$T_c \sim E_F \exp\left[-\frac{F(k_F L)}{k_F r^*}\frac{m}{m^*}\frac{1}{Z^2}\right], \tag{5.27}$$

where we can not determine the pre-exponential coefficient. Therefore, Eq. (5.27) only gives an order of magnitude of T_c. For $k_F L = 0.3$ and $L \approx 50$ nm the Fermi energy of NaLi molecules is about 400 nK, and for, let say, $k_F r_* \approx 2$ the dimer physics is still not important. Then, using the effective mass and factor Z from the Monte Carlo calculations [74] one may think of superfluid transition temperatures of the order of several tens of nanokelvins.

5.5 Concluding remarks

As we see, the novel interlayer p-wave superfluid of polar molecules in the (subwavelength-based) bilayer system with dipoles of one layer opposite to the dipoles of the other one, may have transition temperatures up to several tens of nanokelvins. Together with the earlier proposed s-wave interlayer superfluid [152, 154, 156, 162] and superfluids in multilayer fermionic systems [60, 63, 159–162], it can be a starting point for the creation of more sophisticated layered structures. We think that these superfluids may become quantum simulators of superconductivity in layered condensed matter systems.

Conclusions and perspectives

We have considered the effect of rotonization for a 2D weakly interacting gas of tilted dipolar bosons in a homogeneous layer, and have demonstrated that in contrast to the case of perpendicular dipoles, in a wide range of tilting angles the condensate depletion remains small even when the roton minimum is extremely close to zero. This makes the system interesting for achieving local density waves with controlled short-range order and supersolidity.

We have predicted the effect of rotonization for a weakly correlated Bose gas of dipolar excitons in a semiconductor layer and calculated the stability diagram. According to our estimates, the threshold of the roton instability for a bose-condensed exciton gas with roton-maxon spectrum is achievable experimentally in semiconductor layers. This is another interesting platform for investigation of supersolidity phenomena.

We have then considered p-wave superfluids of identical fermions in 2D lattices. The optical lattice potential manifests itself in an interplay between an increase in the density of states on the Fermi surface and the modification of the fermion-fermion interaction (scattering) amplitude. The density of states is enhanced due to an increase of the effective mass of atoms. For short-range interacting atoms in deep lattices the scattering amplitude is strongly reduced compared to free space due to a small overlap of wavefunctions of fermions sitting in the neighboring lattice sites, which suppresses the p-wave superfluidity. However, we show that for a moderate lattice depth there is still a possibility to create p-wave superfluids with sizable transition temperatures. For fermionic polar molecules, due to a long-range character of the dipole-dipole interaction the effect of the suppression of the scattering amplitude is absent. It is shown that for microwave-dressed polar molecules a stable topological $p_x + ip_y$ superfluid may emerge in the 2D lattice at realistic temperatures.

Finally, we have discussed another interesting novel superfluid of fermionic polar molecules. It is expected in a bilayer system, where dipoles are oriented perpendicularly to the layers and in opposite directions in different layers. We have demonstrated the emergence of interlayer superfluid pairing. In contrast to the already known s-wave interlayer superfluid, where all dipoles are parallel to each other, in our case the s-wave pairing is suppressed and there can be p-wave or higher partial wave superfluids. The interlayer p-wave superfluid in bilayer systems, together with the earlier proposed s-wave interlayer superfluids and superfluids in multilayer fermionic systems, can be a starting point for the creation of more sophisticated layered structures.

Title: Non-conventional many-body phases in ultracold dipolar systems
Author: Aleksey K. Fedorov

Abstract:

The problem of revealing and describing novel macroscopic quantum states characterized by exotic and non-conventional properties is of fundamental importance for modern physics. Such states offer fascinating prospects for potential applications in quantum information processing, quantum simulation, and material research. In the present Thesis we develop a theory for describing non-conventional phases of ultracold dipolar gases. The related systems of large-spin atoms, polar molecules, and dipolar excitons in semiconductors are actively studied in experiments. We put the main emphasis on revealing the role of the long-range character of the dipole-dipole interaction.

We consider the effect of rotonization for a 2D weakly interacting gas of tilted dipolar bosons in a homogeneous layer, and demonstrate that in contrast to the case of perpendicular dipoles, in a wide range of tilting angles the condensate depletion remains small even when the roton minimum is extremely close to zero.

We predict the effect of rotonization for a weakly correlated Bose gas of dipolar excitons in a semiconductor layer and calculate the stability diagram. According to our estimates, the threshold of the roton instability for a bose-condensed exciton gas with the roton-maxon spectrum is achievable experimentally in semiconductor layers.

We then consider p-wave superfluids of identical fermions in 2D lattices. The optical lattice potential manifests itself in an interplay between an increase in the density of states on the Fermi surface and the modification of the fermion-fermion interaction (scattering) amplitude. The density of states is enhanced due to an increase of the effective mass of atoms. For short-range interacting atoms in deep lattices the scattering amplitude is strongly reduced compared to free space due to a small overlap of wavefunctions of fermions sitting in the neighboring lattice sites, which suppresses the p-wave superfluidity. However, we show that for a moderate lattice depth there is still a possibility to create p-wave superfluids with sizable transition temperatures. For fermionic polar molecules, due to a long-range character of the dipole-dipole interaction the effect of the suppression of the scattering amplitude is absent. It is shown that for microwave-dressed polar molecules a stable topological $p_x + ip_y$ superfluid may emerge in the 2D lattice at realistic temperatures.

Finally, we discuss another interesting novel superfluid of fermionic polar molecules. It is expected in a bilayer system, where dipoles are oriented perpendicularly to the layers and in opposite directions in different layers. We demonstrate the emergence of interlayer superfluid pairing. In contrast to the already known s-wave interlayer superfluid, when all dipoles are parallel to each other, in our case the s-wave pairing is suppressed and there can be p-wave or higher partial wave superfluids.

Keywords: Bose–Einstein condensation, superfluidity, magnetic dipole-dipole interaction.

Titre: Phases à N corps non-conventionnelles dans des systèmes ultra-froids dipolaires
Autheur: Aleksey K. Fedorov

Résumé:

Le problème de la détection et de la description des nouveaux états quantiques macroscopiques, caractérisés par des propriétés exotiques et non-conventionnelles, est d'importance fondamentale dans la physique moderne. Ces états offrent des perspectives fascinantes dans le domaine du traitement de l'information, des simulations quantiques et de la recherche des nouveaux types de matériaux. Dans ce travail de thèse, nous développons une théorie qui permet de décrire des phases non-conventionnelles dans des systèmes de gaz ultra-froids dipolaires. Ces systèmes sont activement étudiés expérimentalement en utilisant des atomes à grand spin, des molécules polaires et des excitations dipolaires dans des semiconducteurs. Nous mettons l'accent sur le rôle des interactions dipôle-dipôle à longue portée.

Nous considérons l'effet de "rotonisation" dans un système de gaz de bosons dipolaires tiltés aux interactions faibles dans une couche homogène. Nous étudions la géométrie en deux dimensions. Nous montrons que, contrairement au cas des dipôles perpendiculaires, dans une large variété d'angles de tilt, la fraction condensée reste grande même si le minimum du roton est très proche de zéro.

Nous prédisons l'effet de la "rotonisation" pour un gaz de Bose faiblement corrélé d'excitons dipolaires dans une couche de semiconducteur et nous calculons le diagramme de stabilité. Selon nos estimations, il est possible d'atteindre expérimentalement le seuil d'instabilité du roton dans un condensat de Bose-Einstein du gaz d'excitons avec le spectre roton-maxon dans des couches semiconductrices.

Ensuite, nous considérons des superfluides d'onde-p des fermions dans des réseaux 2D. Le potentiel optique se manifeste par le lien entre l'augmentation de la densité des états sur la surface de Fermi et la modification de l'amplitude d'interaction (diffusion) fermion-fermion. La densité locale des états est amplifiée en raison de l'augmentation de la masse effective des atomes. Pour des atomes dans des réseaux profonds, qui interagissent avec des forces à courte portée, l'amplitude de diffusion est fortement réduite comparée au cas du système libre. Cela s'explique par le fait que le recouvrement des fonctions d'ondes des fermions sur des sites voisins est petit, ce qui élimine la superfluidité d'onde-p. Cependant, nous démontrons que pour des réseaux de profondeur modérée, il est encore possible de créer de la superfluidité en onde-p à des températures de transition suffisamment grandes. Pour des molécules polaires fermioniques, l'effet de suppression de l'amplitude de diffusion est absent, en raison des interactions dipôle-dipôle à longue portée. On montre que pour des molécules polaires habillées par le champ micro-onde, un état superfluide topologique $p_x + ip_y$ stable peut se former dans des réseaux 2D à des températures réalistes.

Finalement, nous discutons un autre état superfluide intéressant de molécules polaires fermioniques, qui devrait apparaître dans des systèmes bicouches. Dans cet état superfluide, les dipôles s'orientent perpendiculairement aux plans des couches dans le sens opposé sur les deux couches différentes. Nous démontrons que l'appariement superfluide apparaît entre les deux couches. Contrairement au cas bien connu d'appariement superfluide

intrecouche d'onde-s, pour lequel tous les dipôles sont parallèles entre eux, dans notre cas l'appariement d'onde-s est supprimé et il devient possible d'avoir le couplage d'onde-p ou d'autres types de superfluides à ondes partielles plus hautes.

Les mots-clefs: condensation de Bose-Einstein, superfluidité, interaction magnétique dipôle-dipôle.

Bibliography

[1] For a review, see J. Thompson and M.D. Lukin, Science **345**, 272 (2014).

[2] For a review, see C. Nayak, S.H. Simon, A. Stern, M. Freedman, and S. Das Sarma, Rev. Mod. Phys. **80**, 1083 (2008).

[3] For a review, see S. Das Sarma, M. Freedman, and C. Nayak, npj Quant. Inform. **1**, 15001 (2015).

[4] M.H. Anderson, J.R. Ensher, M.R. Matthews, C.E. Wieman, and E.A. Cornell, Science **269**, 198 (1995).

[5] K.B. Davis, M.-O. Mewes, M.R. Andrew, N.J. van Druten, D.S. Durfee, D.M. Kurn, and W. Ketterle, Phys. Rev. Lett. **75**, 3969 (1995).

[6] C.C. Bradley, C.A. Sackett, J.J. Tollett, and R.G. Hulet, Phys. Rev. Lett. **75**, 1687 (1995); **79**, 1170 (1997).

[7] For a review, see F. Dalfovo, S. Giorgini, L. Pitaevskii, and S. Stringari, Rev. Mod. Phys. **71**, 463 (1999).

[8] For a review, see S. Giorgini, L. Pitaevskii, and S. Stringari, Rev. Mod. Phys. **80**, 1215 (2008).

[9] For a review, see I. Bloch, J. Dalibard, and W. Zwerger, Rev. Mod. Phys. **80**, 885 (2008).

[10] For a review, see I. Bloch, J. Dalibard, and S. Nascimbéne, Nat. Phys. **8**, 267 (2012).

[11] M. Marinescu and L. You, Phys. Rev. Lett. **81**, 4596 (1998).

[12] L. Santos, G.V. Shlyapnikov, P. Zoller, and M. Lewenstein, Phys. Rev. Lett. **85**, 1791 (2000).

[13] L. Santos, G.V. Shlyapnikov, and M. Lewenstein, Phys. Rev. Lett. **90**, 250403 (2003).

[14] M.A. Baranov, M.S. Mar'enko, Val.S. Rychkov, and G.V. Shlyapnikov, Phys. Rev. A **66**, 013606 (2002).

[15] G.K. Brennen, C.M. Caves, P.S. Jessen, and I.H. Deutsch, Phys. Rev. Lett. **82**, 1060 (1999).

[16] D. Jaksch, J.I. Cirac, P. Zoller, S.L. Rolston, R. Côté, and M.D. Lukin, Phys. Rev. Lett. **85**, 2208 (2000).

[17] D. DeMille, Phys. Rev. Lett. **88**, 067901 (2002).

[18] P. Rabl, D. DeMille, J.M. Doyle, M.D. Lukin, R.J. Schoelkopf, and P. Zoller, Phys. Rev. Lett. **97**, 033003 (2006).

[19] For a review, see L.D. Carr, D. DeMille, R.V. Krems, and J. Ye, New J. Phys. **11**, 055049 (2009).

[20] For a review, see O. Dulieu and C. Gabbanini, Rep. Prog. Phys. **72**, 086401 (2009).

[21] For a review, see S.A. Moses, J.P. Covey, M.T. Miecnikowski, D.S. Jin, and J. Ye, Nat. Phys **13**, 13 (2017).

[22] B.C. Sawyer, B.L. Lev, E.R. Hudson, B.K. Stuhl, M. Lara, J.L. Bohn, and J. Ye, Phys. Rev. Lett. **98**, 253002 (2007).

[23] S. Ospelkaus, A. Peér, K.-K. Ni, J. Zirbel, B. Neyenhuis, S. Kotochigova, P.S. Julienne, J. Ye, and D.S. Jin, Nat. Phys. **4**, 622 (2008).

[24] K.-K. Ni, S. Ospelkaus, M.H.G. de Miranda, A. Pe'er, B. Neyenhuis, J.J. Zirbel, S. Kotochigova, P.S. Julienne, D.S. Jin, and J. Ye, Science **322**, 231 (2008).

[25] S. Ospelkaus, K.-K. Ni, D. Wang, M.H.G. de Miranda, B. Neyenhuis, G. Quéméner, P.S. Julienne, J.L. Bohn, D.S. Jin, and J. Ye, Science **327**, 853 (2010).

[26] K.-K. Ni, S. Ospelkaus, D. Wang, G. Quéméner, B. Neyenhuis, M. H. G. de Miranda, J.L. Bohn, J. Ye, and D.S. Jin, Nature (London) **464**, 1324 (2010).

[27] K. Aikawa, D. Akamatsu, M. Hayashi, K. Oasa, J. Kobayashi, P. Naidon, T. Kishimoto, M. Ueda, and S. Inouye, Phys. Rev. Lett. **105**, 203001 (2010).

[28] M.H.G. de Miranda, A. Chotia, B. Neyenhuis, D. Wang, G. Quéméner, S. Ospelkaus, J.L. Bohn, J. Ye, and D.S. Jin, Nat. Phys. **7**, 502 (2011).

[29] A. Chotia, B. Neyenhuis, S.A. Moses, B. Yan, J.P. Covey, M. Foss-Feig, A.M. Rey, D.S. Jin, and J. Ye, Phys. Rev. Lett. **108**, 080405 (2012).

[30] M.-S. Heo,T.T. Wang, C.A. Christensen, T.M. Rvachov, D.A. Cotta, J.H. Choi, Y.R. Lee, and W. Ketterle, Phys. Rev. A **86**, 021602 (2012).

[31] C.-H. Wu, J.W. Park, P. Ahmadi, S. Will, and M.W. Zwierlein, Phys. Rev. Lett. **109**, 085301 (2012).

[32] T. Takekoshi, L. Reichsollner, A. Schindewolf, J.M. Hutson, C.R. Le Sueur, O. Dulieu, F. Ferlaino, R. Grimm, and H.-C. Nägerl, Phys. Rev. Lett. **113**, 205301 (2014).

[33] P.K. Molony, P.D. Gregory, Z. Ji, B. Lu, M.P. Köppinger, C.R. Le Sueur, C.L. Blackley, J.M. Hutson, and S.L. Cornish, Phys. Rev. Lett. **113**, 255301 (2014).

[34] J.W. Park, S.A. Will, and M.W. Zwierlein, Phys. Rev. Lett. **114**, 205302 (2015); New J. Phys. **17**, 075016 (2015).

[35] S.A. Moses, J.P. Covey, M.T. Miecnikowski, B. Yan, B. Gadway, J. Ye, and D.S. Jin, Science **350**, 659 (2015).

[36] J.P. Covey, S.A. Moses, M. Garttner, A. Safavi-Naini, M.T. Miecnikowski, Z. Fu, J. Schachenmayer, P.S. Julienne, A.M. Rey, D.S. Jin, and J. Ye, Nat. Commun. **7**, 11279 (2016).

[37] A. Griesmaier, J. Werner, S. Hensler, J. Stuhler, and T. Pfau, Phys. Rev. Lett. **94**, 160401 (2005).

[38] M. Lu, N.Q. Burdick, S.H. Youn, and B.L. Lev, Phys. Rev. Lett. **107**, 190401 (2011).

[39] M. Lu, N.Q. Burdick, and B.L. Lev, Phys. Rev. Lett. **108**, 215301 (2012).

[40] K. Aikawa, A. Frisch, M. Mark, S. Baier, A. Rietzier, R. Grimm, and F. Ferlaino, Phys. Rev. Lett. **108**, 210401 (2012).

[41] A.V. Gorbunov and V.B. Timofeev, JETP Lett. **84**, 329 (2006); **87**, 698 (2008); **96**, 138 (2012); Solid State Commun. **157**, 6 (2013).

[42] D.W. Snoke, Advan. Cond. Matt. Phys. **2011**, 938609 (2010).

[43] A.A. High, J.R. Leonard, A.T. Hammack, M.M. Fogler, L.V. Butov, A.V. Kavokin, K.L. Campman, and A.C. Gossard, Nature (London) **483**, 584 (2012).

[44] A.A. High, J.R. Leonard, M. Remeika, L.V. Butov, M. Hanson, and A.C. Gossard, Nano Lett. **12**, 2605 (2012).

[45] Y. Shilo, K. Cohen, B. Laikhtman, K. West, L. Pfeiffer, and R. Rapaport, Nat. Commun. **4**, 2335 (2013).

[46] A.K. Geim and I.V. Grigorieva, Nature (London) **499**, 419 (2013).

[47] M.M. Fogler, L.V. Butov, and K.S. Novoselov, Nat. Commun. **5**, 4555 (2014).

[48] E.V. Calman, C.J. Dorow, M.M. Fogler, L.V. Butov, S. Hu, A. Mishchenko, and A.K. Geim, Appl. Phys. Lett. **108**, 101901 (2016).

[49] For a review, see M.A. Baranov, Phys. Rep. **464**, 71 (2008).

[50] For a review, see T. Lahaye, C. Menotti, L. Santos, M. Lewenstein, and T. Pfau, Rep. Prog. Phys. **72**, 126401 (2009).

[51] For a review, see C. Trefzger, C. Menotti, B. Capogrosso-Sansone, and M. Lewenstein, J. Phys. B: At. Mol. Opt. Phys. **44**, 193001 (2011).

[52] For a review, see M.A. Baranov, M. Delmonte, G. Pupillo, and P. Zoller, Chem. Rev. **112**, 5012 (2012).

[53] H.P. Buchler, E. Demler, M. Lukin, A. Micheli, N. Prokof'ev, G. Pupillo, and P. Zoller, Phys. Rev. Lett. **98**, 060404 (2007).

[54] G.E. Astrakharchik, J. Boronat, I.L. Kurbakov, and Yu.E. Lozovik, Phys. Rev. Lett. **98**, 060405 (2007).

[55] M.A. Baranov, H. Fehrmann, and M. Lewenstein, Phys. Rev. Lett. **100**, 200402 (2008).

[56] T. Pohl, E. Demler, and M.D. Lukin, Phys. Rev. Lett. **104**, 043002 (2010).

[57] I.L. Kurbakov, Yu.E. Lozovik, G.E. Astrakharchik, and J. Boronat, Phys. Rev. B **82**, 014508 (2010).

[58] M. Knap, E. Berg, M. Ganahl, and E. Demler, Phys. Rev. B **86**, 064501 (2012).

[59] S. Gopalakrishnan, I. Martin, and E.A. Demler, Phys. Rev. Lett. **111**, 185304 (2013).

[60] D.-W. Wang and E. Demler, arXiv:0812.1838 (2008).

[61] Y. Yamaguchi, T. Sogo, T. Ito, and T. Miyakawa, Phys. Rev. A **82**, 013643 (2010).

[62] K. Sun, C. Wu, and S. Das Sarma, Phys. Rev. A **82**, 075105 (2010).

[63] N.T. Zinner and G.M. Bruun, Eur. Phys. J. D **65**, 133 (2011).

[64] G.M. Bruun and D.R. Nelson, Phys. Rev. B **89**, 094112 (2014).

[65] J.K. Block and G.M. Bruun, Phys. Rev. B **90**, 155102 (2014).

[66] N.R. Cooper, E. H. Rezayi, and S. H. Simon, Phys. Rev. Lett. **95**, 200402 (2005).

[67] J. Zhang and H. Zhai, Phys. Rev. Lett. **95**, 200403 (2005).

[68] S. Yi and H. Pu, Phys. Rev. A **73**, 061602 (2006).

[69] S. Komineas and N.R. Cooper, Phys. Rev. A **75**, 023623 (2007).

[70] L. Santos and T. Pfau, Phys. Rev. Lett. **96**, 190404 (2006).

[71] B. Pasquiou, E. Maréchal, G. Bismut, P. Pedri, L. Vernac, O. Gorceix, and B. Laburthe-Tolra, Phys. Rev. Lett. **106**, 255303 (2011).

[72] S. Baier, M. J. Mark, D. Petter, K. Aikawa, L. Chomaz, Zi Cai, M.A. Baranov, P. Zoller, and F. Ferlaino, Science **352**, 201 (2016).

[73] Z.-K. Lu and G.V. Shlyapnikov, Phys. Rev. A **85**, 023614 (2012).

[74] N. Matveeva and S. Giorgini, Phys. Rev. Lett. **109**, 200401 (2012).

[75] Z-K. Lu, S.I. Matveenko, and G.V. Shlyapnikov, Phys. Rev. A **88**, 033625 (2013).

[76] K.R.A. Hazzard, B. Gadway, M. Foss-Feig, B. Yan, S.A. Moses, J.P. Covey, N.Y. Yao, M.D. Lukin, J. Ye, D.S. Jin, and A.M. Rey, Phys. Rev. Lett. **113**, 195302 (2014).

[77] N.Y. Yao, C.R. Laumann, S. Gopalakrishnan, M. Knap, M. Müller, E. Demler, and M.D. Lukin, Phys. Rev. Lett. **113**, 243002 (2013).

[78] H. Kadau, M. Schmitt, M. Wenzel, C. Wink, T. Maier, I. Ferrier-Barbut, and T. Pfau, Nature (London) **530**, 194 (2016).

[79] X. Deng, B.L. Altshuler, G.V. Shlyapnikov, and L. Santos, Phys. Rev. Lett. **117**, 020401 (2016).

[80] I. Ferrier-Barbut, H. Kadau, M. Schmitt, M. Wenzel, and T. Pfau, Phys. Rev. Lett. **116**, 215301 (2016).

[81] M. Schmitt, M. Wenzel, F. Böttcher, I. Ferrier-Barbut, and T. Pfau, Nature (London) **539**, 259 (2016).

[82] I. Ferrier-Barbut, M. Schmitt, M. Wenzel, H. Kadau, and T. Pfau, J. Phys. B: At. Mol. Opt. Phys. **49**, 214004 (2016).

[83] For a review, see S. Balibar, Nature (London) **464**, 176 (2010).

[84] For a review, see A.B. Kuklov, N.V. Prokof'ev, and B.V. Svistunov, Physics **4**, 109 (2011).

[85] For a review, see M. Boninsegni and N.V. Prokof'ev, Rev. Mod. Phys. **84**, 759 (2012).

[86] For a review, see S. Balibar, A. D. Fefferman, A. Haziot, and X. Rojas, J. Low Temp. Phys. **168**, 221 (2012).

[87] E.P. Gross, Phys. Rev. **106**, 161 (1957); Ann. Phys. (N.Y.) **4**, 57 (1958).

[88] A.F. Andreev and I.M. Lifshitz, Sov. Phys. JETP **29**, 1107 (1969).

[89] D. A. Kirzhnits and Yu. A. Nepomnyashchii, Sov. Phys. JETP **32**, 1191 (1971).

[90] Y. Pomeau and S. Rica, Phys. Rev. Lett. **72**, 2426 (1994).

[91] P. Noziéres, J. Low Temp. Phys. **137**, 45 (2004); **142**, 91 (2006); **156**, 9 (2009).

[92] E. Kim and M.H.W. Chan, Nature (London) **427**, 225 (2004); Science **305**, 1941 (2004).

[93] D.Y. Kim and M.H.W. Chan, Phys. Rev. Lett. **109**, 155301 (2012).

[94] L.P. Pitaevskii, JETP Lett. **39**, 511 (1984).

[95] G. Baym and C.J. Pethick, Phys. Rev. A **86**, 023602 (2012).

[96] G.V. Shlyapnikov and P. Pedri, Conference on Correlated and Many-Body Phenomena in Dipolar Systems, Max Planck Institute for Complex systems, Dresden, 2006 (2006).

[97] A. Boudjemâa and G.V. Shlyapnikov, Phys. Rev. A **87**, 025601 (2013).

[98] F. Cinti, P. Jain, M. Boninsegni, A. Micheli, P. Zoller, and G. Pupillo, Phys. Rev. Lett. **105**, 135301 (2010).

[99] N. Henkel, R. Nath, and T. Pohl, Phys. Rev. Lett. **104**, 195302 (2010).

[100] A.E. Golomedov, G.E. Astrakharchik, and Yu.E. Lozovik, Phys. Rev. A **84**, 033615 (2011).

[101] S. Saccani, S. Moroni, and M. Boninsegni, Phys. Rev. B **83**, 092506 (2011).

[102] R.M. Wilson, S. Ronen, J.L. Bohn, and H. Pu, Phys. Rev. Lett. **100**, 245302 (2008).

[103] R.M. Wilson, C. Ticknor, J.L. Bohn, and E. Timmermans, Phys. Rev. A **86**, 033606 (2012).

[104] U.R. Fischer, Phys. Rev. A **73**, 031602 (2006).

[105] Z.-K, Lu, Y. Li, D.S. Petrov, and G.V. Shlyapnikov, Phys. Rev. Lett. **115**, 075303 (2015).

[106] V.P. Mineev and K.V. Samokhin, *Introduction to Unconventional Superconductivity* (CRC Press, 1999).

[107] G.E. Volovik, *Exotic Properties of Superfluid* ^{3}*He* (World Scientific, Singapore, 1992).

[108] N. Read and D. Green, Phys. Rev. B **61**, 10267 (2000).

[109] K.D. Nelson, Z.Q. Mao, Y. Maeno, and Y. Liu, Science **306**, 1151 (2004).

[110] T.M. Rice, Science **306**, 1142 (2004).

[111] S. Das Sarma, C. Nayak, and S. Tewari, Phys. Rev. B **73**, 220502 (2006).

[112] L.N. Bulaevskii, Sov. Phys. JETP **37**, 1133 (1973).

[113] M.J. Graf, D. Rainer, and J.A. Sauls, Phys. Rev. B **47**, 12089 (1993).

[114] P. Fulde and R.A. Ferrell, Phys. Rev **135**, A550 (1964).

[115] A.I. Larkin and Y.N. Ovchinnikov, Sov. Phys. JETP **20**, 762 (1965).

[116] For a review see R. Casalbuoni and G. Nardulli, Rev. Mod. Phys. **76**, 263 (2004).

[117] For a review, see V. Gurarie and L. Radzihovsky, Ann. Phys. (Amsterdam) **322**, 2 (2007).

[118] V. Gurarie, L. Radzihovsky, and A.V. Andreev, Phys. Rev. Lett. **94**, 230403 (2005).

[119] Y. Nishida, Ann. Phys. **324**, 897 (2009).

[120] Y. Nishida, L. Santos, and C. Chamon, Phys. Rev. B **82**, 144513 (2010).

[121] M.S. Foster, V. Gurarie, M. Dzero, and E.A. Yuzbashyan, Phys. Rev. Lett. **113**, 076403 (2014).

[122] N.R. Cooper and G.V. Shlyapnikov, Phys. Rev. Lett. **103**, 155302 (2009).

[123] J. Levinsen, N.R. Cooper, and G.V. Shlyapnikov, Phys. Rev. A **84**, 013603 (2011).

[124] A. Stern, Ann. Phys. **323**, 204 (2008).

[125] G. Möller, N.R. Cooper, and V. Gurarie, Phys. Rev. B **83**, 014513 (2011).

[126] D.A. Ivanov, Phys. Rev. Lett. **86**, 268 (2001).

[127] A.Yu. Kitaev, Ann. Phys. **303**, 2 (2003).

[128] A. Bulgac, M.M. Forbes, and A. Schwenk, Phys. Rev. Lett. **97**, 020402 (2006); A. Bulgac and S. Yoon, Phys. Rev. A **79**, 053625 (2009).

[129] D.V. Efremov and L. Viverit, Phys. Rev. B **65**, 134519 (2002).

[130] C. Zhang, S. Tewari, R. M. Lutchyn, and S. Das Sarma, Phys. Rev. Lett. **101**, 160401 (2008).

[131] M. Sato, Y. Takahashi, and S. Fujimoto, Phys. Rev. Lett. **103**, 020401 (2009).

[132] S. Tewari, S. Das Sarma, C. Nayak, C. Zhang, and P. Zoller, Phys. Rev. Lett. **98**, 010506 (2007).

[133] J.D. Sau, R.M. Lutchyn, S. Tewari, and S. Das Sarma, Phys. Rev. Lett. **104**, 040502 (2010).

[134] C.A. Regal, C. Ticknor, J.L. Bohn, and D.S. Jin, Phys. Rev. Lett. **90**, 053201 (2003).

[135] C. Ticknor, C.A. Regal, D.S. Jin, and J.L. Bohn, Phys. Rev. A **69**, 042712 (2004).

[136] K. Günter, T. Stöferle, H. Moritz, M. Köhl, and T. Esslinger, Phys. Rev. Lett. **95**, 230401 (2005).

[137] J. Zhang, E.G.M. Van Kempen, T. Bourdel, L. Khaykovich, J. Cubizolles, F. Chevy, M. Teichmann, L. Tarruell, S.J.J.M.F. Kokkelmans, and C. Salomon, Phys. Rev. A **70**, 030702 (2004).

[138] C.H. Schunck, M.W. Zwierlein, C.A. Stan, S.M.F. Raupach, W. Ketterle, A. Simoni, E. Tiesinga, C.J. Williams, and P.S. Julienne, Phys. Rev. A **71**, 045601 (2005).

[139] F. Chevy, E.G.M. van Kempen, T. Bourdel, J. Zhang, L. Khaykovich, M. Teichmann, L. Tarruell, S.J.J.M.F. Kokkelmans, and C. Salomon, Phys. Rev. A **71**, 062710 (2005).

[140] J. Fuchs, C. Ticknor, P. Dyke, G. Veeravalli, E. Kuhnle, W. Rowlands, P. Hannaford, and C.J. Vale, Phys. Rev. A **77**, 053616 (2008).

[141] Y. Inada, M. Horikoshi, S. Nakajima, M. Kuwata-Gonokami, M. Ueda, and T. Mukaiyama, Phys. Rev. Lett. **101**, 100401 (2008); **101**, 139901 (2008).

[142] K. Martiyanov, V. Makhalov, and A. Turlapov, Phys. Rev. Lett. **101**, 100401 (2010); V. Makhalov, K. Martiyanov, and A. Turlapov, Phys. Rev. Lett. **112**, 045301 (2014).

[143] T. Nakasuji, J. Yoshida, and T. Mukaiyama, Phys. Rev. A **88**, 012710 (2013).

[144] J. Levinsen, N.R. Cooper, and V. Gurarie, Phys. Rev. Lett. **99**, 210402 (2007).

[145] J. Levinsen, N.R. Cooper, and V. Gurarie, Phys. Rev. A **78**, 063616 (2008).

[146] M. Jona-Lasinio, L. Pricoupenko, and Y. Castin, Phys. Rev. A **77**, 043611 (2008).

[147] A.M. Rey, R. Sensarma, S. Fölling, M. Greiner, E. Demler, and M.D. Lukin, Europhys. Lett. **87**, 60001 (2009).

[148] A.V. Gorshkov, S.R. Manmana, G. Chen, J. Ye, E. Demler, M.D. Lukin, and A.M. Rey, Phys. Rev. Lett. **107**, 115301 (2011); Phys. Rev. A **84**, 033619 (2011).

[149] K.A. Kuns, A.M. Rey, and A.V. Gorshkov, Phys. Rev. A **84**, 063639 (2011).

[150] R. Barnett, D. Petrov, M. Lukin, and E. Demler, Phys. Rev. Lett. **96**, 190401 (2006).

[151] A. Micheli, G.K. Brennen and P. Zoller, Nat. Phys. **96**, 190401 (2006).

[152] A. Pikovski, M. Klawunn, G.V. Shlyapnikov, and L. Santos, Phys. Rev. Lett. **105**, 215302 (2010).

[153] D.-W. Wang, Phys. Rev. Lett. **98**, 060403 (2007).

[154] M. Klawunn, A. Pikovski, and L. Santos, Phys. Rev. A **82**, 044701 (2010).

[155] R.M. Lutchyn, E. Rossi, and S. Das Sarma, Phys. Rev. A **82**, 061604 (2010).

[156] M.A. Baranov, A. Micheli, S. Ronen, and P. Zoller, Phys. Rev. A **83**, 043602 (2011).

[157] A. Pikovski, M. Klawunn, A. Recati, and L. Santos, Phys. Rev. A **84**, 061605 (2011).

[158] N.T. Zinner, B. Wunsch, D. Pekker, and D.-W. Wang, Phys. Rev. A **85**, 013603 (2012).

[159] D.-W. Wang, M.D. Lukin, and E. Demler, Phys. Rev. Lett. **97**, 180413 (2006).

[160] A.C. Potter, E. Berg, D.-W. Wang, B.I. Halperin, and E. Demler, Phys. Rev. Lett. **105**, 220406 (2010).

[161] M. Babadi and E. Demler, Phys. Rev. A **84**, 235124 (2011).

[162] A.G. Volosniev, J.R. Armstrong, D.V. Fedorov, A.S. Jensen, and N.T. Zinner, Few-Body Syst. **54**, 707 (2013).

[163] W. Yi, A. Daley, G. Pupillo, and P. Zoller, New J. Phys. **10**, 073015 (2008).

[164] B. Dubetsky and P. Berman, Phys. Rev. A **66**, 045402 (2002); Laser Phys. **12**, 1161 (2002).

[165] S. Nascimbene, N. Goldman, N.R. Cooper, and J. Dalibard, Phys. Rev. Lett. **115**, 140401 (2015).

[166] M. Gullans, T.G. Tiecke, D.E. Chang, J. Feist, J.D. Thompson, J.I. Cirac, P. Zoller, and M. D. Lukin, Phys. Rev. Lett. **109**, 235309 (2012).

[167] O. Romero-Isart, C. Navau, A. Sanchez, P. Zoller, and J.I. Cirac, Phys. Rev. Lett. **111**, 145304 (2013).

[168] C. Huang, F. Ye, Z. Sun, and X. Chen, Opt. Express **22**, 30108 (2014).

[169] V.Y.F. Leung, A. Tauschinsky, N.J. Druten, and R.J.C. Spreeuw, Quantum Inf. Process. **10**, 955 (2011).

[170] A. González-Tudela, C.-L. Hung, D.E. Chang, J.I. Cirac, and H.J. Kimble, Nat. Photonics **9**, 320 (2015).

[171] J.D. Thompson, T.G. Tiecke, N.P. de Leon, J. Feist, A.V. Akimov, M. Gullans, A.S. Zibrov, V. Vuletic, and M.D. Lukin, Science **340**, 1202 (2013).

[172] J.S. Douglas, H. Habibian, C.-L. Hung, A. V. Gorshkov, H.J. Kimble, and D.E. Chang, Nat. Photonics **9**, 326 (2015).

[173] M. Lacki, M.A. Baranov, H. Pichler, and P. Zoller, Phys. Rev. Lett. **117**, 233001 (2016).

[174] F. Jendrzejewski, S. Eckel, T. G. Tiecke, G. Juzeliunas, G. K. Campbell, L. Jiang, A.V. Gorshkov, Phys. Rev. A **94**, 063422 (2016).

[175] A.K. Fedorov, I.L. Kurbakov, Y.E. Shchadilova, and Yu.E. Lozovik, Phys. Rev. A **90**, 043616 (2014).

[176] A.K. Fedorov, I.L. Kurbakov, and Yu.E. Lozovik, Phys. Rev. B **90**, 165430 (2014).

[177] A.K. Fedorov, S.I. Matveenko, V.I. Yudson, and G.V. Shlyapnikov, Sci. Rep. **6**, 27448 (2016).

[178] A.K. Fedorov, V.I. Yudson, and G.V. Shlyapnikov, Phys. Rev. A **95**, 043615 (2017).

[179] P.L. Kapitza, Nature (London) **141**, 74 (1938).

[180] L.D. Landau, J. Phys. USSR **5**, 71 (1941).

[181] R.P. Feynman, Rev. Mod. Phys. **29**, 205 (1957).

[182] For a review, see C. Chin, R. Grimm, P. Julienne, and E. Tiesinga, Rev. Mod. Phys. **82**, 1225 (2010).

[183] C. Ticknor, R.M. Wilson, and J.L. Bohn, Phys. Rev. Lett. **106**, 065301 (2011).

[184] P. Muruganandam and S.K. Adhikari, Phys. Lett. A **376**, 480 (2012).

[185] B.C. Mulkerin, D.H.J. O'Dell, A.M. Martin, and N.G. Parker, J. Phys. Conf. Ser. **497**, 012025 (2014).

[186] A. Macia, F. Mazzanti, J. Boronat, and R.E. Zillich, Phys. Rev. A **84**, 033625 (2011).

[187] A. Macia, D. Hufnagl, F. Mazzanti, J. Boronat, and R.E. Zillic, Phys. Rev. Lett. **109**, 235307 (2012).

[188] M. Ruggeri, arXiv:1305.6007 (2013).

[189] A. Macia, J. Boronat, and F. Mazzanti, Phys. Rev. A **90**, 061601 (2014).

[190] Y. Cai, M. Rosenkranz, Z. Lei, and W. Bao, Phys. Rev. A **82**, 043623 (2010).

[191] A.K. Fedorov, I.L. Kurbakov, and Yu.E. Lozovik, J. Phys. Conf. Ser. **414**, 012036 (2013).

[192] D. Baillie, R.N. Bisset, C. Ticknor, and P.B. Blakie, Phys. Rev. Lett. **113**, 265301 (2014).

[193] D. Baillie and P.B. Blakie, New J. Phys. **17**, 033028 (2015).

[194] M. Raghunandan, C. Mishra, K. Lakomy, P. Pedri, L. Santos, and R. Nath, Phys. Rev. A **92**, 013637 (2015).

[195] G.M. Bruun and E. Taylor, Phys. Rev. Lett. **101**, 245301 (2008); **107**, 169901 (2011).

[196] G.M. Bruun, C. Hainzl, and M. Laux, J. Mod. Opt. **63**, 1777 (2016).

[197] F. Mazzanti, R.E. Zillich, G.E. Astrakharchik, and J. Boronat, Phys. Rev. Lett. **102**, 110405 (2009).

[198] D.S. Petrov, D.M. Gangardt, and G.V. Shlyapnikov, J. Phys. IV France **116**, 3 (2004).

[199] D.S. Petrov, M. Holzmann, and G.V. Shlyapnikov, Phys. Rev. Lett. **84**, 2551 (2000).

[200] T. Belyaev, Sov. Phys. JETP **7**, 299 (1958).

[201] Yu.E. Lozovik and V.I. Yudson, Phys. A **93**, 493 (1978).

[202] E.L. Bolda, E. Tiesinga, and P.S. Julienne, Phys. Rev. A **68**, 032702 (2003).

[203] S.-M. Shih and D.-W. Wang, Phys. Rev. A **79**, 065603 (2009).

[204] C. Ticknor, Phys. Rev. A **80**, 052702 (2009); **81**, 042708 (2010); **84**, 032702 (2011).

[205] Y. Wang and C.H. Greene, Phys. Rev. A **85**, 022704 (2012).

[206] A.G. Volosniev, D.V. Fedorov, A.S. Jensen, and N.T. Zinner, Phys. Rev. Lett. **106**, 250401 (2011).

[207] T. Lahaye, J. Metz, B. Fröhlich, T. Koch, M. Meister, A. Griesmaier, T. Pfau, H. Saito, Y. Kawaguchi, and M. Ueda, Phys. Rev. Lett. **101**, 080401 (2008).

[208] T. Koch, T. Lahaye, J. Metz, B. Fröhlich, A. Griesmaier and T. Pfau, Nat. Phys. **4**, 218 (2008).

[209] A.A. Abrikosov, L.P. Gorkov, and I.E. Dzyaloschinskii, *Methods of Quantum Field Theory in Statistical Physics* (Prentice-Hall, 1965).

[210] V.N. Popov, *Functional Integrals in Quantum Field Theory and Statistical Physics* (D. Reidel, Dordrecht, 1983).

[211] C. Mora and Y. Castin, Phys. Rev. A **67**, 053615 (2003).

[212] M. Lara, J.L. Bohn, D.E. Potter, P. Soldán, and J.M. Hutson, Phys. Rev. A **75**, 012704 (2007).

[213] D.S. Jin and J. Ye, Phys. Today **64**, 27 (2011).

[214] S.Y.T. van de Meerakker, P.H.M. Smeets, N. Vanhaecke, R.T. Jongma, and G. Meijer, Phys. Rev. Lett. **94**, 023004 (2005).

[215] A.O.G. Wallis and J.M. Hutson, Phys. Rev. Lett. **103**, 183201 (2009).

[216] J. Deiglmayr, A. Grocola, M. Repp, K. Morlbauer, C. Gluck, J. Lange, O. Dilieu, R. Wester, and M. Weidemuller, Phys. Rev. Lett. **101**, 133004 (2008).

[217] G. Quéméner and J.L. Bohn, Phys. Rev. A **81**, 060701 (2010).

[218] A. Micheli, Z. Idziaszek, G. Pupillo, M. A. Baranov, P. Zoller, and P. S. Julienne, Phys. Rev. Lett. **105**, 073202 (2010).

[219] V.L. Ginzburg, Contemp. Phys. **9**, 355 (1968).

[220] L.V. Keldysh and A.N. Kozlov, Sov. Phys. JETP **27**, 521 (1968).

[221] For a review, see S.A. Moskalenko and D.W. Snoke, *Bose-Einstein Condensation of Excitons and Biexcitons and Coherent Nonlinear Optics with Excitons* (Cambridge University Press, New York, 2000).

[222] For a review, see M. Combescot, O. Betbeder-Matibet, and F. Dubin, Phys. Rep. **463**, 215 (2008).

[223] Yu.E. Lozovik, *in Proceeding of Dielectric Electronics Workshop* (Tashkent, 1973), p. 63.

[224] Yu.E. Lozovik and V.N. Nishanov, Sov. Phys. Solid State **18**, 1905 (1976).

[225] Yu.E. Lozovik and V.I. Yudson, JETP Lett. **22**, 274 (1975); JETP **44**, 389 (1976); Solid State Commun. **19**, 391 (1976). **21**, 211 (1977).

[226] L. Liu, L. Swierkowski, and D. Neilson, Physica B **249-251**, 594 (1998).

[227] V.V. Solov'ev, I.V. Kukushkin, J. Smet, K. von Klitzing, and W. Dietsche, JETP Lett. **83**, 553 (2006); **84**, 222 (2006).

[228] A. Filinov, P. Ludwig, Yu.E. Lozovik, M. Bonitz, and H. Stolz, J. Phys.: Conf. Ser. **35**, 197 (2006).

[229] Yu.E. Lozovik and A.A. Sokolik, JETP Lett. **87**, 55 (2008); Eur. Phys. J. B **73**, 195 (2010).

[230] H. Min, R. Bistritzer, J.-J. Su, and A.H. MacDonald, Phys. Rev. B **78**, 121401 (2008).

[231] Yu.E. Lozovik, S.L Ogarkov, and A.A. Sokolik, Phys. Rev. B **86**, 045429 (2012).

[232] A. Perali, D. Neilson, and A.R. Hamilton, Phys. Rev. Lett. **110**, 146803 (2013).

[233] B. Seradjeh, J.E. Moore, and M. Franz, Phys. Rev. Lett. **103**, 066402 (2009).

[234] G.Y. Cho and J.E. Moore, Phys. Rev. B **84**, 165101 (2011).

[235] N. Hao, P. Zhang, and Y. Wang, Phys. Rev. B **84**, 155447 (2011).

[236] D. Tilahun, B. Lee, E.M. Hankiewicz, and A.H. MacDonald, Phys. Rev. Lett. **107**, 246401 (2011).

[237] D.K. Efimkin, Yu.E. Lozovik, and A.A. Sokolik, Phys. Rev. B **86**, 115436 (2012).

[238] D.K. Efimkin and Yu.E. Lozovik, Phys. Rev. B **88**, 235420 (2013).

[239] D. Neilson, A. Perali, and A.R. Hamilton, Phys. Rev. B **89**, 060502 (2014).

[240] Yu.E. Lozovik and O.L. Berman, JETP **84**, 1027 (1997).

[241] Yu.E. Lozovik, O.L. Berman, and M. Willander, J. Phys.: Condens. Matter **14**, 12457 (2002).

[242] P. Pieri, D. Neilson, and G.C. Strinati, Phys. Rev. B **75**, 113301 (2007).

[243] Yu.E. Lozovik and O.L. Berman, JETP Lett. **64**, 573 (1996); Phys. Scr. **55**, 491 (1997).

[244] Yu.E. Lozovik, O.L. Berman, and V.G. Tsvetus, Phys. Rev. B **59**, 5627 (1999).

[245] O.L Berman, Yu.E. Lozovik, D.W. Snoke, and R.D. Coalson, J. Phys.: Condens. Matter **19**, 386219 (2007).

[246] Yu.E. Lozovik, Phys.-Usp. **52**, 286 (2009).

[247] S.I. Shevchenko, Phys. Rev. Lett. **72**, 3242 (1994).

[248] A.V. Balatsky, Y.N. Joglekar, and P.B. Littlewood, Phys. Rev. Lett. **93**, 266801 (2004).

[249] J. Keeling and N.G. Berloff, Phys. Rev. Lett. **100**, 250401 (2008).

[250] E.B. Sonin, Phys. Rev. Lett. **102**, 106407 (2009).

[251] A.A. Pikalov and D.V. Fil J. Phys.: Condens. Matter **23**, 265301 (2011).

[252] D. Neilson, A. Perali, and A.R. Hamilton, Phys. Rev. **B** 89, 060502 (2014).

[253] Yu.E. Lozovik and A.V. Poushnov, Phys. Lett. A **228**, 399 (1997).

[254] Yu.E. Lozovik, I.L. Kurbakov, and I.V. Ovchinnikov, Solid State Commun. **126**, 269 (2003).

[255] J. Keeling, L.S. Levitov, and P.B. Littlewood, Phys. Rev. Lett. **92**, 176402 (2004).

[256] J. Ye, T. Shi, and L. Jiang, Phys. Rev. Lett. **103**, 177401 (2009).

[257] A.V. Kavokin, M. Vladimirova, B. Jouault, T.C.H. Liew, J.R. Leonard, and L.V. Butov, Phys. Rev. B **88**, 195309 (2013).

[258] A.A. High, A.T. Hammack, J.R. Leonard, S. Yang, L.V. Butov, T. Ostatnický, M. Vladimirova, A.V. Kavokin, T.C.H. Liew, K.L. Campman, and A.C. Gossard, Phys. Rev. Lett. **110**, 246403 (2013).

[259] A.V. Nalitov, M. Vladimirova, A.V. Kavokin, L.V. Butov, and N.A. Gippius, Phys. Rev. B **89**, 155309 (2014).

[260] I.A. Shelykh, T. Taylor, and A.V. Kavokin, Phys. Rev. Lett. **105**, 140402 (2010); **105**, 199902 (2010).

[261] Y.G. Rubo and A.V. Kavokin, Phys. Rev. B **84**, 045309 (2011).

[262] R. Combescot and M. Combescot, Phys. Rev. Lett. **109**, 026401 (2012).

[263] H. Sigurdsson, T.C.H. Liew, O. Kyriienko, and I.A. Shelykh, Phys. Rev. B **89**, 035302 (2014).

[264] D.S. Smirnov and M.M. Glazov, Phys. Rev. B **90**, 085303 (2014).

[265] A.V. Gorbunov and V.B. Timofeev, JETP **119**, 115 (2014).

[266] J.P. Eisenstein and A.H. MacDonald, Nature (London) **432**, 691 (2004).

[267] J.J. Su and A.H. MacDonald, Nat. Phys. **4**, 799 (2008).

[268] D. Nandi, A.D.K. Finck, J.P. Eisenstein, L.N. Pfeiffer, and K.W. West, Nature (London) **488**, 481 (2012).

[269] K. Yang, Phys. Rev. Lett. **87**, 056802 (2001).

[270] Yu.E. Lozovik and I.V. Ovchinnikov, JETP Lett. **79**, 76 (2004).

[271] V.V. Krivolapchuk, E.S. Moskalenko, and A.L. Zhmodikov, Phys. Rev. B **64**, 045313 (2001).

[272] V.B. Timofeev and A.V. Gorbunov, J. Appl. Phys. **101**, 081708 (2007).

[273] A.V. Gorbunov, V.B. Timofeev, D.A. Demin, and A.A. Dremin, JETP Lett. **90**, 146 (2009).

[274] Y. Shilo, K. Cohen, B. Laikhtman, K. West, L. Pfeiffer, and R. Rapaport, Nat. Commun. **4**, 2335 (2013).

[275] M. Stern, V. Umansky, and I. Bar-Joseph, Science **343**, 55 (2014).

[276] M. Combescot, R. Combescot, M. Alloing, and F. Dubin, Europhys. Lett. **105**, 47011 (2014); M. Alloing, M. Beian, D. Fuster, Y. Gonzalez, L. Gonzalez, R. Combescot, M. Combescot, and F. Dubin, Europhys. Lett. **107**, 10012 (2014).

[277] Yu.E. Lozovik, I.L. Kurbakov, G.E. Astrakharchik, J. Boronat, and M. Willander, Solid State Commun. **144**, 399 (2007).

[278] M. Matuszewski, T. Taylor, and A.V. Kavokin, Phys. Rev. Lett. **108**, 060401 (2012).

[279] C. Schindler and R. Zimmermann, Phys. Rev. B **78**, 045313 (2008).

[280] M. Combescot, O. Betbeder-Matibet, and R. Combescot, Phys. Rev. Lett. **99**, 176403 (2007).

[281] G. Baym and C.J. Pethick, Phys. Rev. Lett. **76**, 6 (1996).

[282] D.H.J. O'Dell, S. Giovanazzi, and C. Eberlein, Phys. Rev. Lett **92**, 250401 (2004).

[283] A. Griffin, Phys. Rev. B **53**, 9341 (1996).

[284] M. de Dios-Leyva, C.A. Duque, and L.E. Oliveira, Phys. Rev. B **75**, 035303 (2007).

[285] L.V. Butov, A.V. Mintsev, Yu.E. Lozovik, K.L. Campman, and A.C. Gossard, Phys. Rev. B **62**, 1548 (2000).

[286] A. Parlangeli, P.C.M. Christianen, J.C. Maan, I.V. Tokatly, C.B. Soerensen, and P.E. Lindelof, Phys. Rev. B **62**, 15323 (2000).

[287] L.V. Butov, C.W. Lai, D.S. Chemla, Yu.E. Lozovik, K.L. Campman, and A.C. Gossard, Phys. Rev. Lett. **87**, 216804 (2001).

[288] L.V. Butov, A.L. Ivanov, A. Imamoglu, P.B. Littlewood, A.A. Shashkin, V.T. Dolgopolov, K.L. Campman, and A.C. Gossard, Phys. Rev. Lett. **86**, 5608 (2001).

[289] O. Carmel, H. Shtrikman, and I. Bar-Joseph, Phys. Rev. B **48**, 1955 (1993).

[290] H. Stolz, R. Schwartz, F. Kieseling, S. Som, M. Kaupsch, S. Sobkowiak, D. Semkat, N. Naka, T. Koch, and H. Fehske, New J. Phys. **14**, 105007 (2012).

[291] G.J. Schinner, E. Schubert, M.P. Stallhofer, J.P. Kotthaus, D. Schuh, A.K. Rai, D. Reuter, A.D. Wieck, A.O. Govorov, Phys. Rev. B **83**, 165308 (2011).

[292] A.T. Hammack, M. Griswold, L.V. Butov, L.E. Smallwood, A.L. Ivanov, and A.C. Gossard, Phys. Rev. Lett. **96**, 227402 (2006).

[293] A.A. High, A.K. Thomas, G. Grosso, M. Remeika, A.T. Hammack, A.D. Meyertholen, M.M. Fogler, L.V. Butov, M. Hanson, and A.C. Gossard, Phys. Rev. Lett. **103**, 087403 (2009).

[294] G. Chen, R. Rapaport, L.N. Pffeifer, K. West, P.M. Platzman, S. Simon, Z. Vörös, and D. Snoke, Phys. Rev. B **74**, 045309 (2006); Z. Vörös, D.W. Snoke, L. Pffeifer, and K. West, Phys. Rev. Lett. **97**, 016803 (2006).

[295] K. Kowalik-Seidl, X.P. Vögele, F. Seilmeier, D. Schuh, W. Wegscheider, A.W. Holleitner, and J.P. Kotthaus, Phys. Rev. B **83**, 081307 (2011); K. Kowalik-Seidl, X.P. Vögele, B.N. Rimpfl, G.J. Schinner, D. Schuh, W. Wegscheider, A.W. Holleitner, and J.P. Kotthaus, Nano Lett. **12**, 326 (2012).

[296] K. Yoshioka, Y. Morita, K. Fukuoka, and M. Kuwata-Gonokami, Phys. Rev. B **88**, 041201 (2013).

[297] M. Bauer, J. Keeling, M.M. Parish, P. López Ríos, and P. B. Littlewood, Phys. Rev. B **87**, 035302 (2013).

[298] R. Maezono, P.L. Ríos, T. Ogawa, and R.J. Needs, Phys. Rev. Lett. **110**, 216407 (2013).

[299] A. Filinov, M. Bonitz, P. Ludwig, and Yu.E. Lozovik, Phys. Status Solidi C **3**, 2457 (2006).

[300] Yu.E. Lozovik, O.L. Berman, and V.G. Tsvetus, JETP Lett. **66**, 332 (1997).

[301] M.D. Fraser, H.H. Tan, and C. Jagadish, Phys. Rev. B **84**, 245318 (2011).

[302] M.V. Kochiev, V.A. Tsvetkov, and N.N. Sibeldin, JETP Lett. **95**, 481 (2012).

[303] A.V. Gorbunov, V.B. Timofeev, and D.A. Demin, JETP Lett. **94**, 800 (2012).

[304] A. Amo, M. D. Martín, L. Viña, A.I. Toropov, and K.S. Zhuravlev, Phys. Rev. B **73**, 035205 (2006).

[305] W. Hofstetter, J.I. Cirac, P. Zoller, E. Demler, and M.D. Lukin, Phys. Rev. Lett. **89**, 220407 (2002).

[306] D.-W. Wang, M.D. Lukin, and E. Demler, Phys. Rev. A **72**, 051604 (2005).

[307] M. Iskin and C.A.R. Sá de Melo, Phys. Rev. B **72**, 224513 (2005); R.W. Cherng and C.A.R. Sá de Melo, arXiv:0808.1426.

[308] J.K. Chin, D.E. Miller, Y. Liu, C. Stan, W. Setiawan, C. Sanner, K. Xu, and W. Ketterle, Nature (London) **443**, 961 (2006).

[309] Y.-J. Han, Y.-H. Chan, W. Yi, A. J. Daley, S. Diehl, P. Zoller, and L.-M. Duan, Phys. Rev. Lett. **103**, 070404 (2009).

[310] P. Massignan, A. Sanpera, and M. Lewenstein, Phys. Rev. A **81**, 031607 (2010).

[311] A. Bühler, N. Lang, C.V. Kraus, G. Möller, S.D. Huber, and H.P. Büchler, Nat. Commun. **5**, 4504 (2014).

[312] B. Liu, X. Li, B. Wu, and W.V. Liu, Nat. Commun. **5**, 5064 (2014).

[313] K. Miyake, Prog. Theor. Phys. **69**, 1794 (1983).

[314] L.P. Gor'kov and T.K. Melik-Barkhudarov, Sov. Phys. JETP **13**, 1018 (1961).

[315] X. Dong and B. Wu, Laser Phys. **17**, 190 (2007).

[316] A. Negretti, R. Gerritsma, Z. Idziaszek, F. Schmidt-Kaler, and T. Calarco, Phys. Rev. B **90**, 155426 (2014).

[317] E.M. Lifshitz and L.P. Pitaevskii, *Statistical Physics, Part 2* (Pergamon Press, Oxford, 1980).

[318] A. Micheli, G. Pupillo, H.P. Büchler, and P. Zoller, Phys. Rev. A **76**, 043604 (2007).

[319] A.V. Gorshkov, P. Rabl, G. Pupillo, A. Micheli, P. Zoller, M.D. Lukin, and H.P. Büchler, Phys. Rev. Lett. **101**, 073201 (2008).

[320] L. Pricoupenko, Phys. Rev. Lett. **100**, 170404 (2008).

[321] M.W. Zwierlein, J.R. Abo-Shaeer, A. Schirotzek, C.H. Schunck, and W. Ketterle, Nature (London) **435**, 1047 (2005).

[322] E. Grosfeld, N.R. Cooper, A. Stern, and R. Ilan, Phys. Rev. B **76**, 104516 (2007).

[323] M. Lara, B.L. Lev, and J.L. Bohn, Phys. Rev. A **78**, 033433 (2008).

[324] S. Hoekstra, V. Metsälä, P.C. Zieger, L. Scharfenberg, J.J. Gilijamse, G. Meijer, and S.Y.T. van de Meerakker, Phys. Rev. A **76**, 063408 (2007).

[325] Yu. Kagan, B.S. Svistunov, and G.V. Shlyapnikov, JETP Lett. **42**, 209 (1988).

université PARIS-SACLAY | ÉCOLE DOCTORALE Physique en Île-de-France (EDPIF)

Titre : Phases à N corps non-conventionnelles dans des systèmes ultra-froids dipolaires

Mots clés : condensation de Bose-Einstein, superfluidité, interaction magnétique dipôle-dipôle

Résumé : Le problème de la détection et de la description des nouveaux états quantiques macroscopiques, caractérisées par des propriétés exotiques et non-conventionnelles, est d'importance fondamentale dans la physique moderne. Ces états offrent des perspectives fascinantes dans le domaine de traitement d'information, de simulations quantiques et de recherche des nouveaux types des matériaux. Dans ce travail de thèse nous développons une théorie qui permet de décrire des phases non-conventionnelles dans des systèmes des gaz ultra-froids dipolaires. Ces systèmes sont activement étudiés expérimentalement en utilisant des atomes à grand-spins, des molécules polaires et des excitations dipolaires dans des semi-conducteurs. Nous mettons l'accent sur la révélation du rôle de l'interaction dipôle-dipôle à long porté. Nous considérons l'effet de rotonization dans un système de gaz des bosons dipolaires «tiltés» aux interactions faibles dans une couche homogène. Nous prédisons l'effet de rotonization pour un gaz de Bose faiblement corrélé des excitons dipolaires dans une couche de semi-conducteur et nous calculons le diagramme de stabilité. Ensuite, nous considérons des superfluides d'onde-p des fermions identiques dans des réseaux 2D. Finalement, nous faisons une discussion sur un autre état superfluide intéressant des molécules polaires fermioniques, qui devrait apparaitre dans des systèmes bicouches.

Title : Non-conventional many-body phases in ultracold dipolar systems

Keywords : Bose–Einstein condensation, superfluidity, magnetic dipole-dipole interaction

Abstract : The problem of revealing and describing novel macroscopic quantum states character- ized by exotic and non-conventional properties is of fundamental importance for modern physics. Such states offer fascinating prospects for potential applications in quantum in- formation processing, quantum simulation, and material research. In the present Thesis we develop a theory for describing non-conventional phases of ultracold dipolar gases. The related systems of large-spin atoms, polar molecules, and dipolar excitons in semi-conductors are actively studied in experiments. We put the main emphasis on revealing the role of the long-range character of the dipole-dipole interaction. We consider the effect of rotonization for a 2D weakly interacting gas of tilted dipolar bosons in a homogeneous layer. We predict the effect of rotonization for a weakly correlated Bose gas of dipolar excitons in a semiconductor layer and calculate the stability diagram. We then consider p-wave superfluids of identical fermions in 2D lattices. Finally, we discuss another interesting novel superfluid of fermionic polar molecules.